AD NUMBER

ADB093690

NEW LIMITATION CHANGE

TO

Approved for public release, distribution unlimited

FROM

Distribution authorized to U.S. Gov't. agencies only; Test and Evaluation; 30 MAY 1984. Other requests shall be referred to Naval Weapons Center, China Lake, CA 93555-6001.

AUTHORITY

Naval Air Warfare Center, Weapons Div, Code 4T42AOD, China Lake, CA ltr dtd 23 Sep 1999

AD-B093 690

Thermostructural Evaluation of Four Infrared Seeker Dome Materials

Part 2. Thermal and Mechanical Properties

by
John R. Koenig
Southern Research Institute
for the
Ordnance Systems Department

APRIL 1985

DTIC
ELECTE
JUL 8 1985
B

**NAVAL WEAPONS CENTER
CHINA LAKE, CA 93555-6001**

DTIC FILE COPY

85 0

Naval Weapons Center
AN ACTIVITY OF THE NAVAL MATERIAL COMMAND

FOREWORD

This is the final report of work conducted at the Southern Research Institute (SRI), Birmingham, Ala., during 1983 and 1984 under Naval Weapons Center (NWC) contract N60530-83-C-0031, as part of the Multimode Guidance Program. This program is under the direction of NAVSEA 62R, SEATASK 62R210003008150186.

In the interest of economy, this report is published in its original form as submitted by SRI and does not follow the established NWC technical publication (TP) format. The report is published in the NWC TP series to ensure accountability and retrievability of the data.

To reduce the size of this report (originally 318 pages), three appendixes containing raw test data were omitted. These data are summarized in the body of the report. Copies of these appendixes may be obtained from the Naval Weapons Center, Attn: Don Gay, Code 3942, China Lake, California 93555-6001.

This report is published in two parts: Part 1 covers test and analysis conducted at NWC; Part 2 herein covers thermal and structural analysis conducted at the Southern Research Institute under NWC contract.

Approved by
C. L. SCHANIEL, *Head*
Ordnance Systems Department
16 April 1985

Under authority of
K. A. DICKERSON
Capt., U.S. Navy
Commander

Released for publication by
B. W. HAYS
Technical Director

REPORT DOCUMENTATION PAGE

1a REPORT SECURITY CLASSIFICATION		1b RESTRICTIVE MARKINGS			
UNCLASSIFIED		N/A			
2a SECURITY CLASSIFICATION AUTHORITY		3 DISTRIBUTION/AVAILABILITY OF REPORT			
N/A		Statement B; test and evaluation;			
2b DECLASSIFICATION/DOWNGRADING SCHEDULE		30 May 1984 *SAME AS COVER*			
N/A					
4 PERFORMING ORGANIZATION REPORT NUMBER(S)		5 MONITORING ORGANIZATION REPORT NUMBER(S)			
SoRI-EAS-84-1096-5155-1-F		NWC TP 6539, Part 2			

6a NAME OF PERFORMING ORGANIZATION	6b OFFICE SYMBOL (If applicable)	7a NAME OF MONITORING ORGANIZATION
Southern Research Institute Thermophysical Division	N/A	Naval Weapons Center

6c ADDRESS (City, State, and ZIP Code)	7b ADDRESS (City, State, and ZIP Code)
Birmingham, AL 32555-5305	China Lake, CA 93555-6001

8a NAME OF FUNDING/SPONSORING ORGANIZATION	8b OFFICE SYMBOL (If applicable)	9 PROCUREMENT INSTRUMENT IDENTIFICATION NUMBER
Naval Weapons Center	Code 3921	NWC Contract N60530-83-C-0031

8c ADDRESS (City, State, and ZIP Code)	10 SOURCE OF FUNDING NUMBERS			
	PROGRAM ELEMENT NO	PROJECT NO	TASK NO	WORK UNIT NO
China Lake, CA 93555-6001	PE63318N	S0186	21003	N/A

11 TITLE (Include Security Classification)
THERMOSTRUCTURAL EVALUATION OF FOUR INFRARED SEEKER DOME MATERIALS. PART 2. THERMAL AND MECHANICAL PROPERTIES

12 PERSONAL AUTHOR(S)
John R. Koenig

13a TYPE OF REPORT	13b TIME COVERED	14 DATE OF REPORT (Year, Month, Day)	15 PAGE COUNT
Final	FROM 1983 TO 1984	1985, April	158

16 SUPPLEMENTARY NOTATION

17 COSATI CODES			18 SUBJECT TERMS (Continue on reverse if necessary and identify by block number)
FIELD	GROUP	SUB-GROUP	IR seeker dome materials Dome thermostructural limits
16	04	04.2	Dome material properties Fractographic studies
17	08		Dome thermal properties (Contd. on back)

19 ABSTRACT (Continue on reverse if necessary and identify by block number)

(U) Four candidate IR seeker dome materials were evaluated in this study for their thermal and mechanical properties. The materials evaluated included sapphire, spinel, zinc sulfide, and zinc selenide. The mechanical properties evaluated were tension, compression, and flexure at ambient and elevated temperatures. The thermal properties evaluated were thermal expansion, thermal conductivity, and specific heat.

(U) This report is published in two parts. Part 1 covers test and analysis conducted at the Naval Weapons Center. Part 2 herein covers thermal and structural analysis conducted at the Southern Research Institute under NWC contract.

20 DISTRIBUTION/AVAILABILITY OF ABSTRACT	21 ABSTRACT SECURITY CLASSIFICATION	
☐ UNCLASSIFIED/UNLIMITED ☐ SAME AS RPT ☒ DTIC USERS	UNCLASSIFIED	
22a NAME OF RESPONSIBLE INDIVIDUAL	22b TELEPHONE (Include Area Code)	22c OFFICE SYMBOL
Don Gay	619-939-3341	NWC, Code 3942

DD FORM 1473, 84 MAR   83 APR edition may be used until exhausted
All other editions are obsolete

UNCLASSIFIED

18. (Contd.)
     Sapphire domes
     Spinel domes
     Zinc sulfide domes
     Zinc selenide domes

Accession For

NTIS GRA&I
DTIC TAB
Unannounced
Justification

By
Distribution/

Availability Codes

Dist	Avail and/or special
B-3	

CONTENTS

LIST OF FIGURES

LIST OF FIGURES (Continued)

LIST OF FIGURES (Continued)

LIST OF TABLES

LIST OF TABLES (Continued)

THERMAL AND MECHANICAL PROPERTIES OF
CANDIDATE OPTICAL MATERIALS FOR IR WINDOWS

1.0   INTRODUCTION

This is the final report of the effort conducted at Southern
Research for the Naval Weapons Center, China Lake, California under Contract
Number N60530-83-C-0031. The purpose of this program was to determine the
thermal and mechanical properties of several optical materials. There were
four materials evaluated in this study: Sapphire, Spinel, Zinc Selenide
(ZnSe) and Zinc Sulphide (ZnS).

The mechanical properties used in the evaluation include tension,
compression and flexure at room temperature and elevated temperatures. The
thermal properties used were thermal expansion, thermal conductivity, and
specific heat. In addition to these properties, nondestructive measurements
(NDC) were made to aid in the interpretation of the data and fractographic
studies were made of the tested specimens to understand the results. The NDC
results provide a tool to judge typicality and variation in future materials.

Planned applications for IR seeker systems for the intermediate
and long term time frame, particularly for air to air systems, require sur-
vival of the windows in more extreme aerodynamic heating conditions. This
requires the materials to survive more severe thermostructural loads which
exceed the capability of currently used optical materials. The materials
listed above were selected based on several criteria, including cost, optical
properties, rain erosion resistance, fabricability and, particularly, thermal
stress resistance. The matrices selected for this program were designed to
address, particularly, the thermal stress issue.

This report will cover the test matrices used for the charac-
terization of these materials, a discussion of some of the parameters to be
considered when conducting tests on these materials, the apparatuses and
procedures used, the experimental results obtained and a comparison and
summary of the materials. Some of the discussion of the data reduction
techniques will be integrated with the data reduction.

2.0   TEST MATRICES

The test matrices used for the evaluation of these materials are
presented in Tables 1 through 3.* They were designed to obtain sufficient in-
formation for comparative design studies and screening of the material with
emphasis on those properties which are anticipated to be most critical for a
thermostructural environment. The matrices for the ZnS and ZnSe are different
from the matrices for the spinel and sapphire due to anticipated differences
in the temperature limitations of the materials. These are somewhat different
from the planned matrices as shown in Tables 3 and 4 due to the specimens
received and decisions made during the course of the testing to optimize the
data set.

The objective of a screening matrix is to identify promising can-
didate materials for a given application with a minimum expenditure. This is
more straight forward in this program in that the driving load, thermal stress,
had been defined apriori. It is still somewhat of a challenge to define a
matrix which addresses the critical intrinsic properties with minimal expendi-
ture of resources.

The thermal stress resistance was investigated using thermal expan-
sion, thermal conductivity, specific heat, compression, tension and flexure.
Sensitivity studies conducted on this class of materials (see Appendix) show
the critical properties which control the thermal stress response for the
general heating rates and geometries of interest here to be the thermal
expansion, tensile strength or strain to failure and the ratio of the high
temperature compressive modulus to low temperature tensile modulus. The
other properties measured have a second order effect on the thermal stress
response, but are important for other critical responses. For example, the
thermal conductivity and specific heat, in addition to being necessary to
predict the thermal fields for thermal stress prediction, also affect in
depth heating of other system components and with the thermal expansion, aid
in thermal deformation compatibility design with the collar structure (the
intermediate body between the missile main body and the dome).

---

*All tables and figures are located at the end of the report.

2

The tensile tests conducted on these materials, as seen in Tables 1 through 3, were limited to room temperature only. This was done to limit the expenditure on fabricating these relatively complex specimens. As will be noted later, this was perhaps an unfortunate decision. It was also decided to machine these specimens to a fixed surface finish which would be matched on a dedicated set of flexure specimens (discussed below). The rest of the flexure specimens would be finished to the equivalent level as anticipated for IR domes. The effect of surface finish (for the spinel and sapphire) was to be accounted for by correlation between the flexure and tensile specimens. The temperature trend was also to be obtained from the flexure data. Five tensile tests were planned at room temperature, sufficient to obtain a reasonable estimate of the mean.

Three compressive tests were conducted in a nondestructive mode (loading to low stresses in the elastic response regime) at a series of temperatures up to the limit of the material. Tests were conducted at intervals of 200 °F. This provided a good estimate of the compressive elastic modulus as a function of temperature. It was not deemed important to obtain the compressive strength for these materials as compressive failure is unlikely. Poisson's ratio was measured at room temperature on the compressive specimens.

The flexure tests were conducted at a series of temperatures providing both the flexural modulus and strength. In the case of the sapphire additional tests were conducted at room temperature and 2000 degrees to evaluate the response at the 60 degree orientation. For both the spinel and sapphire five tests were conducted at room temperature with the surface ground to the same finish as the tensile specimens. In each case some latitude was taken with the number of replications at temperature to optimize the data set.

The thermal expansion was measured up to the material limit. The expansion of the sapphire was measured in both the 0 and 60 degree orientation. The specific heat and thermal conductivity were both measured up to the material limit. As will be discussed later the conductivity was measured at different temperature gradients to inspect how to appropriately model these materials where a significant radiation component is present.

3

The nondestructive tests consisted of measuring the bulk density and sonic velocity of each specimen plus a careful visual examination. The surface roughness was inspected using optical and SEM microscopy. SEM microscopy was used for the fractography.

3.0 MATERIALS

The specimens were all received from the fabricators in final machined condition. Each specimen was numbered by the fabricator and that identification was maintained through the testing. There were some differences in the number of specimens received of various orientations and finishes between what was received and what was anticipated as discussed herein and the matrices were adjusted accordingly.

The ZnS and ZnSe were fabricated by CVD, Inc. of Woburn, Massachusetts. Both are isotropic in nature and transparent with an amber shade. They are both fabricated using chemical vapor deposition.

The spinel ($MgAl_2O_4$) was fabricated by Coors Porcelain of Golden, Colorado using a hot pressing technique and the sapphire was made by growing a single crystal boule by Crystal Systems, Inc. The spinel has a cubic structure and is isotropic while the sapphire has a hexagonal structure.

4.0 MECHANICAL PROPERTY TESTING OF BRITTLE MATERIALS

The measurement of basic mechanical properties of brittle materials, such as tensile strength, using the methods which have been developed for ductile materials, is typically very unsatisfactory. There is typically a wide scatter in results when apparently identical tests are conducted on identical specimens of the same material. Some of the variation is caused by the inherent variability in the properties of the material, which is a result of the sensitivity of the material to local stress concentrations, caused by flaws, voids, microcracks, inclusions and other defects in the material. Part of the variability is caused by test technique due to the sensitivity of brittle materials to local stress concentrations or parasitic stresses.

Typically in the mechanical property testing of materials, there are many effects which leau to disturbances either in what would otherwise be a uniform or at least a simple distribution of stress across the gage section of the test specimen, or in the magnitude of the loads actually applied to the test section. Some of these sources of stress variations in the tensile test are tolerances in specimen and load train dimensions, eccentricities in the specimen and load train, kinks in the load train, friction in the universal joints, extraneous crosshead motion of the test machine, failure to apply load along the centerline, as well as many others. They result from the inability to carry out every step of the test perfectly and from the practical requirement that tolerances must be applied to every specimen, every piece of hardware and every activity connected with the test. Some of these variations are evident, such as the difficulty of aligning the applied load perfectly through the centroid of the cross-section of the specimen, or the difficulty of eliminating friction at ball joints in the load train, or the difficulty of designing and manufacturing a specimen such that loads can be applied without stress concentrations occurring in the gage. All of these effects, however, lead to locaiized stresses which are different from the nominal stress determined from the load at failure, the geometry of the failed cross-section, the specimen geometry, and assumptions of a uniform homogeneous material having simple elastic stress-strain properties. Since the material is brittle it will fail, generally speaking, when the peak stress reaches the limiting stress of the material at some particular location, regardless of how localized this location might be. A ductile material will yield locally and will fail only when the average stress over a significant portion of the cross-section reaches the limiting strength of the material.

There have been two bioad approaches taken in attempts to resolve this difficulty. One method is to select the test technique for its relative simplicity and to accept a complex stress distribution within the specimen. Reliance is then placed on refined stress analysis to determine the maximum stresses and, hence, material strength from the measured loads at failure. This approach may or may not be low in cost depending on the specimen configuration which is used. Frequently a complex specimen, such as the theta specimen, which is designed to provide areas of uniform

stress, is used to minimize the stress analysis problem by substituting specimens which are expensive to fabricate, although the test technique is simple. Alternatively, simple low cost specimens may be used with complete dependence on stress analysis to determine maximum stresses. The latter type of test is frequently used for comparative data on large numbers of specimens.

The flexural test used in this program is an example of such a test. In addition to its dependence on stress analysis, this approach involves a stress gradient at the location of fracture, so that a simple uniaxial strength is not determined. The complex stress state also inhibits the study of basic phenomena such as volume effects, rate dependence, or tensile stress-strain response since the flexural response is a combination of both tension and compression. This was understood when the matrices for this program were developed and the objective of the effort was to understand this data by correlation to the tensile data. As will be discussed, there was an additional problem in that the specimens received did not have a "break" at the corners (as is standard practice), the effect of which will be discussed later.

The other approach is to use the type of test that will produce simple stress distributions which can be readily and accurately determined from the measured loads and geometry, and to concentrate on refinement of technique, apparatus and specimen configuration in order to minimize the effects noted earlier. This is the approach taken for the gas bearing tensile tests reported herein and discussed in the next section. Some of the more obvious advantages of this test are:

1. Homogeneous stress field
2. Well defined volume under peak stress
3. Well defined surface under peak stress
4. Sufficient volume of uniform strain to allow good strain measurements
5. Unique fracture surface
6. Ready extension of the technique to elevated temperatures
7. Strain or stress rate control

5.0   APPARATUSES AND PROCEDURES

This section of the report presents discussions of the equipment and methods used for the evaluation of the properties determined in this program. It also shows the specimen configurations selected for each determination and gives the conditions under which the tests were conducted.

5.1   Tension

The tensile evaluations were performed in a gas bearing tensile facility. This facility utilizes gas bearing universals in the load linkage to prevent the introduction of unknown bending moments in the load train from the crosshead motion or eccentricity and allows monitoring cf the straightness of the load train.

A typical tensile facility is shown in Figure 1 and schematically in Figures 2 and 3. The primary components are the gas bearings, the load frame, the mechanical drive system, the 5500 degree furnace (not used in this effort), the optical strain analyzers and associated instrumentation for measurement of load and strain. The load capacity is 15,000 pounds.

The load frame and mechanical drive system are similar to those of many good systems. The upper crosshead is positioned by a small electric motor connected to a precision screw jack. This crosshead is stationary during loading and is moved only during assembly of the load train. The lower crosshead is used to apply the load to the specimen through a precision screw jack chain driven by a variable speed motor and gear reducer.

Nonuniaxial loading, and therefore bending stresses, may be introduced in tensile specimens not only from (1) misalignment of the load train at the attachment to the crossheads, but also from (2) eccentricity or nonstraightness within the load train, (3) unbalance of the load train, and (4) external forces applied to the load train by such items as electrical leads or clip-on extensometers. Although the bending moments from these sources may seem relatively slight, the resulting stresses can be quite significant in the evaluation of extremely sensitive brittle materials.

Elimination of nonuniaxial loading at the point of attachment of the load train to the crossheads has been confirmed by measuring the torque required to produce initial motion within the system with the bearings in operation under 5000 pounds load. This torque was found to be a maximum of 0.0066 inch-pounds. The stress that could be induced in a specimen due to this bending moment is 0.16 psi.

Emphasis in the design of the load train is placed on (1) large length to diameter ratios at each connection, (2) close sliding fits of all mating surfaces (3) elimination of threaded connections, (4) the use of pin connections wherever possible and (5) increasing the size of components to permit precise machining of all mating surfaces. All members are machined true and concentric to within 0.0005 inches, and the entire load train is checked regularly with an alignment bar to check overall alignment.

Strain measurements were made using an optical extensometer tracking the elongation between flags mounted on both sides of the specimen. The signals from both sides are averaged in reporting the strain values. On some (typically three) of the specimens of each material, strain gages were also used. Load was measured with a commercial flat load cell. The cell received a constant dc voltage input from a power supply and transmitted a millivolt signal (directly proportional to load) to an x-y recorder. Simultaneously, the optical strain analyzer measured the axial strain and transmitted a millivolt signal to the recorder. Similar plots were made using the output of the strain gages. Thus, continuous plots of stress-strain were recorded and are presented as the raw data in the appendix of this report.

The specimen used for the tensile tests for this program is shown in Figure 4. The spinel specimens were slightly modified for a total length of 4.5 inches. Both the zinc sulfide and zinc selenide specimens had a gage diameter of 0.250 inches.

5.2 Compression

The compressive evaluations were performed in a gas bearing compressive apparatus of similar design to the tensile apparatus described above. The compressive facility is shown in a photograph in Figure 5 and schematically in Figure 6. It consisted primarily of a load frame, gas bearings, load train, 50 ton screw jack, variable speed mechanical drive system, strain analyzers, 5500 °F furnace, and associated instrumentation for the measurement of load and strain.

Gas bearings were installed at each end of the load train to permit precise alignment of the load train to the specimen. The upper bearing was spherical on a radius of 6.5 inches, which is the distance from the top of the specimen to the bearing surface. The lower bearing is flat allowing transverse alignment of the load train. The gas bearings are floated only during the initial portion of the loading. The instrumentation is similar to that for the tensile facility.

A sketch of the 5500 °F furnace is shown in Figure 7. The furnace consists of a resistively heated graphite element insulated from a water cooled shell by thermatomic carbon. The furnace and specimen were purged in helium to provide an inert atmosphere. Temperatures were monitored with thermocouples at lower temperatures and with optical pyrometers at higher temperatures.

In order to obtain a good definition of the modulus-temperature relationship with only three specimens per material, the specimens were cycled through load-unload sequences at temperature increments of 200 °F. This is referred to as nondestructive mechanicals (NDM). At room temperature both strain gages and optical techniques were used. Strain gages monitored both the axial and lateral strains allowing measurement of the Poisson's ratio as well as the Young's modulus. The specimen used for the compressive evaluations is shown in Figure 8.

5.3   Flexure

Beam flexural evaluations were performed in the flexural apparatus shown in Figure 9 which consists of a load frame, load cell, load train, graphite resistance furnace, deflection measurement system and associated equipment for continuous measurement of load and deflection. Load was applied to the specimen from the lower end of the load train, and load measurements are made by the load cell at the upper end. As the load is applied to the specimen, midpoint deflection of the specimen is measured by means of a rod contacting the specimen midpoint and extending down to a differential transformer. The differential transformer is supported by a tube that attaches to the support bar eliminating load train motion from the deflection measurement. A new molybdenum loading system was designed and fabricated for this effort.

From the plot of load versus midpoint deflection, the values of modulus of rupture and flexural modulus were measured. The ultimate strength is calculated from the equation:

$$S = \frac{mc}{I}$$

which simplifies to

$$S = \frac{PL}{bh}$$

for a specimen with a rectangular cross-section employing the third span loading method, and where fracture occurs within the middle one-third of the specimen span length. The four point loading system is shown schematically in Figure 10. In these equations:

    S = modulus of rupture

    P = maximum applied load

    L = span length

    b = width of specimen

    h = height of the specimen

    m = moment

    c = length over which moment is measured

    I = moment of inertia

The initial modulus in flexure was calculated from the equation:

$$E_f = \frac{6P \ [a^3/3 + ac/2 \ (a + c/4]}{\delta \ bh^3}$$

where

E = elastic modulus in flexure

P/δ = ratio of load to corrected midpoint deflection at any point along the elastic portion of the curve

a and c = distances between the supports and loading points

The above equation neglects the deformation due to shear and assumes that the neutral axis coincides with the center of the cross-section.

5.4 Thermal Conductivity

The apparatus used for the evaluation of the thermal conductivity of these materials through 1800 °F is known as the comparative rod apparatus (CRA). The CRA compares the conductivity of the specimen being characterized to the known conductivity of a reference piece. Several types of references are available and their conductivities are traceable to NBS data or other reliable sources. In this effort references of Pyroceram and slipcast fused silica were used.

The CRA consists of a series of cylindrical pieces stacked in a vertical column as illustrated in Figure 11. The specimen and reference pieces are placed in the order reference-specimen-reference. Above the top reference is an electric heater that serves as the heat source for the experiment. AlSiMag insulators are placed above the heater and a steel rod forms the top of the column, receiving a compaction weight through a steel ball. Below the bottom reference is another electric heater or insulator, another steel rod, and a cooling sink, if required. The entire column is supported upon a steel ball for elimination of lateral forces that could deform the structure.

11

In assembling the apparatus, a large annular shell of aluminum or transite is moved down around the stacked pieces. The central core of the shell is wound with five electric coils which are guard heaters, each separately controlled to match the temperature gradient through the stacked column, thereby controlling radial heat losses.

The annular space between the central core and the stacked column is filled with diatomaceous earth, thermatomic carbon, or other insulating material selected to be compatible with the specimen. The entire shell is also filled with insulation.

Thermocouples are used to measure temperatures at all key points in the apparatus, including typically three points in the references and specimens, two points in the upper and lower guards, and one point in the middle guard.

For specimens with a conductivity of greater than 10 Btu-in./hr-ft -°F, the temperature gradient through the column is considered to be linear and the radial heat losses to be negligible. The calculations are made in a straightforward manner from Fourier's equation for one-dimensional heat flow:

$$q'' = \Delta t \, k/l$$

where q'' = heat flow through the material

Δt = temperature drop across the gage section

k = conductivity of the piece

l = gage length of the piece

The heat flow is calculated for the reference pieces directly since their conductivities are known and the temperature drops and gage lengths have been measured. It is then solved for the conductivity of the specimen using the arithmetic average of the q'' of the upper and lower references.

The radial inflow apparatus (RIA) was used to measure the thermal conductivity of the spinel and sapphire specimens from 1500 to up to 5500 °F. In this apparatus a water calorimeter located at the centerline of the specimen removes heat that flows inward from an external heat source. The heat source

is a high temperature furnace, into which the entire apparatus is placed. The water flow rate and the temperature rise give a direct measure of the heat flow through the specimen per unit time. Temperature measurements at two radial locations in each of the four specimen parts give the temperature drop across the specimen. These data enable the calculation of the thermal conductivity of the specimen.

A completely assembled RIA is shown schematically in Figure 12. In this figure a cylindrical specimen is shown rather than the four piece specimen used in this program. Figure 13 shows an assembled four piece specimen. Referring to Figure 12, the calorimeter water enters at 32 °F at the bottom and passes up through the insulation, the specimen, and more insulation, leaving the apparatus at the top. Two thermocouples placed 1/2 inch apart measure the temperature rise in the water stream as it passes through the gage section of the specimen. A flowmeter in the external water circuit measures the flow rate, which can be adjusted by a control valve. Vertical sight tubes are run down through the upper insulation material and aligned with holes in the specimen, so that thermocouple or optical pyro-meter readings can be taken of the specimen temperature. Vertical holes are drilled to the center of the specimen near the furnace side to determine the high temperature, and near the calorimeter side to determine the low temperature.

The apparatus is assembled on the water calorimeter tube by sliding cylindrical pieces down into position. The lower insulating pieces are graphite tubes filled with thermatomic carbon. The specimen holder is also a graphite tube, but of a slightly smaller diameter, such that it fits snugly into the lower insulating tube. The upper insulation piece is assembled with their vertical sight tubes in their precise positions and thermatomic packed around them. The upper insulation piece fits snugly around the specimen holder so that the assembly is physically stable and properly aligned. The position of the specimen holder is adjusted vertically so that the two thermocouples in the calorimeter are spaced equally above and below the center of the specimen. A radial hole in the specimen holder tube is aligned with an optical port in the side of the furnace when the apparatus is inserted into the furnace and secured in place.

13

To perform an evaluation, the specimens are assembled around the calorimeter, and the unit is installed in the furnace with the sight tubes and optical port properly aligned. Thermocouples are inserted into the sight tubes for the initial temperature measurement. The helium purge, calorimeter water flow, and power to the furnace are then turned on. The first temperature check is performed at approximately 1500 °F, which is made with thermocouples. When the desired temperature is achieved, the thermocouple readings and water flow are recorded.

For higher temperatures, the thermocouples are removed and the voltage to the furnace is adjusted upward. When the desired temperature is achieved, the thermocouple readings and water flow are recorded.

Special modifications of this technique had to be made to properly model the radiation effects. This was due to the material being transmissive to the near infrared. The specimens were machined down to a thickness of 0.25 inches and placed between two strips of graphite which contained the holes for temperature measurement. The inner packing around the calorimeter was varied to provide different temperature drops across the specimen. The reduction of these data is discussed with the data presentation.

5.5   Thermal Expansion

Thermal expansion measurements were made using quartz tube dilatometers modified from the Bureau of Standards design for measurements up to 1800 °F. Improvements have been made to prevent lateral movement of the quartz tube, thus eliminating possible erroneous readings.

The specimen was placed in a quartz tube that is firmly secured to the body of the apparatus, which is mounted on a work bench. A second quartz tube of slightly smaller diameter was inserted into the outer tube such that it rests on the specimen end. A quartz rod that is free to move vertically was then placed into the apparatus such that one end is in contact with the dial gage piston. The body of the dial gage was firmly attached to the apparatus. Any expansion or contraction of the specimen is transferred through the inner quartz tube, the quartz push rod, and the dial gage piston to registe a displacement on the gage. The quartz tube and specimen are located within a cylindrical electrical heater and can be heated to 1800 °F in the apparatus. The dial gage is calibrated in 0.0001 inch displacements and has an accuracy of ±0.0001 inch at any point in its range (0-0.5 inch).

The use of quartz for both the fixed and movable parts of the apparatus eliminates any difference in expansion rates and allows the apparatus to record only the expansion or contraction of the specimen. The recorded raw data are then corrected based on calibration data for that dilatometer developed from regular calibration runs on traceable standards. The specimen used for this program is illustrated in Figure 14.

For temperatures up to the maximum use temperature of the sapphire and spinel, graphite dilatometers were used which are capable of temperatures up to 5500 °F. The graphite dilatometers used for this effort consist of a graphite tube into which the specimen is placed and a graphite pushrod which is in contact with both the specimen and the precision dial gage. The entire assembly is placed in a furnace capable of elevating the temperature of the specimen to 5500 °F. Temperature readings are made with Chromel-Alumel thermocouples up to 2000 °F and with an optical pyrometers through sight glasses in the furnace at higher temperatures. The values from the dial gage readings as a function of temperature, corrected for the calibration of the dilatometer, are plotted to provide the thermal expansion curve.

5.6   Heat Capacity

The heat capacity to 1000 °F was determined from data obtained in an adiabatic calorimeter. In this apparatus the heated specimen was dropped into a thermally guarded, calibrated cup, and the enthalpy is measured as a function of the increase in temperature of the cup. The heat capacity is the slope of the enthalpy-temperature curve.

A tubular furnace was used to bring the specimen to temperature. The furnace pivots over the cup allowing the unit also to be used with a cold box for temperatures down to -300 °F. When the furnace is in place and the desired temperature is reached, the specimen is released from a suspension assembly which is triggered externally. Thermocouples are used to measure the specimen temperature.

Specimens of the material were heated to the desired temperature, and following a stabilization period, are dropped into the calorimeter cup. Adiabatic conditions are maintained during each run by manually adjusting the cup guard bath temperature.

The covered cup of the calorimeter is approximately 2.5 inches diameter by 2 inches deep. Three thermocouple wells are located in the bottom wall of the cup. The cup is mounted on cork supports, which rest in a silver-plated copper jacket. The jacket is immersed in a bath of ethylene glycol which is maintained at the temperature of the cup by means of a heater and copper cooling coils immersed in the liquid. A double-bladed stirrer maintains uniform bath temperature.

In the calorimeter six copper-constantan thermocouples, differentially connected between calorimeter cup and jacket, indicate temperature difference between the cup and bath. The six thermocouples allow a difference of 0.03 °F to be detected. This difference is maintained to within 0.15 °F. During the run, absolute temperature measurements of the cup are determined by means of the three thermocouple junctions, series-connected, in the bottom of the calorimeter cup.

The enthalpy of the specimen at any initial temperature is calculated from the equation:

$$h = K/W_s (t_2 - t_1)$$

where h = enthalpy above t_2

K = calorimeter constant, 0.2654 Btu/°F

W_s = sample weight in lbs

t_1 = initial cup temperature in °F

t_2 = final cup temperature in °F

The calorimeter constant of 0.2654 Btu/°F was determined by measuring the enthalpy of an electrolytic copper specimen of known specific heat. The enthalpy is referred to a common base temperature of 85 °F using linear interpolation. The enthalpy-temperature curve established is used to determine heat capacity (specific heat) by measuring its slope at different temperatures. This is done both graphically and by analytical methods.

The accuracy of the apparatus has been confirmed by measuring the enthalpy of sapphire (SRM 734 from NBS) and other standard specimens. The results of the comparison on sapphire and other data indicate that the overall uncertainty of the apparatus is ±3 percent.

The heat capacity of the spinel and sapphire were measured up to their use temperature using an ice calorimeter which employs the drop technique in which the specimen is heated in a furnace and then dropped into the ice calorimeter. The calorimeter contains a cup surrounded by a frozen ice mantle. Water at an inlet temperature of 32 °F is circulated through an annulus surrounding the mantle in order to absorb heat leak from the surroundings. The entire system is insulated with glass wool. The enthalpy of the specimen is sensed as a change in volume of the water ice ystem of the calorimeter as the ice melts. The annulus containing the flooded ice mantle communicates with the atmosphere through a mercury column in order that the change in volume can be read directly in a burette.

17

The specimen is placed in either a graphite or stainless steel basket and heated in the furnace in a controlled atmosphere such as Helium. The specimen and basket are dropped into the calorimeter and the volume change due to the melting ice is measured. The flutter valve immediately above the cup and the diaphragm valve immediately below the furnace are major features of the apparatus since the first blocks off radiation gains from the specimen up to the drop tube, and the second blocks radiation gains from the furnace down the drop tube just prior to dropping. The volume changes due to the baskets are measured and correction curves are established. Separate basket calibration minimizes the radiation error accompanying drop techniques.

The heat necessary to melt enough ice to cause a volume change of 1 cc has been established by NBS at 3.487 BTU. The correction of the basket is subtracted from the measured mercury displacement and the result used to calculate specimen enthalpy above 32 °F. The heat capacity, which is by definition the slope of the enthalpy curve, is determined both graphically and analytically.

5.7 Bulk Density

The bulk density of the specimens was measured on the regular specimens (all but the tensile and compressive specimens) by gravimetric techniques. The specimens were measured with micrometers and weighed on a Mettler balance. The reported density is simply the mass, in grams, divided by the calculated volume in cubic centimeters.

5.8 Ultrasonic Velocity

The ultrasonic velocity was measured on each of the specimens in the direction of test. The measurement was made using a through transmission technique. The setup is shown schematically in Figure 15.

The basic apparatuses used for measuring ultrasonic velocity were a Sperry UM 721 Reflectoscope and a Tektronix oscilloscope. In using the through-transmission, elapsed-time technique for measuring velocity, a short pulse of longitudinal mode sound was transmitted through the specimen. An electrical pulse from the pulse generator was applied to the crystal in the transducer. The pulse generated by the transducer was transmitted through a short delay line and inserted into the specimen. The time of insertion of the leading edge of this sound beam was the reference point on the time base of the oscilloscope which was used as a high speed stop watch. When the leading edge of this pulse of energy reaches the second transducer it was displayed on an oscilloscope. The difference between the entrance and exit times was used with the specimen length to calculate the sonic velocity.

6.0 DATA AND DISCUSSION

6.1 Gravimetric Density

Tne gravimetric density was measured on each of the mechanical and thermal specimens with the exception of the tensile and compressive specimens. The results are given on each of the mechanical data tables. The average densities measured were:

Sapphire - 3.97 gms/cc

Spinel - 3.58 gms/cc

ZnSe - 5.24 gms/cc

ZnS - 4.08 gms/cc

all of which are close to the anticipated value for theoretically dense material.

6.2 Ultrasonic Velocity

The ultrasonic velocity was measured on all specimens tested, the results given in the data tables. The average ultrasonic velocity for each material is

	Flex Specimens	Tensile Specimens
Sapphire 60°	0.4081 in./µsec	0.407 in./µsec
Sapphire 0°	0.4375 in./µsec	-
Spinel	0.3837 in./µsec	0.352
ZnSe	0.1741 in./µsec	0.174
ZnS	0.2121 in./µsec	0.211

Note the distinctive lower velocity of the 60° sapphire specimens.

These data can be used, along with the density values, to calculate a sonic modulus for each material. The average values of sonic modulus for the four materials, based on the velocity values measured on the tensile specimens are:

Sapphire	61.9×10^6 psi	$(47.2 \times 10^6$ psi$)$
Spinel	41.7×10^6 psi	$(30.1 \times 10^6$ psi$)$
ZnS	17.1×10^6 psi	$(9.1 \times 10^6$ psi$)$
ZnSe	14.9×10^6 psi	$(13.2 \times 10^6$ psi$)$

The values shown are the thin rod modulus. Those values in parentheses are are calculated according to:

$$E_{sonic} = \rho \, v^2 \frac{(1 + \nu)\,(1 - 2\nu)}{(1 - \nu)}$$

where ρ is density, v is velocity, and ν is the Poisson ratio.

6.3   Flexure

The flexural tests were conducted on each material with the surfaces maintained as received. Care was taken to avoid contact with this surface prior to testing. All handling was done with gloves. As mentioned earlier, there was no definition of "breaks" in the finishing of the corners of the tensile surface. This should be standard practice in the testing of brittle materials but was not called out on the specimen drawings. This will tend to give lower ultimate flexural strength values than would otherwise be obtained. The trends as a function of temperature will still be valid if the modes do not change. This is not necessarily the case for these materials.

6.3.1   Flexural Results for Sapphire

The results of the flexural tests on the sapphire specimens are given in Table 4. The first five 70 °F specimens were the zero-degree specimens with the polished finish. The second five 70 °F specimens had the 60/40 finish. There is no significant difference in either the density and sonic velocity between the two sets. As expected there was also no significant difference in the measured flexural modulus. The strength showed a dramatic difference. The average of the polished finished specimens was 130,151 psi while those with the 60/40 finish had an average strength of 73,567 psi.

The next five 70 °F specimens were oriented 60° to the first ten 70 °F specimens. The flexural moduli were much lower (52.5 versus 64.8 x 10⁶ psi). This is also reflected in the ultrasonic velocities (0.409 versus 0.438 inches/µsec). The flexural strengths of these specimens was lower than either of the 0° specimens despite the polished finish which was equivalent to the first set. The average was 73,490 psi. The average modulus was 52.47 x 10⁶ psi, significantly lower than the 64.8 average of the first two sets (0° orientation). The failure surfaces of these 60° specimens was distinctly different from the 0° specimens. A typical example of the 60° failure is shown in Figure 16 and has a conchoidal nature.

The failure surfaces on the 0° specimens are distinctly different as seen in Figure 17, the fracture tracking cleavage planes in a step-wise fashion.

The strength (and moduli) of the zero-degree-oriented specimens are lower at 2000° and continuously decrease in value as a function of temperature. Specimen F-18 at 2000 °F had a dramatically lower value. The fracture initiation site is shown in Figure 18.

The 60° specimens tested at 2000 °F showed a larger decrease in strength (45 percent of room temperature values) than the 0° specimens (81 percent of room temperature, ignoring F-18). The mean value was 33,223 psi, considerably weaker than even the 3000 °F 0° specimens.

The trends of the flexural moduli as a function of temperature are shown on Figure 19. The data are relatively well grouped and showed consistent trends. Figure 20 shows the strength as a function of temperature. Again a consistent trend is seen although, as expected, the coefficient of variation is much higher. Also, the coefficient of variation of the ground specimens is higher (20 percent) than that of the polished specimens. F-18 is anomalously low, having a value in the range of the 60° specimens.

6.3.2 Flexural Results for Spinel

The results of the flexural tests on spinel are shown on Table 5. No distinction was seen between the "ground" and "polished" specimens so that these values are lumped in the 70 °F data set. The mean strength at 70 °F was 13460 psi and the flexural modulus was 40.2 x 10⁶ psi. Again recall that the corners were not "broken" on these specimens. The apparent reason for the lack of distinction between the degrees of polish is that there was porosity in the parts which was larger than the scratches from the grinding or polishing process. An example of this is seen in Figure 21. A typical fracture surface is shown in Figure 22 which shows the grain size, presence of voids, and suspected initiation site which is, as anticipated, at a corner. Note also that the failure appears to propagate between, rather than through, grains.

Several specimens had chips on one surface. These were oriented so that the chips were on the compressive face. The chips did not have any apparent effect.

Figure 23 shows the trend of the flexural modulus as a function of temperature. It decreases about linearly to 2000 °F then more rapidly. Figure 24 shows the strength values as a function of temperature.

6.3.3 Flexural Results for Zinc Sulfide

The results of the flexural tests on the zinc sulfide specimens are given in Table 6. The modulus values are relatively consistent and decrease linearly as a function of temperature. The stress strain curves were nonlinear at 1500 and 1800 °F. This is illustrated in Figure 25. The flexural strength, however shows an increase as a function of temperature up to 1500 °F and, at 1800 °F, the strength is at least that at room temperature. The cause of this effect is not known. It may be that there is a process of defect healing occurring. If so, the rate of this event would determine if the increase would be effective in application. The flexural strength-temperature relationship is shown in Figure 26.

6.3.4   Flexural Results for Zinc Selenide

The flexure properties measured on the zinc selenide specimens are given in Table 7. The modulus, as in the ZnS results, decreases almost linearly as a function of temperature. This is illustrated in Figure 27. Again the stress strain curves were nonlinear at higher temperatures, being extremely nonlinear at 1000 °F and above with a "yield point" of about 1500 psi at 1000 °F and 1000 psi at 1500 °F and 1800 °F. Most of the 1500 and 1800 °F specimens did not provide an ultimate flexural strength because the specimens bottomed out in the fixture. After the tests, the unfractured specimens maintained the curved shape.

The strength increased at 500 °F over the room temperature values and was still higher than the room temperature values at 1000 °F as illustrated in Figure 28.

6.4   Tension

Tensile tests were conducted on each of the materials at room temperature only. Strain gages were used on several of the specimens in addition to clip-on optical extensometers. Good agreement was seen between the two techniques. Other specimens were ungaged as a standard, making sure that the gages did not affect ultimate values.

6.4.1   Tensile Response of Sapphire

The results of the tensile tests on the sapphire material are given in Table 8. The specimens were oriented in the 60° orientation. The sonic velocities agreed well with the 60° flex specimens. The calculated ρv^2 modulus for these specimens is 61.9×10^6 psi and, considering Poisson effects, the bulk sonic modulus is 47.2×10^6 psi. These values bracket the measured initial modulus which averaged 51.2×10^6 psi. The tensile modulus is also in good agreement with the room temperature flexural modulus which averaged 52.5×10^6 psi.

One of the five tensile specimens (T-1) failed in the head of the specimen. The failure was at a low stress level as calculated in the gage section (39,350 psi) and an even lower number value in the head, the value of which is affected by the stress concentration at the failure location. The failure surface for T-1 is shown in Figure 29.

The average tensile strength without specimen T-1 was 45,440 psi. A typical failure surface is shown in Figure 30 and the failure initiation in Figure 31. The tensile stress-strain curves for the sapphire are shown in Figure 32.

6.4.2   Tensile Response of Spinel

One of the five spinel tensile specimens was broken giving only four specimens for testing. The results of these tests are given in Table 9. Examples of the failure surfaces are shown in Figures 33 to 36. As with the flexure specimens, the failure propagated between the grains; the average strength of the four specimens was 14,200 psi. Two specimens broke at a lower value (12,500 psi average) and two at a higher value (15,900 psi average). No distinction was seen between the pairs in fractography. The two lower-strength specimens did have the lower velocity measurements but not significantly lower. The strains to failure also sorted as the moduli were essentially the same and the stress strain curves were linear to failure as illustrated in Figure 37. The average strain to failure was 0.00035 in./in.

6.4.3   Tensile Response of Zinc Sulfide

The results of the tensile tests for the zinc sulfide specimens are given in Table 10. The average strength of these specimens was 3565 psi. The response was very linear to failure as illustrated in Figure 38. Fracture faces and failure initiation points for the weakest (T-1) and strongest (T-2) specimens are shown in Figures 39 and 40. The average modulus was 11.4×10^6 psi and the strain to failure 0.00031 inches/inch. The stiffness is just slightly higher than the flexural modulus, 10.6×10^6 psi.

25

6.4.4   Tensile Response of Zinc Selenide

The tensile stress-strain data for zinc selenide are given in Table 11. The stiffness is again slightly higher than the flexural modulus (11.5 versus 10.3 x 10^6 psi) probably reflecting a shear contribution in the flexural data. The stress-strain curves were quite linear (except for T-2 as measured by the clip-ons). This is illustrated in Figure 41, a composite of the stress-strain curves. Specimen T-2 was linear as measured by the strain gages. The average strength was 2665 psi and the average strain to failure 0.00024 inches/inch. A typical tensile failure surface and initiation site (specimen T-2) are shown in Figure 42. Figures 43 and 44 show sequential magnifications of the failure surface of specimen T-4.

6.5   Compression

The compressive measurements were made by sequentially loading the specimens at increasing temperatures as discussed in the procedures section. The results reported for each specimen are obtained (typically averaged) from three replications per specimen at each temperature. Measurements were made up until nonlinearities were noted at the low stress levels used.

6.5.1   Compressive Results for Sapphire

The results of the compressive NDM measurements for sapphire are given in Table 12. These are plotted in Figure 45 and the average plotted in Figure 46. Figure 46 also shows a comparison with the tensile modulus at 70° and the flexural modulus at 70 and 2000°. There is good agreement between them, the tensile modulus being a little low at 70 °F.

6.5.2   Compressive Results for Spinel

The results of the compressive NDM measurements for spinel are given in Table 13. Specimen C-3 gave dramatically softer response than the other two specimens as illustrated on Figure 47. The other two specimens

were averaged to obtain the curve shown on Figure 48. The curve developed is higher (stiffer) than indicated by the tensile and flexure data.

6.5.3 Compressive Results for Zinc Sulfide

The results of the compressive NDM measurements for zinc sulfide are given in Table 14 and plotted on Figure 49. The average values agree well with the tensile and flexure results at 70° but tend to be stiffer than the flexural moduli at higher temperatures as illustrated in Figure 50.

6.5.4 Compressive Results for Zinc Selenide

The zinc selenide NDM compressive data are provided in Table 15 and plotted on Figure 51. The average values (Figure 52) agree well with the tensile and flexure results.

6.6 Thermal Expansion

6.6.1 Thermal Expansion of Sapphire

Figure 53 is a plot of the thermal expansion of 60° sapphire from room temperature to 3400 °F. The expansion was measured in a quartz dilatometer for temperatures up to 1500 °F. For temperatures greater than 1500 °F a graphite dilatometer was used. Again, this is good duplication of data and the expansion appears stable throughout the tested temperature range. The maximum expansion is 18.5×10^{-3} in./in. at 3400 °F. Tables 16 to 19 give the measured results by test.

Figure 54 is the thermal expansion of 0° sapphire. Its expansion is also stable but lower than 60° sapphire. The maximum expansion is 17.25 $\times 10^{-3}$ in./in. at 3400 °F. Plotted along with the 0° sapphire expansion is the expansion data of an NBS standard sapphire. Excellent agreement was obtained. Tables 20 to 23 give the individual test results.

6.6.2   Thermal Expansion of Spinel

Figure 55 is a plot of the thermal expansion of spinel from room temperature to about 2900 °F. Again, both quartz and graphite dilatometers were used. The expansion is stable and increases linearly to a maximum value of 15.5×10^{-3} in./in. at 2900 °F. Tables 24 to 27 give the thermal expansion test results.

6.6.3   Thermal Expansion of Zinc Sulfide

Figure 56 is a plot of the thermal expansion of zinc sulfide versus temperature. The expansion was measured from room temperature to 1800 °F using a quartz dilatometer (described earlier). As can be seen there is good agreement between the specimens. The expansion is somewhat linear attaining a maximum value of 8.4×10^{-3} in./in. at 1800 °F. The tabular results are provided in Tables 28 and 29.

6.6.4   Thermal Expansion of Zinc Selenide

Figure 57 is a plot of the thermal expansion of zinc selenide from room temperature to 1800 °F as measured in a quartz dilatometer. There is good duplication of data. The expansion is linear up to about 1200 °F. After 1200 °F there is a slight "hump" in the data which peaks at about 1400 °F. The "hump" is no longer detectable after 1600 °F as the expansion returns to its linearity. The peak expansion is 7.0×10^{-3} in./in. at 1800 °F. The "hump" in the thermal expansion data is probably due to some phase change within the material. This change could be either recrystallization or precipitation of the parent materials. A review of the mechanical data shows that the flexural modulus, flexural strength, and compressive modulus all decrease somewhere between 1000 °F and 1500 °F. Infrared absorption data from Hughes (Reference 1) indicates optical degradation of the material at about 1200 °F. The results by test are given in Tables 30 and 31.

6.6.5   Comparison of Thermal Expansions

Figure 58 is a composite plot of the thermal expansions of all
four materials. At 1800 °F ZnSe had the highest expansion. ZnS, spinel and
60° sapphire are all next with roughly the same expansions. 0° sapphire
had the lowest expansion.

6.7   Heat Capacity of the Four Materials

The heat capacity of the four window materials was measured
using an adiabatic calorimeter (for temperatures less than 1000 °F) and an
ice calorimeter (for temperatures greater than 1000 °F). Both of these
techniques were described earlier. To obtain heat capacity enthalpy,
changes of the material are first determined. The enthalpy changes are
plotted and the slope of the enthalpy curve (heat capacity) is determined
graphically. Figures 59 through 62 are the enthalpy curves for Sapphire,
Spinel, Zinc Sulfide and Zinc Selenide, respectively. Figures 63 through
66 are the corresponding heat capacity curves. Figure 67 is a composite
plot of the heat capacity of all four materials. Zinc Selenide had the
lowest heat capacity. The heat capacity of the Zinc Selenide increased
linearly until about 120 °F, where it began to level off. This is
probably due to material degradation as described earlier. The heat
capacity of zinc selenide increased from 0.08 Btu/lb-F (200 °F) to 0.125
Btu/lb-F (1800 °F). Zinc sulfide had the next lowest heat capacity which
increased from 0.115 Btu/lb-F (200 °F) to 0.135 Btu/lb-F (1800 °F). The
heat capacity of the sapphire increased sharply from 0.215 Btu/lb-F at
200 °F to 0.295 Btu/lb-F at 1500 °F. After 1500 °F the heat capacity
increases slightly to 0.325 Btu/lb-F at 3250 °F. The heat capacity of
NBS sapphire increased sharply from 0.215 Btu/lb-F at 200 °F to 0.295 at
1500 °F. After 1500 °F the heat capacity increases slightly to 0.325 Btu/
lb-F at 3250 °F. The heat capacity of NBS sapphire (Reference 720) is also
plotted. As can be seen there is good agreement with the NBS standard
sapphire. The heat capacity of the spinel starts off about the same as

the sapphire (0.215 at 200 °F). The heat capacity of the spinel is slightly
lower than the sapphire until about 1250 °F. At this point the heat capacity
of the spinel increases, exceeding the sapphire, to a maximum value of 0.37
Btu/lb-F at 3000 °F.

Tables showing the individual data points for each of the
materials are provided as Tables 32 to 39.

6.8 Thermal Conductivity of Sapphire

Sapphire absorbs significant amounts of radiation at certain
wavelengths. This radiation is then reemitted within the sapphire providing
a radiative transport mechanism within the medium. The ordinary (true)
thermal conduction is thus augmented by a radiation conduction. The apparent
measured conductivity, a combination of the true thermal conduction and the
radiation conduction, is termed a thermal conductance.

Figure 68 is a plot of the thermal conductance of sapphire
versus temperature. Conductance from 250 °F to 1500 °F was measured in the
comparative rod apparatus (CRA), discussed earlier. Conductance from 1500 °F
to about 3250 °F was measured in the radial inflow apparatus (RIA), also
discussed earlier. Figure 68 shows a difference in the values of conductance
at 1500 °F as measured by both facilities. This difference is attributed
to radiation effects involving specimen thicknesses, transmission coefficients
and view factors. Radiation effects can be compensated for analytically if
one assumes that conduction and radiation are independent of one another
(References 2, 3, and 4), that is,

$$q_{total} = q_{conduction} + q_{radiation} \tag{1}$$

Let $q_{conduction}$ be simple conduction governed by Fourier's law
for steady-state heat flow (Reference 5)

$$q_{conduction} = \frac{k\,(T_1 - T_2)}{D} \tag{2}$$

and let $q_{radiation}$ be defined as radiant heat transfer between two flat
plates with some transmitting-absorbing media in between (References 6
and 7),

30

$$q_{radiation} = \frac{N \sigma (T_1^4 - T_2^4)}{\left[\frac{3(1-\tau)}{4} D \left|\frac{1}{\epsilon_1} + \frac{1}{\epsilon_2} - 1\right|\right] F} \qquad (3)$$

where the terminology is as follows:

T_1 = Temperature Hot Surface

T_2 = Temperature Cold Surface

K = Thermal Conductivity

D = Specimen Thickness

σ = Stefan-Boltzman Constant

τ = Transmission Coefficient

ϵ_1 = Emissivity Surface 1

ϵ_2 = Emissivity Surface 2

F = View Factor = 1 for RIA = 0.2 for CRA

N = Amount of Energy below Wavelength for Blackbody at T

If the above equations are used in conjunction with the transmission plots of sapphire (Figures 69 and 70 supplied by NWC (Reference 8)), a value of true thermal conductivity can be solved for. This is shown in Figure 71. The dashed line represents literature values (Reference 9 and 10). There is good agreement between data sets as shown.

The issue of the difference between the CRA results and the RIA results is further clouded by the misorientation of the RIA specimens which were aligned 90° to the intended orientation. The effect of this on the values measured is unknown but, given the relatively good agreement in the calculated values, appears to be less than 20 percent.

6.9 Thermal Conductivity of Spinel

Figure 72 is a plot of the thermal conductance of spinel versus temperature. Again there is disagreement at 1500 °F between facilities. If the data are treated in the same manner as the sapphire data and the analytical equations used in conjunction with the transmission plots (Figures 73 and 74), a corrected thermal conductivity curve is obtained (Figure 75). The dashed line represents the average value of the data. There were no literature values available on spinel for comparison. Data above 2500 °F is questionable

since 2500 °F is the approximate hot pressing temperature of the material.

6.10   Thermal Conductivity of Zinc Sulfide (ZnS)

Figure 76 is a plot of the thermal conductivity of zinc sulfide (ZnS) as a function of temperature. The conductivity was measured in the comparative rod apparatus only. Data above 1470 °F is questionable as this is the reported degradation temperature of the material[5]. Since the conductivity was measured at temperatures less than 1500 °F, radiation effects need not be considered. The data in Figure 76 represents the true conductivity. The values of conductivity range from about 95 Btu-in./hr-ft^2-°F at 260 °F to 45 Btu-in./hr-ft^2-°F at 1000 °F.

6.11   Thermal Conductivity of Zinc Selenide (ZnSe)

Figure 77 is a plot of the thermal conductivity of zinc selenide (ZnSe) as a function of temperature. The conductivity was measured in the comparative rod apparatus only. Data above 1112 °F is questionable as this is the reported degradation temperature of the material[8]. Since the conductivity was measured at temperatures less than 1500 °F, radiation effects need not be considered. The data in Figure 77 represents the true conductivity. The values of conductivity range from about 93 Btu-in./hr-ft^2-°F at 190 °F to 40 Btu-in./hr-ft^2-°F at 1000 °F.

7.0   SUMMARY OF PROPERTIES

Tables 40 through 43 provide a quick summary of the properties of each of the four materials. Flexural strength values are suspect due to the lack of a "break" on the corners. Thermal conductivity values are corrected for radiation where appropriate. As expected tensile values, rather than flexure, give a good comparison to the predicted tensile loads in full scale thermostructural testing as given in Part 1 of this report and shown in Table 44. Table 45 provides a comparison of the four materials.
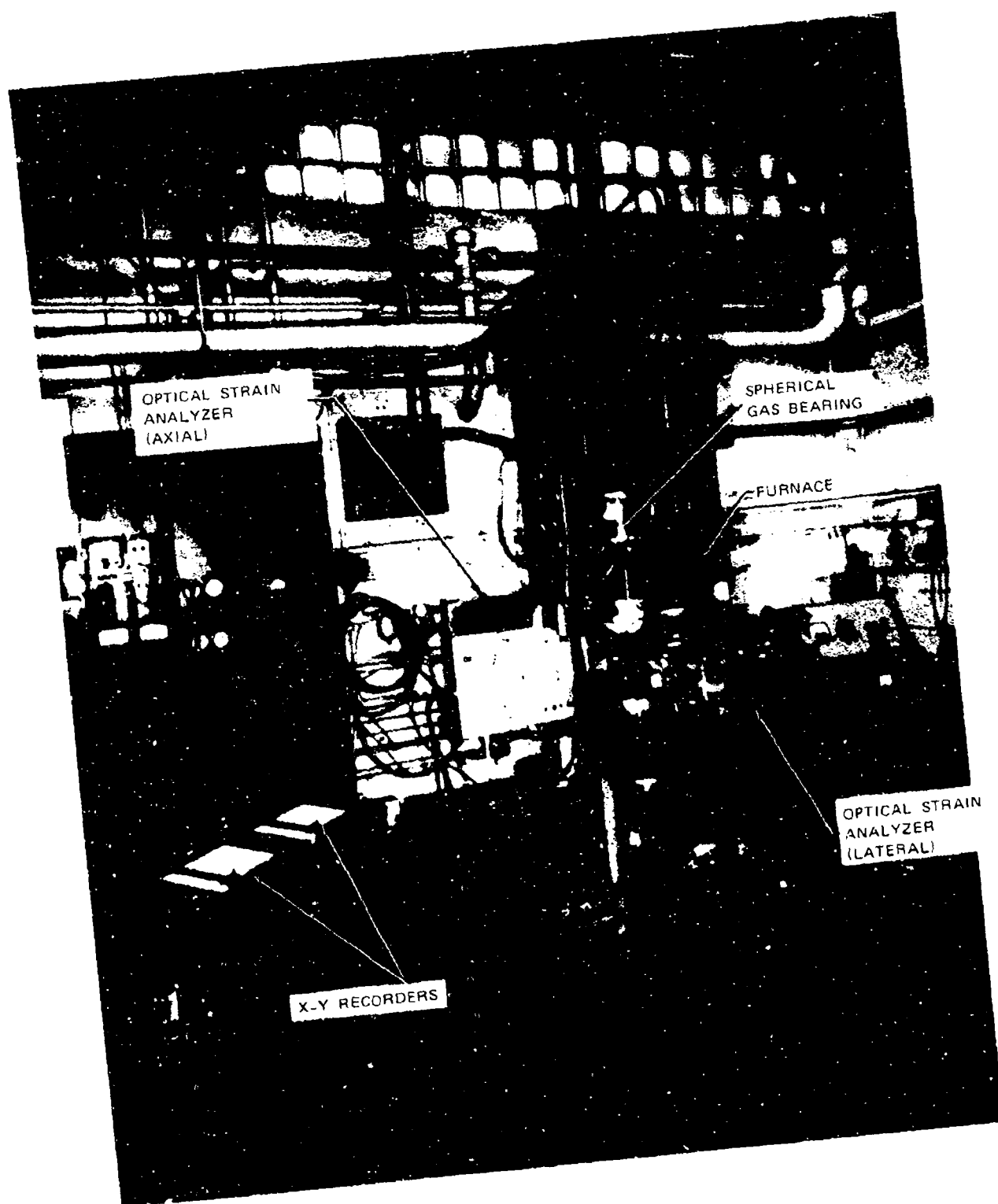
Figure 1. Photograph of a Tensile Stress-Strain Facility
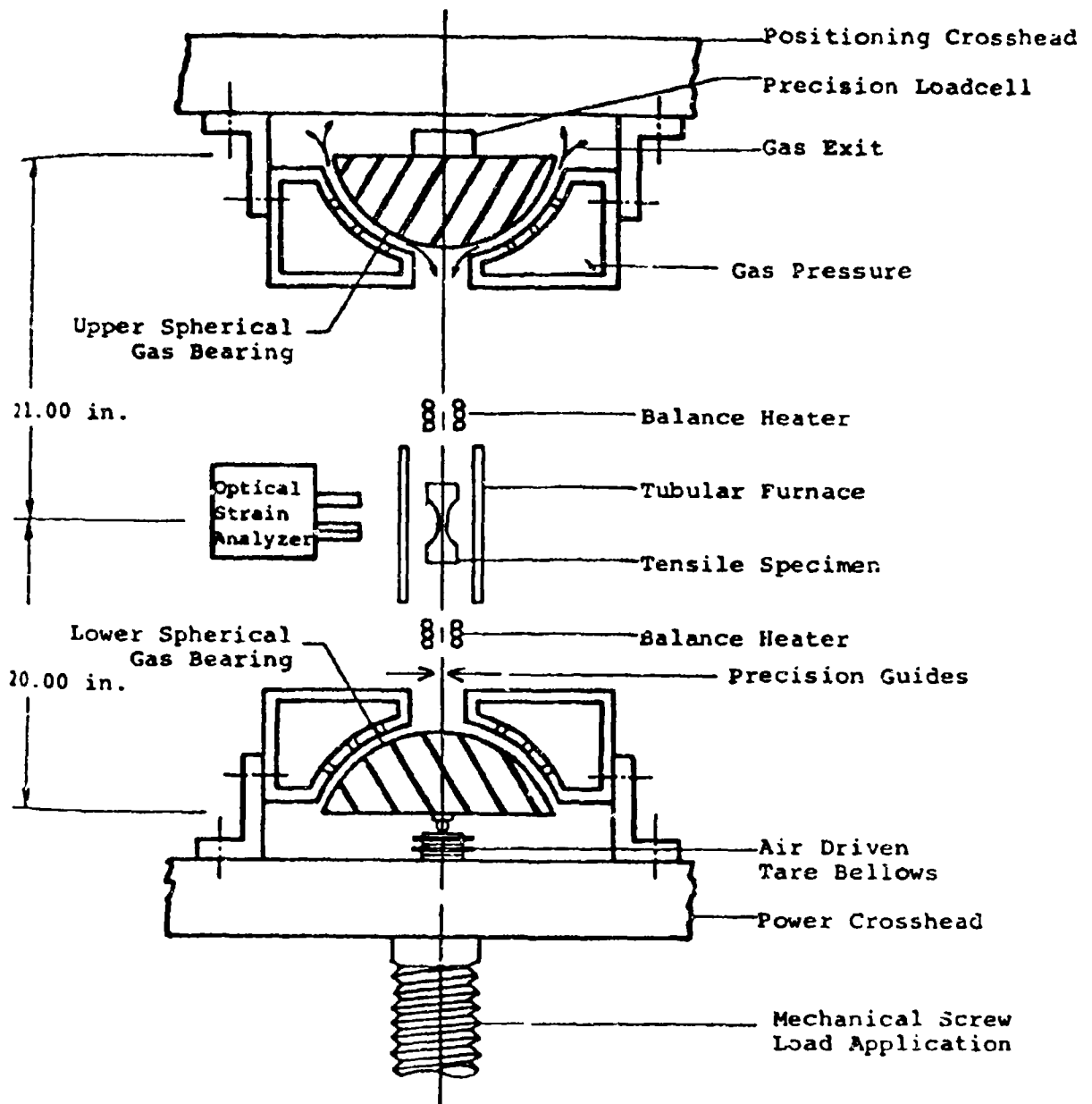
Figure 2. Schematic arrangement of the gas-bearing universals, specimen and load train
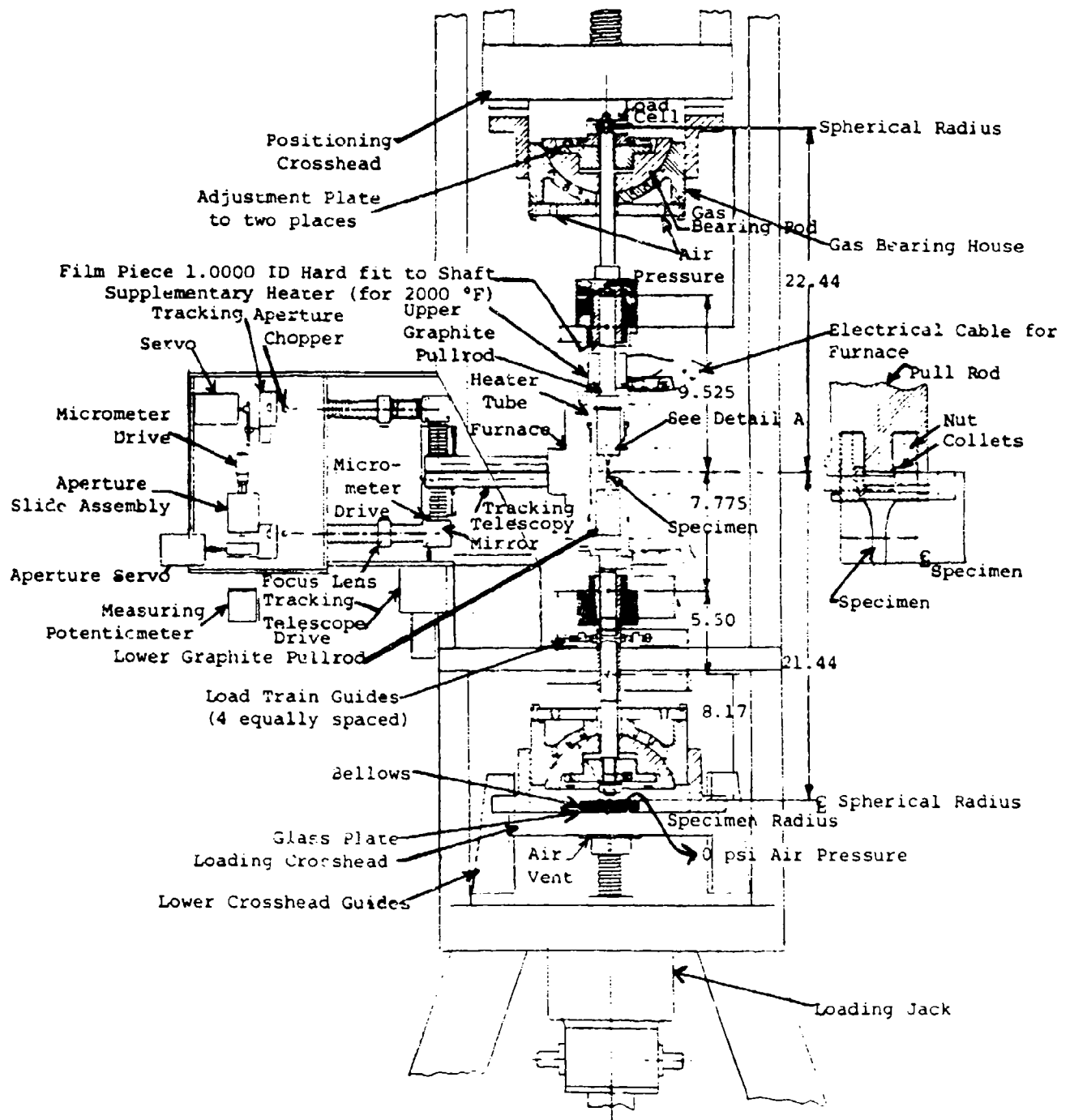
Figure 3.   Schematic arrangement of gas-bearing universals, specimen and load train

Notes: 1. All diameters true and concentric to 0.0005".
        2. Both ends flat and perpendicular to 0.0005".
        3. Finish grind gage section axially.
        4. Tolerances unless otherwise noted: Decimals x.xx – 0.005"
                                                 Decimals x.xxx– 0.001"

0.500" Dia.

0.453 Dia.

0.156" Dia. ±.001

0.2

2"R

-0.2

0.516"

1.250"

5.00"

0.250"
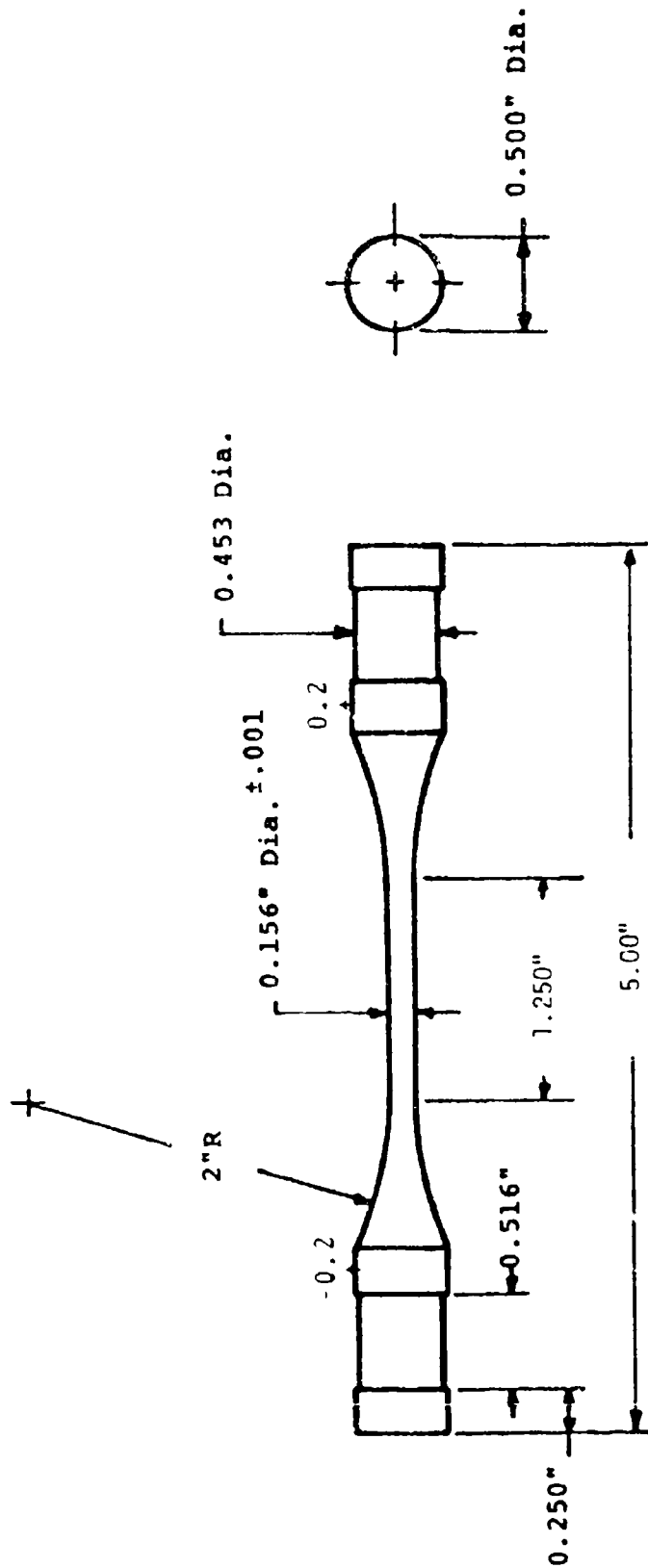
Figure 4. Tensile Specimen Configuration

36
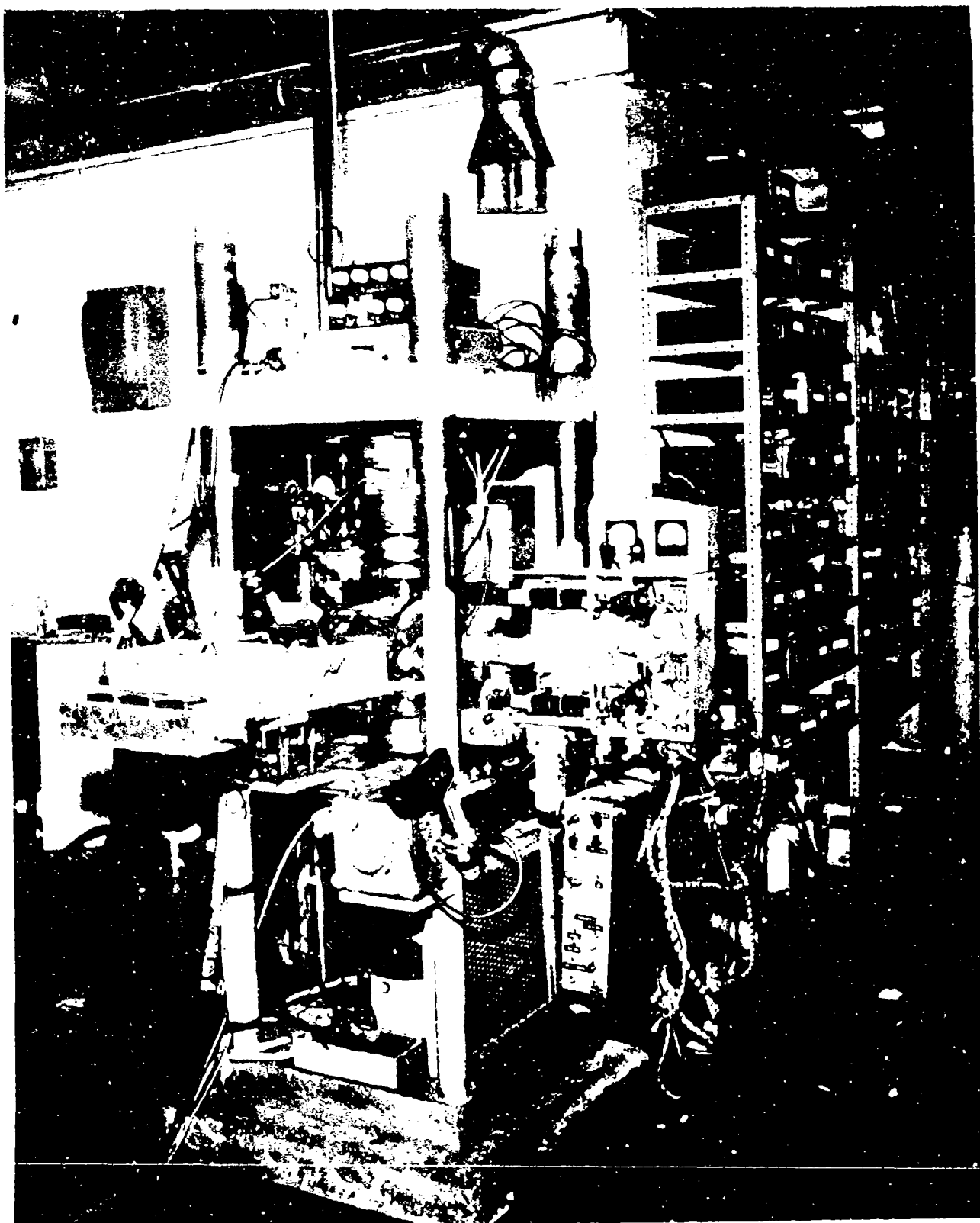
Figure 1. Picture of the combustion facility after its baseline and other measurements.
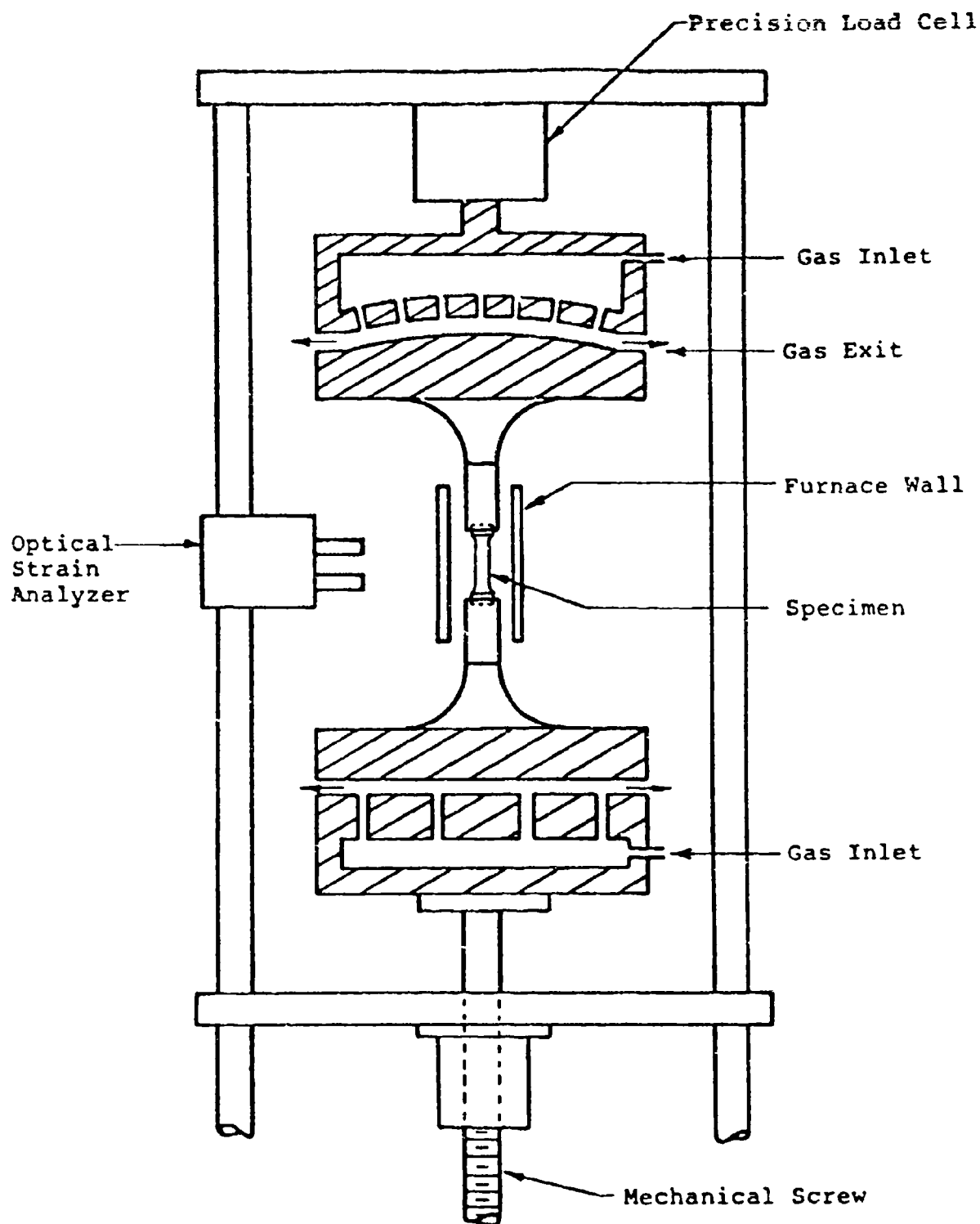
Figure 6. Schematic arrangement of Gas-Bearing universals, Specimen and
Load Train
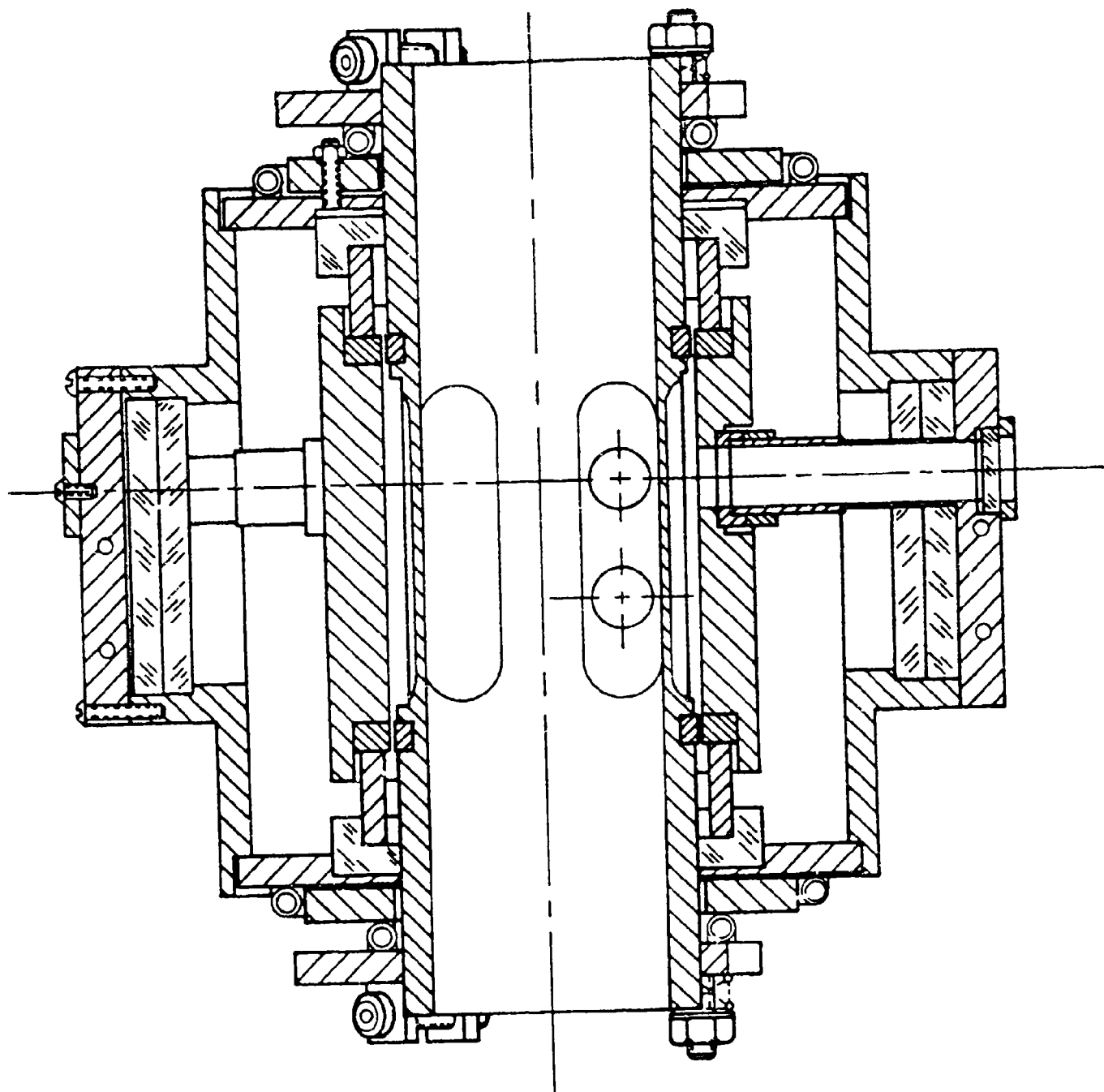
Figure 7. Small 5500 °F Graphite Resistance Furnace
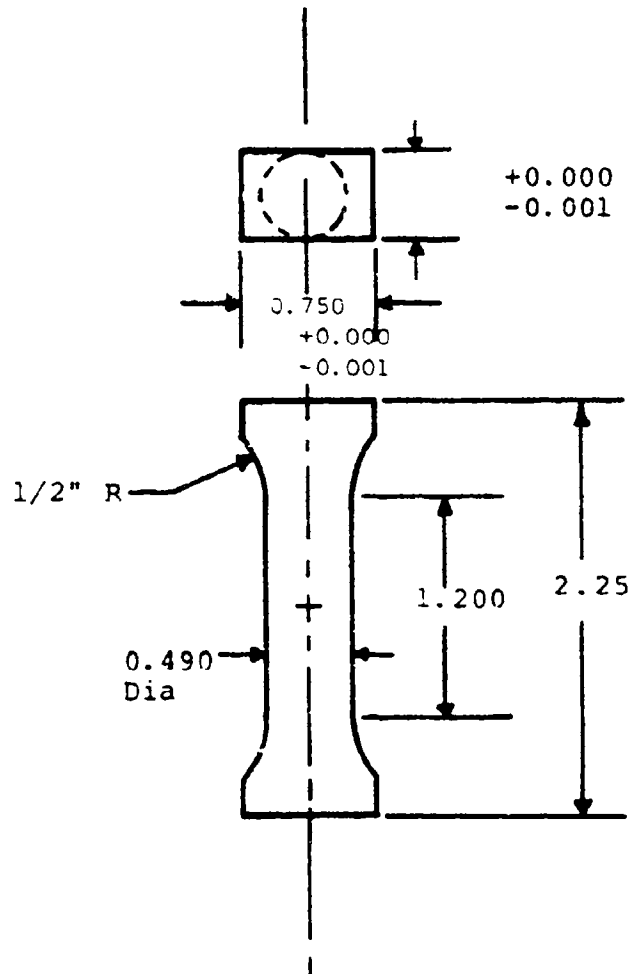
Notes: 1. Tolerances unless noted: Fractions ± 1/64"
                                     Decimals ± 0.001"
       2. Both ends flat and perpendicular to 0.0005"

Figure 8. Compression Specimen Configuration
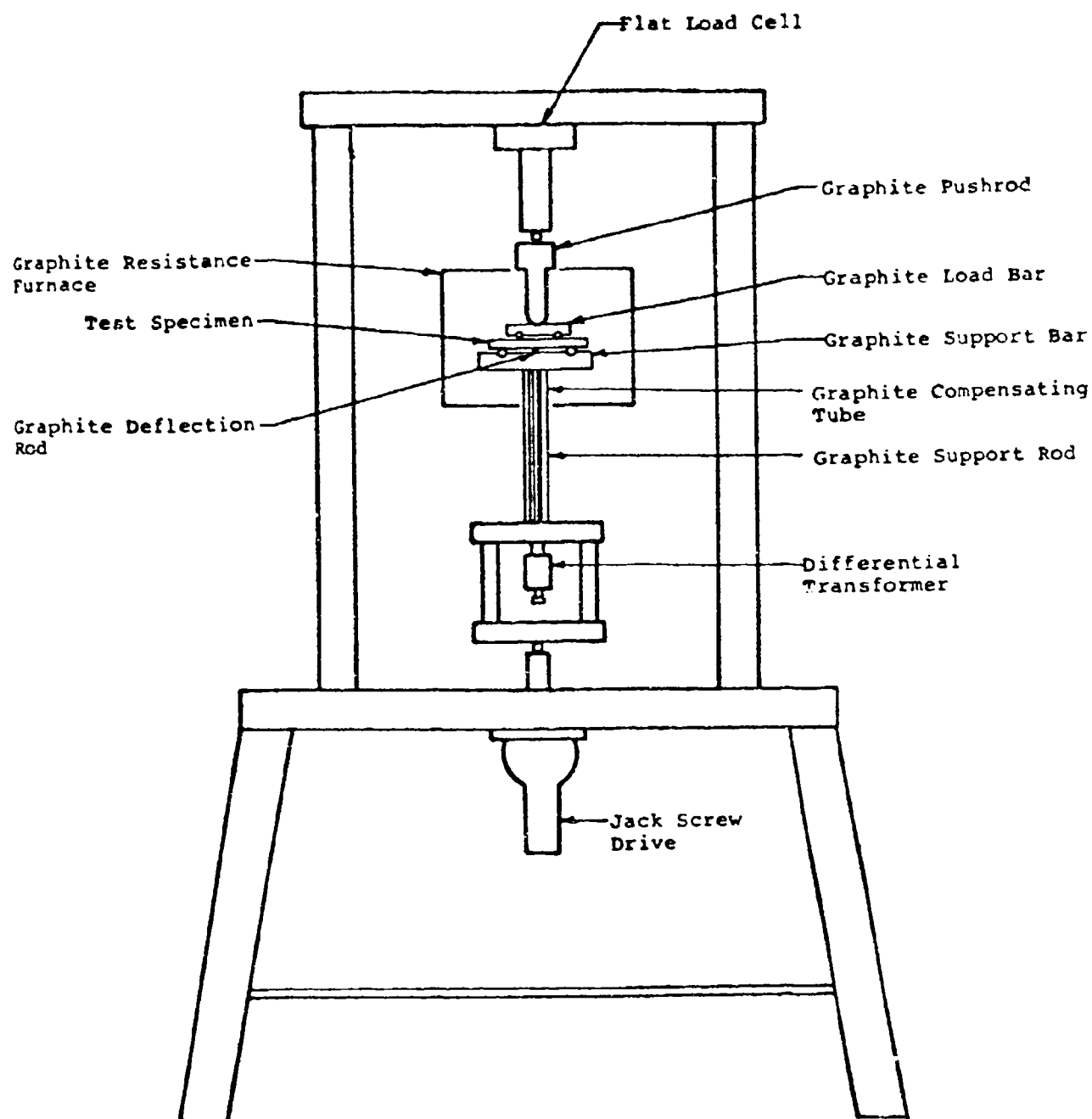
Figure 9.   Schematic of high temperature flexural apparatus

41
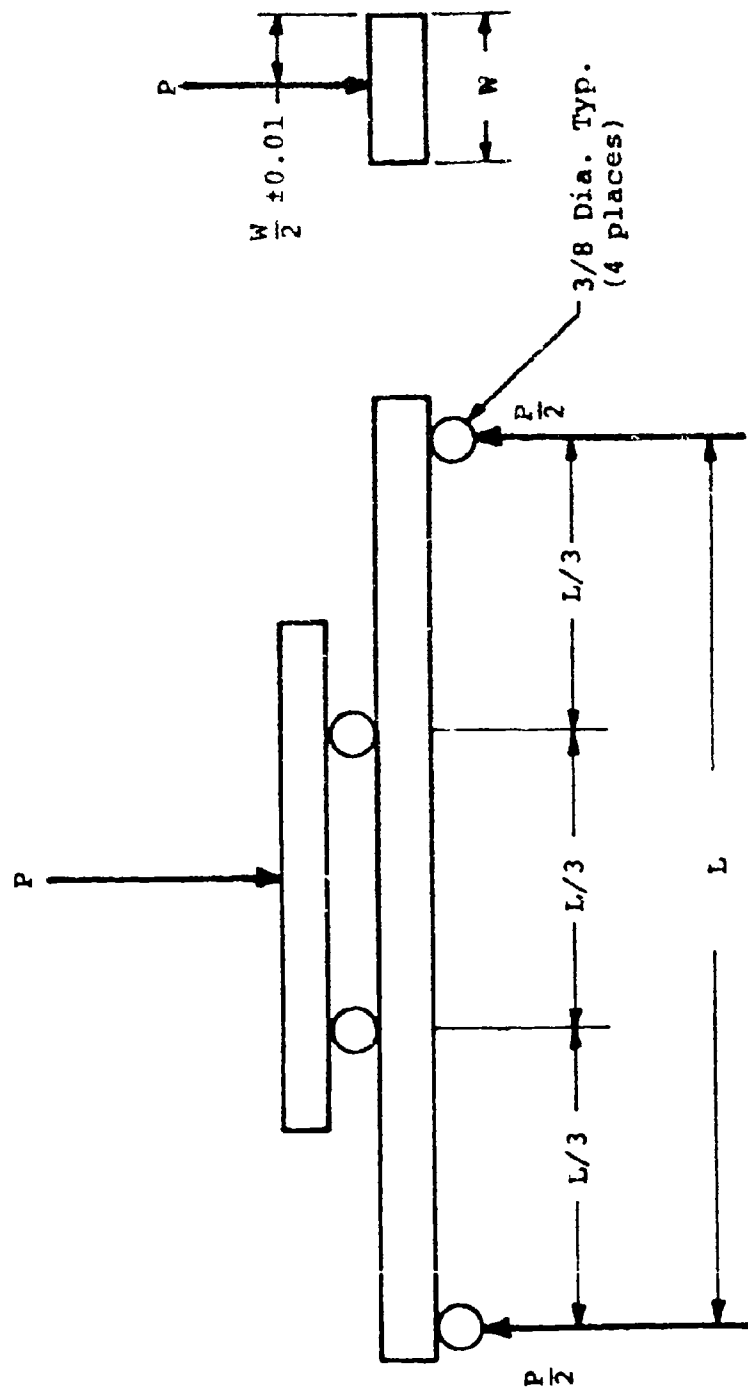
Figure 10. Flexural four-point loading set-up
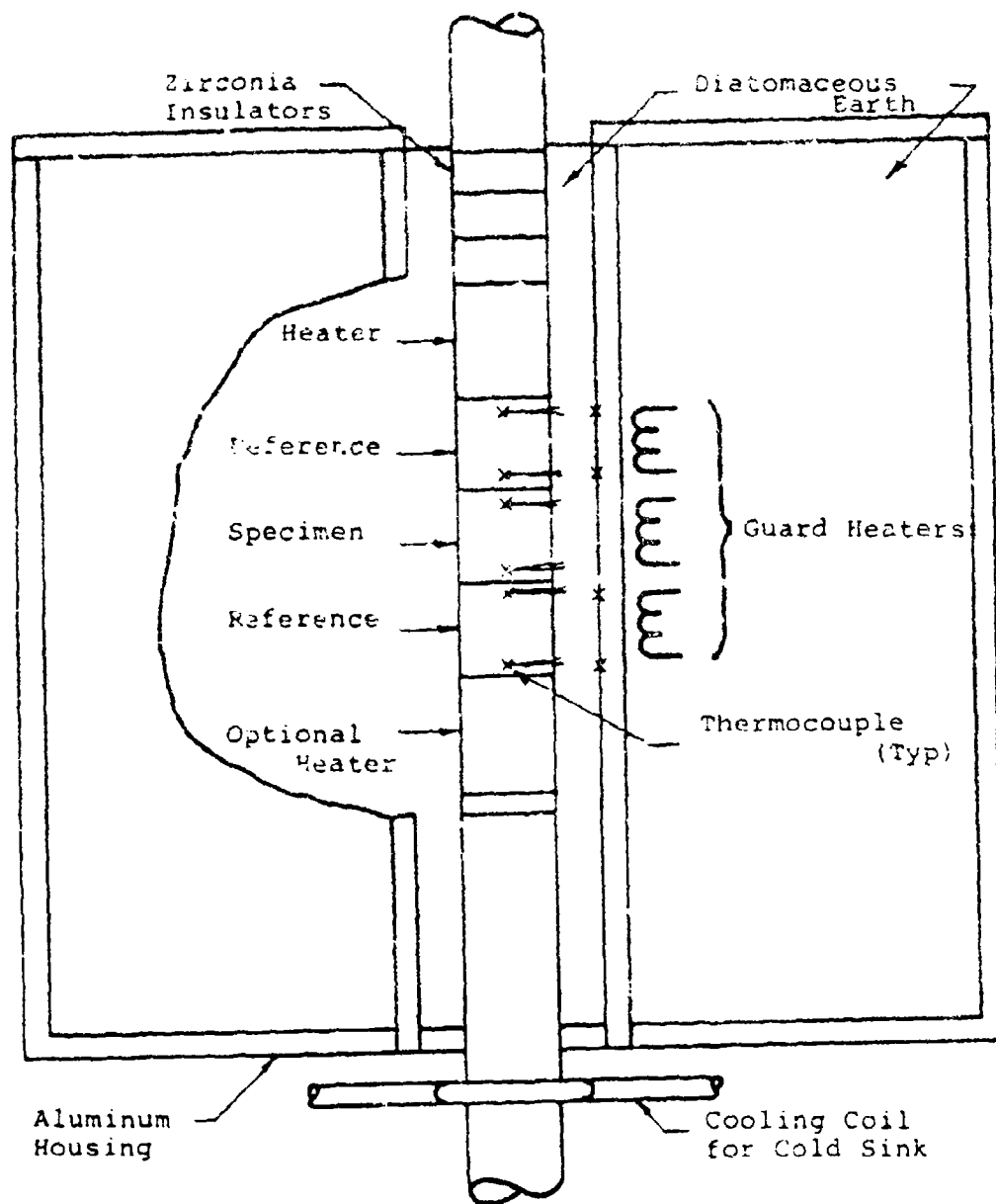
Figure 11. Schematic of Comparative Rod Thermal Conductivity Apparatus
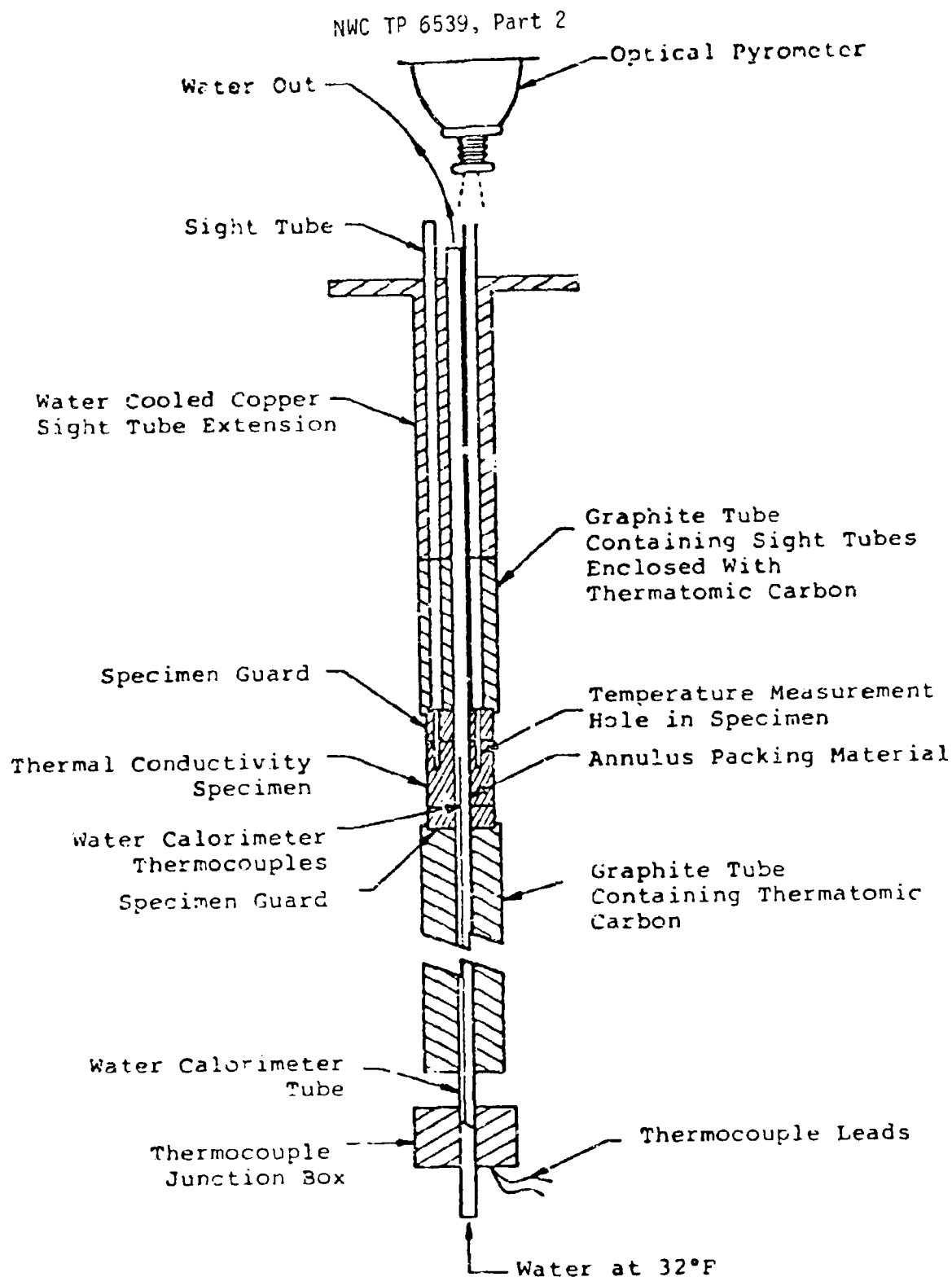
Figure 12. Cross-section schematic of an assembled RIA showing a cylindrical specimen

44
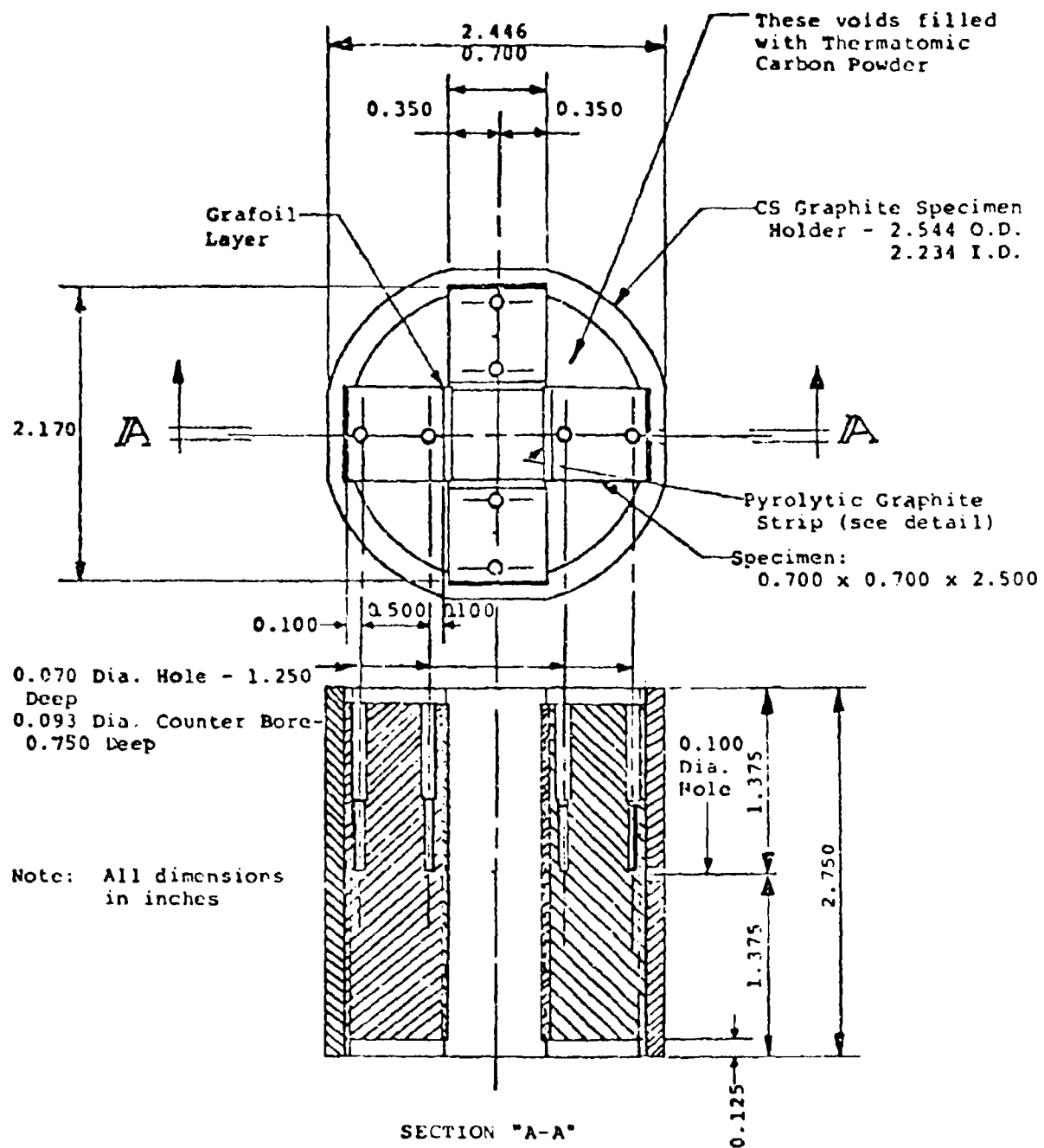
Figure 13. Radial Inflow Apparatus specimen holder and specimen configuration

0.500

0.500

3.000

Three-Inch Spherical Radius Both Ends
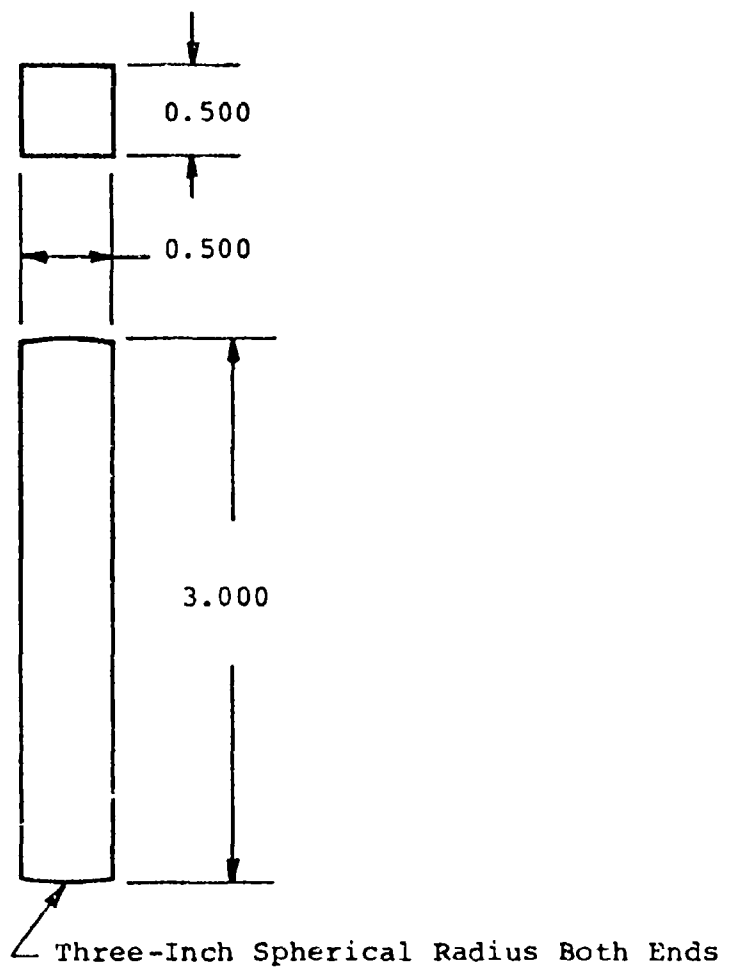
Notes: All dimensions in inches

Figure 14. Thermal Expansion specimen
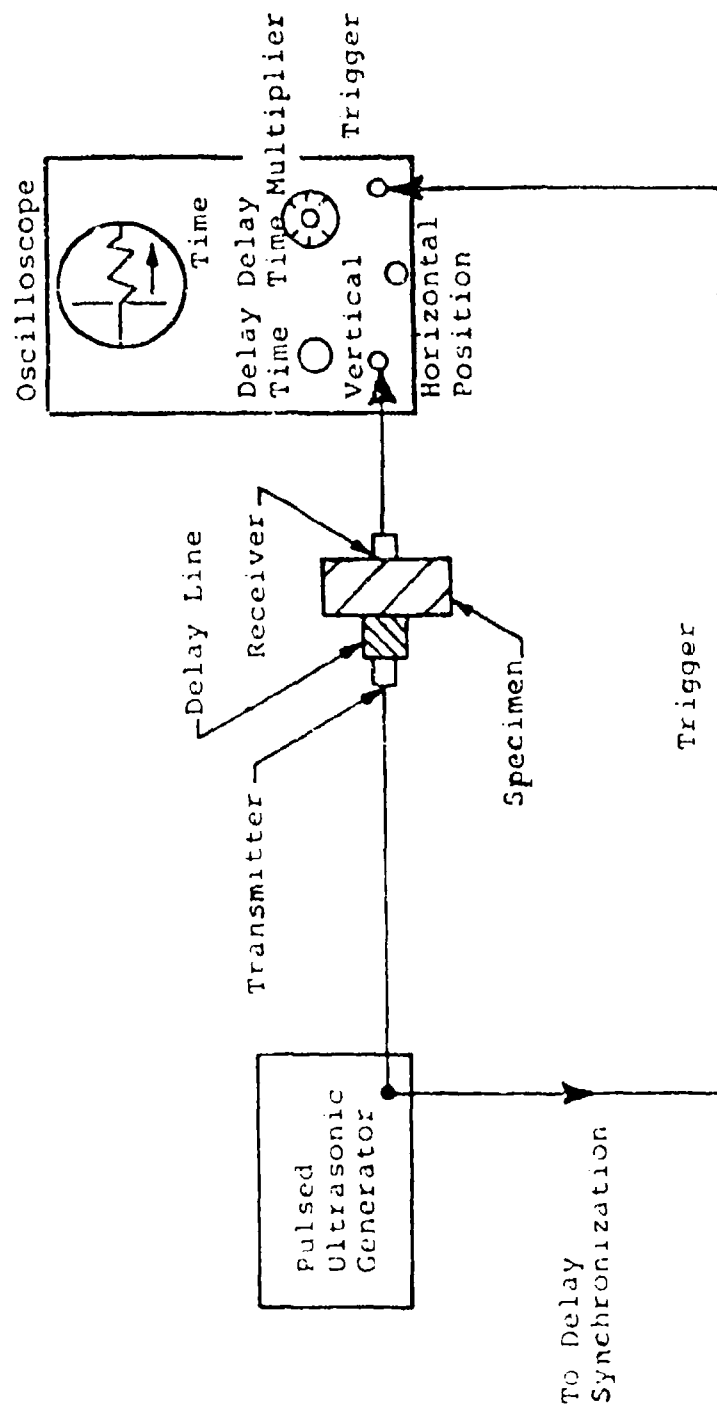
Figure 15. Ultrasonic Velocity-Measuring Apparatus Schematic

Figure 16. Failure surface of sapphire flexure specimen F-10 (60°) showing
typical conchoidal nature of failure

Figure 17. Fracture face of 0° oriented flexure specimen
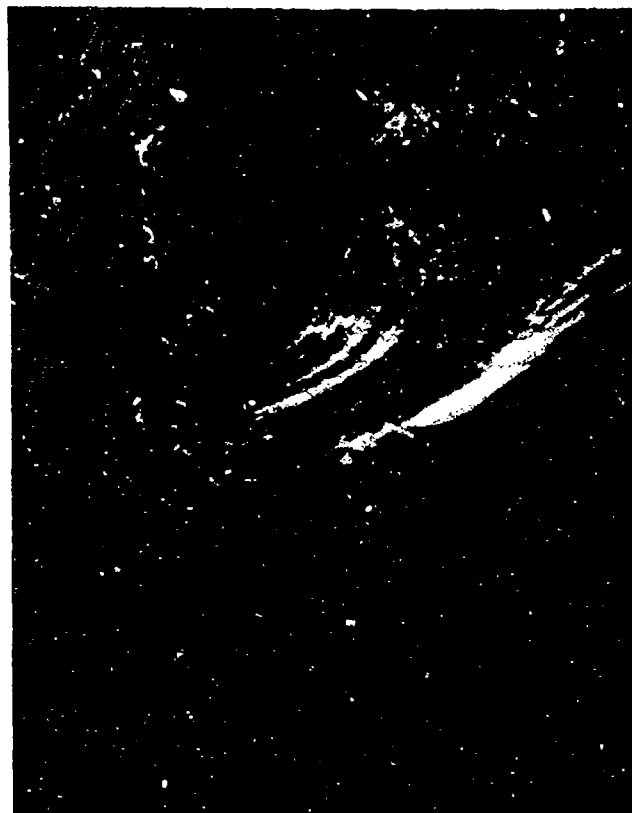
Figure 18. Apparent fracture initiation site for specimen F-18
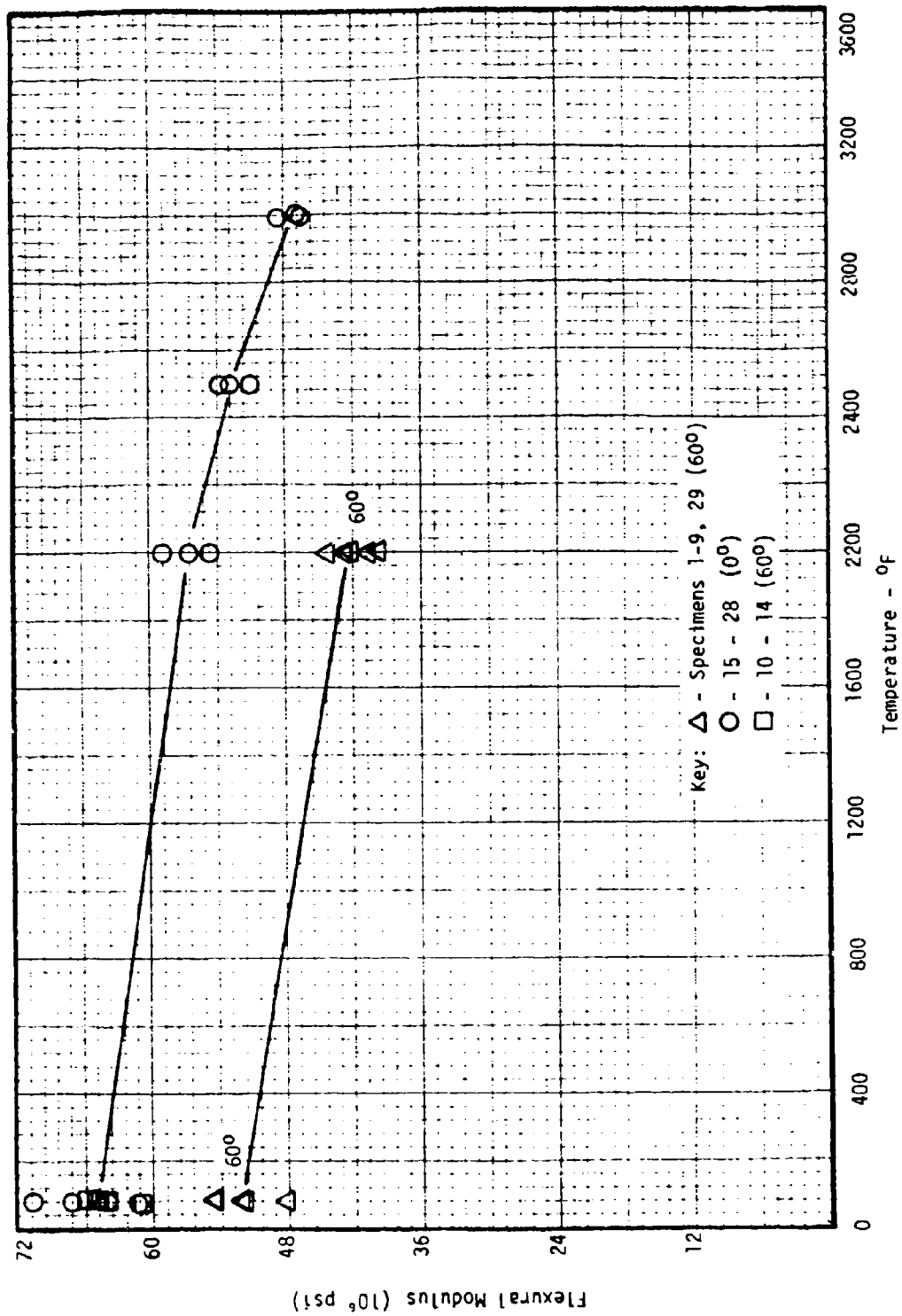
Figure 19. Flexural Modulus vs. Temperature for Sapphire
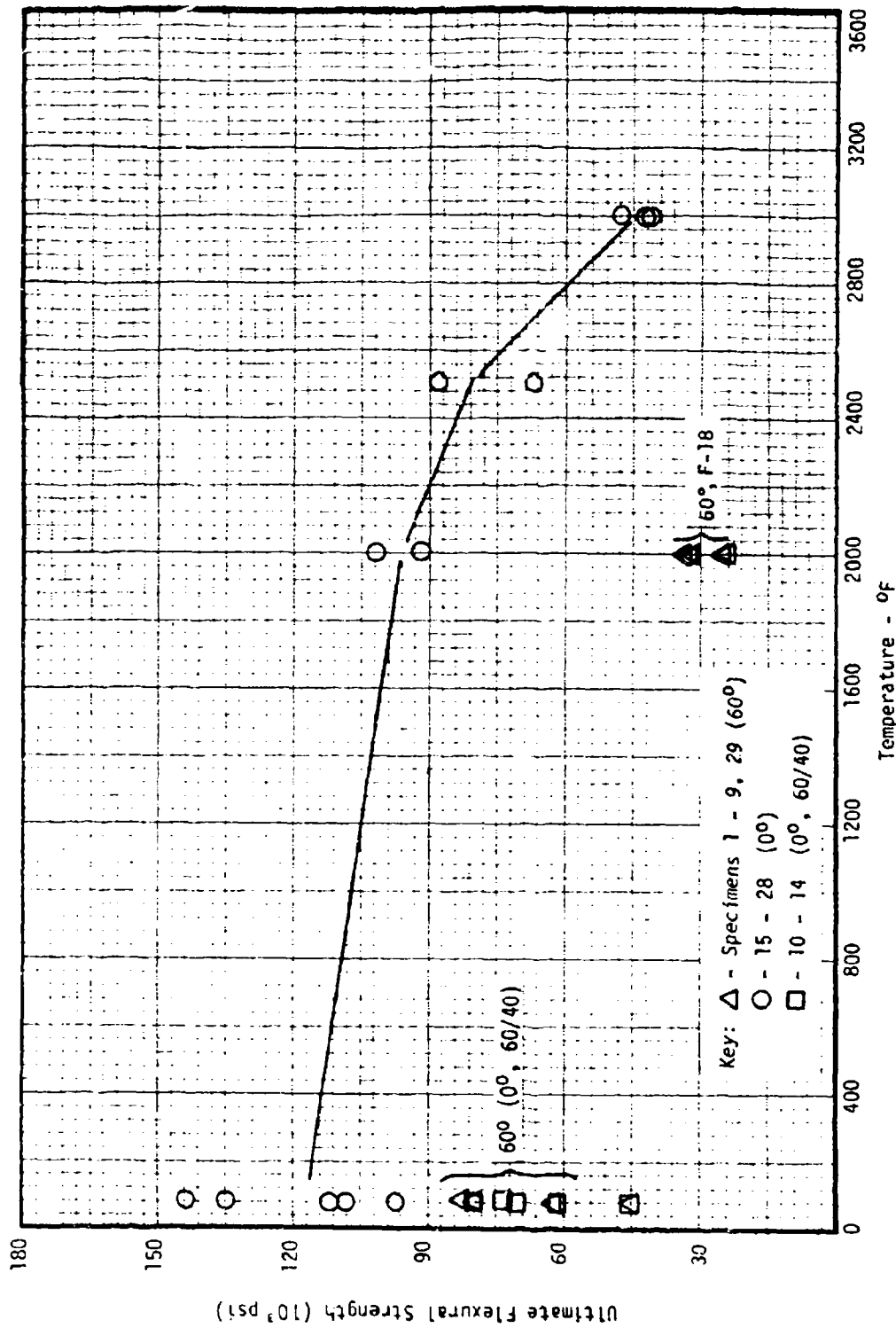
Figure 20. Ultimate Flexural Strength vs. Temperature for Sapphire

Figure 21. Voids in Spinel flexural specimen F-16
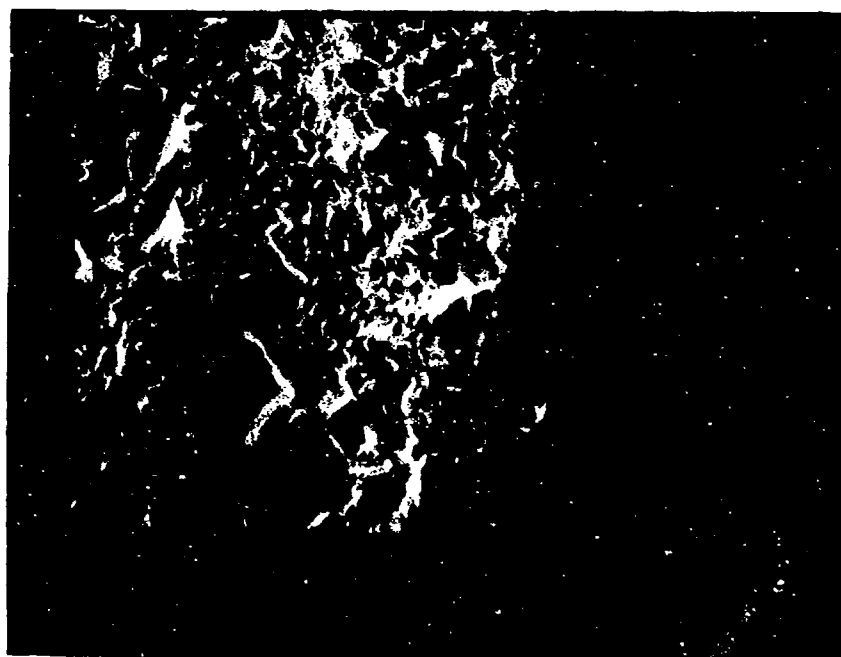
Figure 22. Fracture surface of Spinel flexure specimen F-3
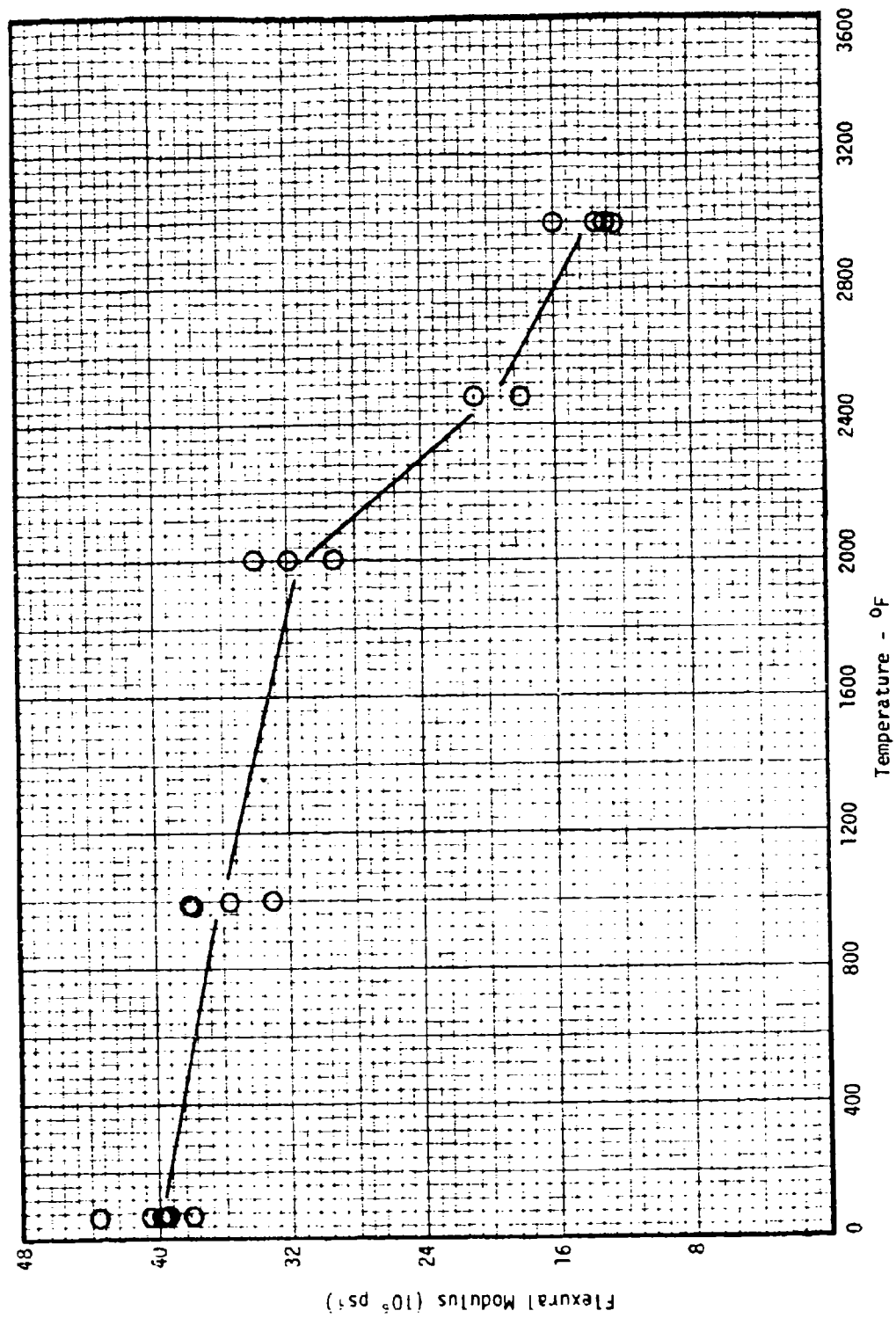
Figure 23. Flexural modulus versus temperature for Spinel
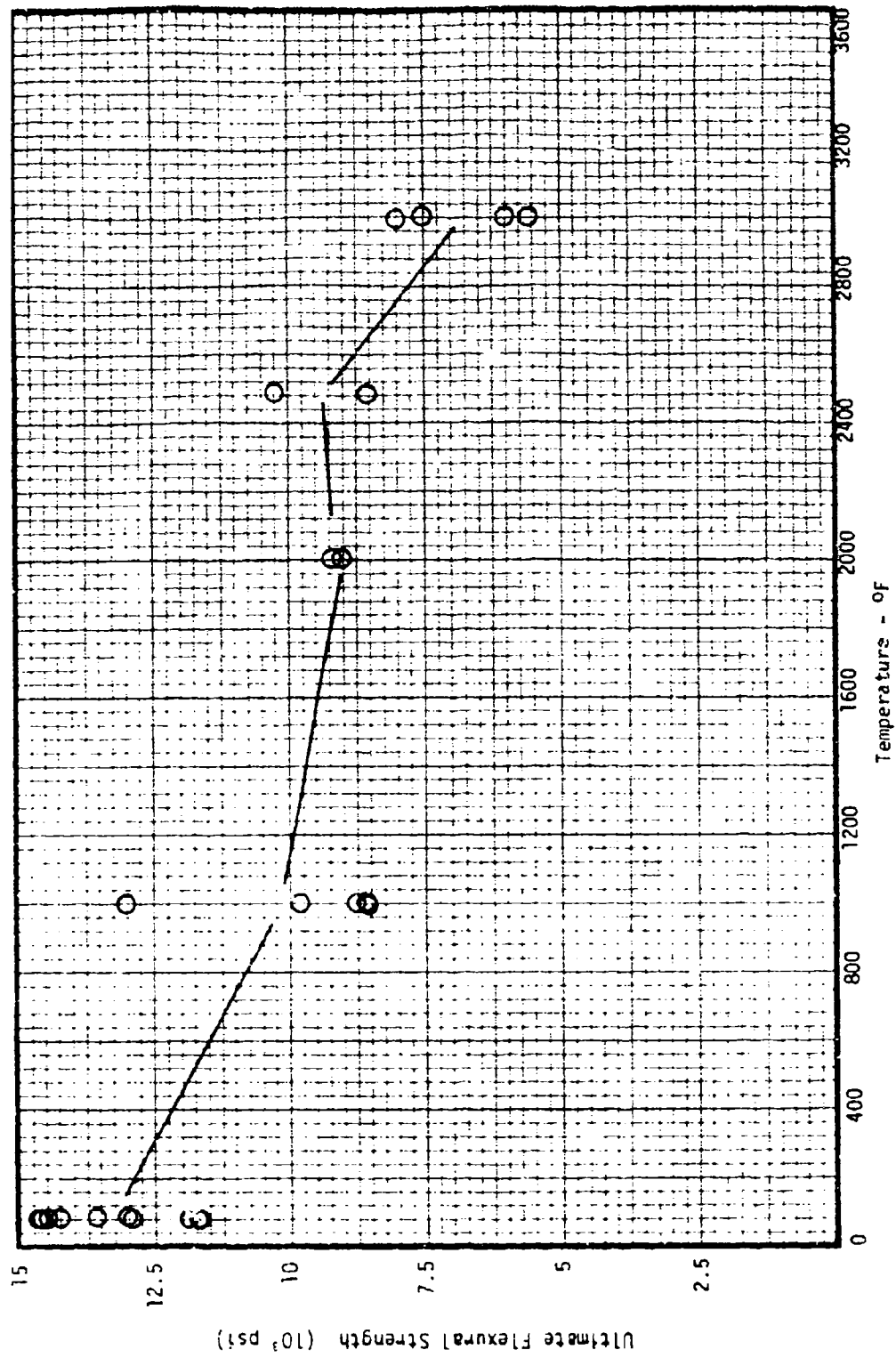
Figure 24. Ultimate flexural strength versus temperature for Spinel
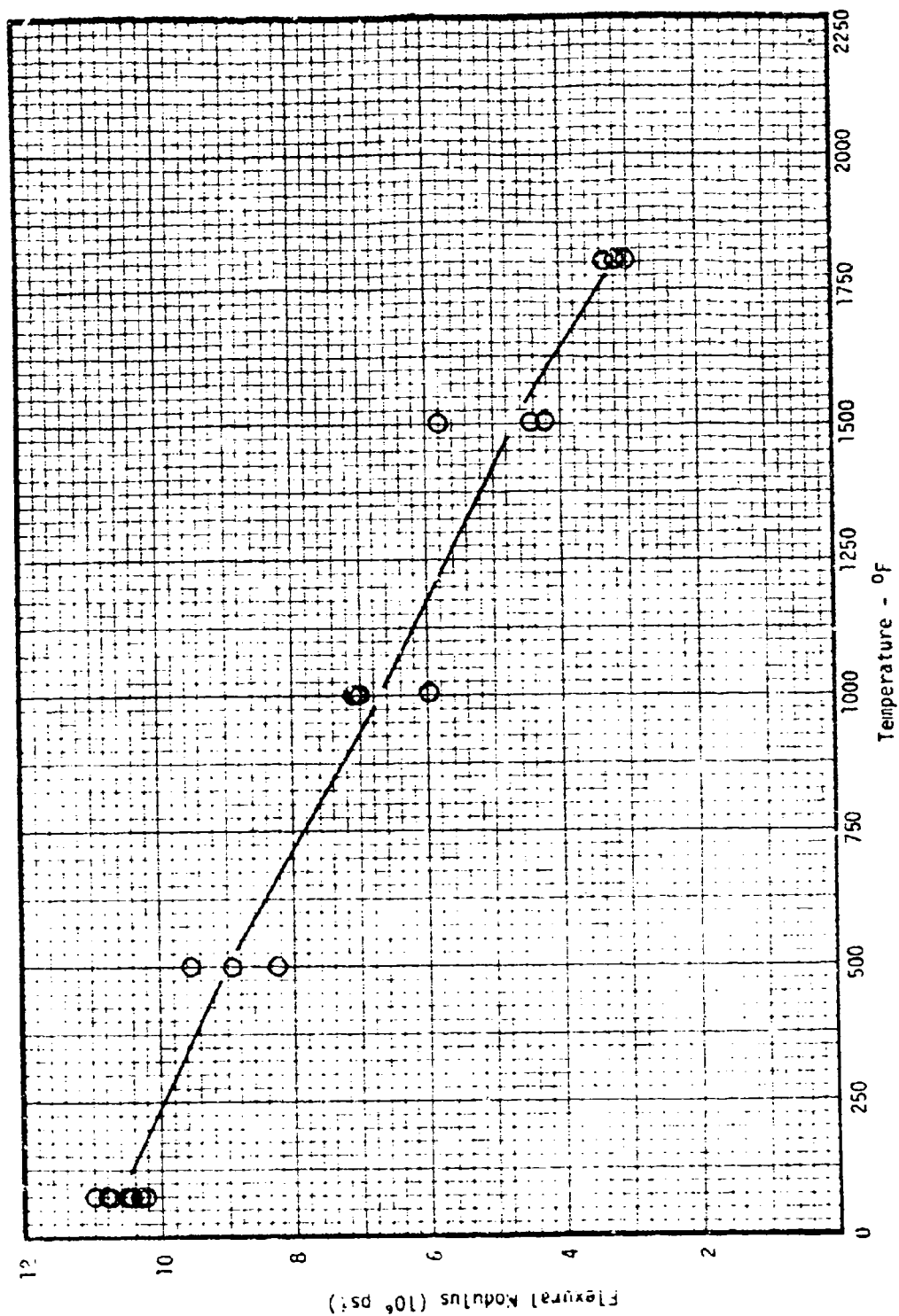
Figure 25. Flexural modulus versus temperature for ZnS.

57
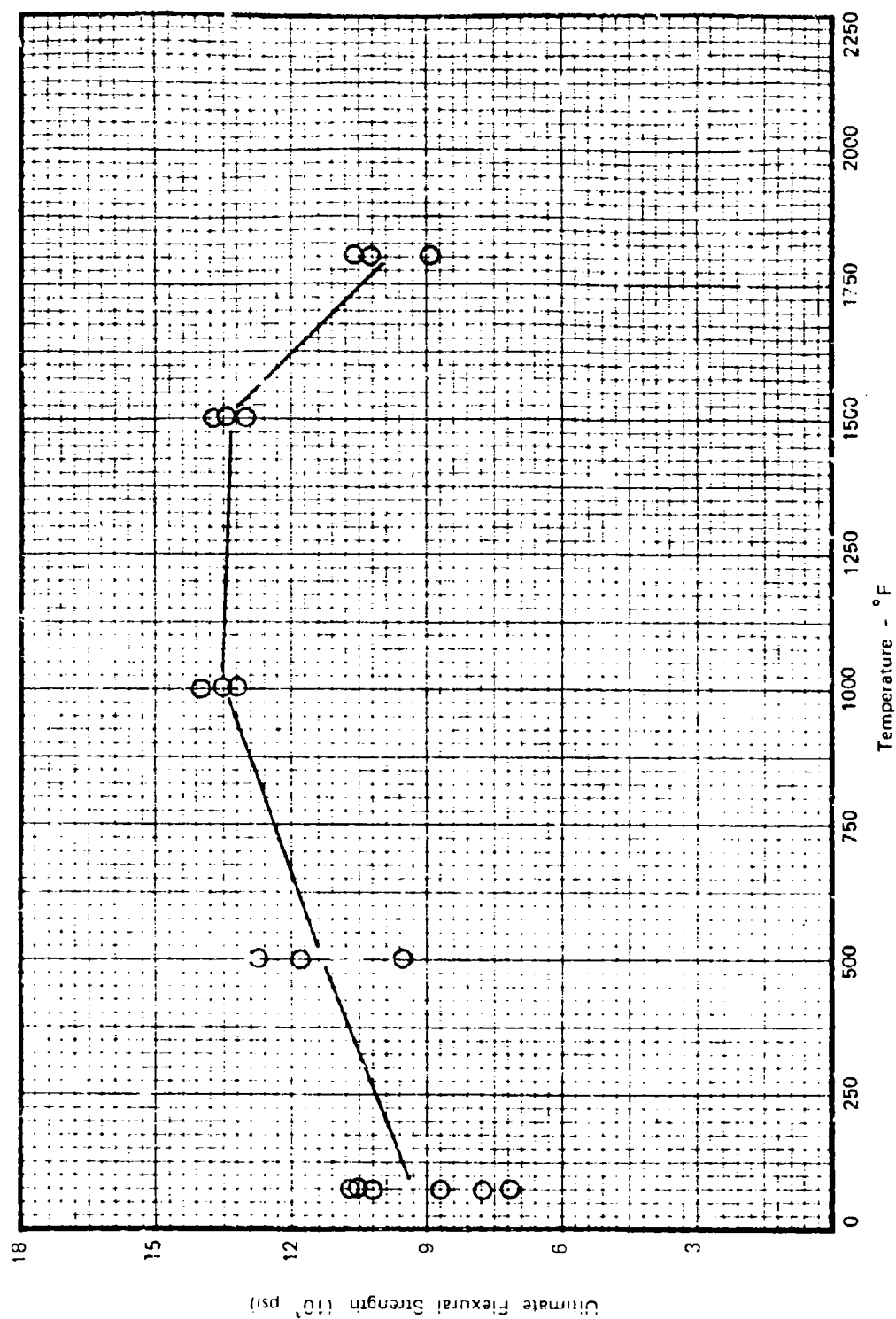
Figure 26. Ultimate flexural strength versus temperature for ZnS

58
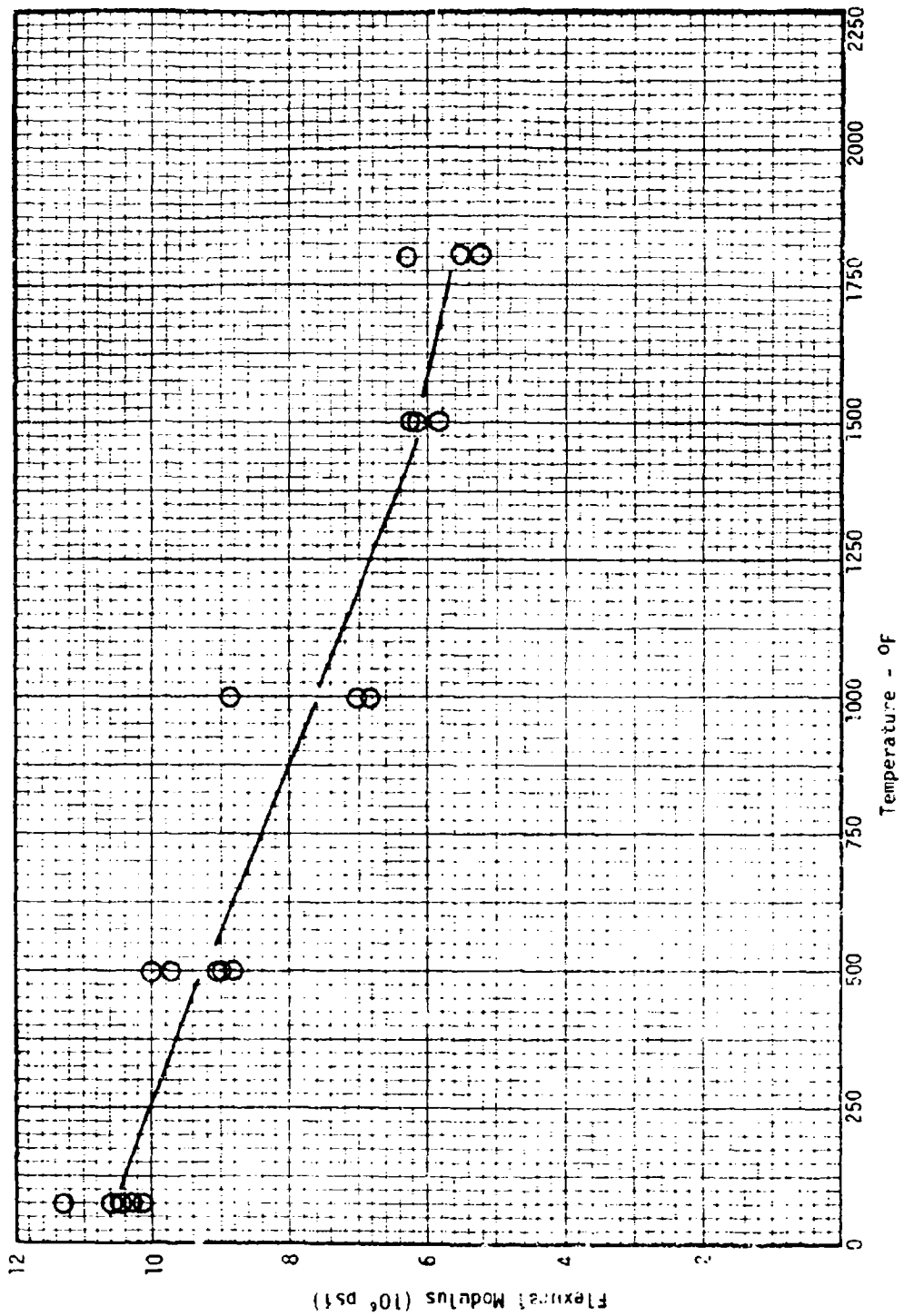
Figure 27. Flexural modulus versus temperature for ZnSe
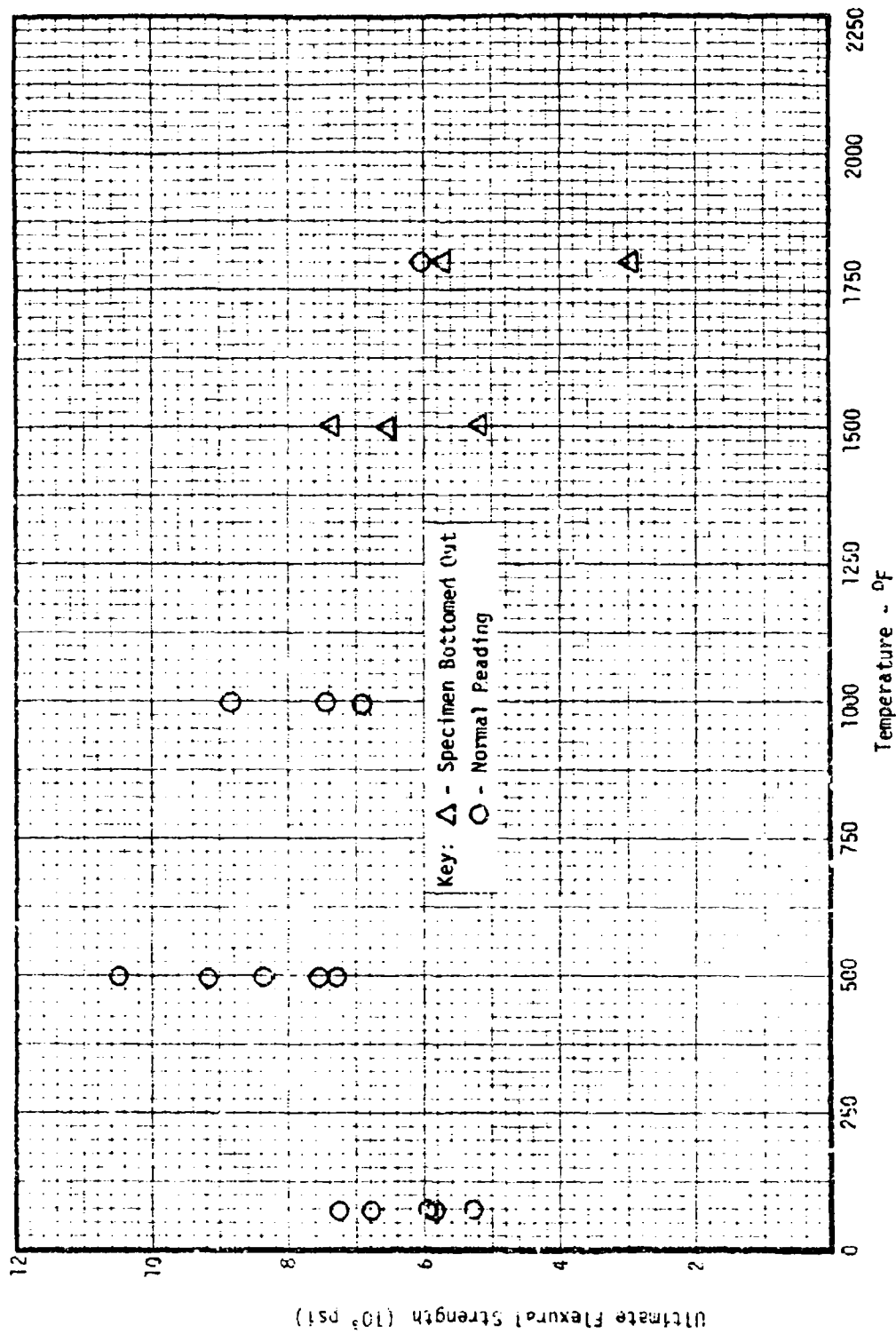
Figure 28. Ultimate flexural strength versus temperature for ZnSe

Figure 29.   Failure surface (head failure) of Sapphire tensile specimen T-1

Figure 30.   Fracture surface of Sapphire tensile specimen T-2

Figure 31. Failure initiation site for specimen shown in Figure 30.
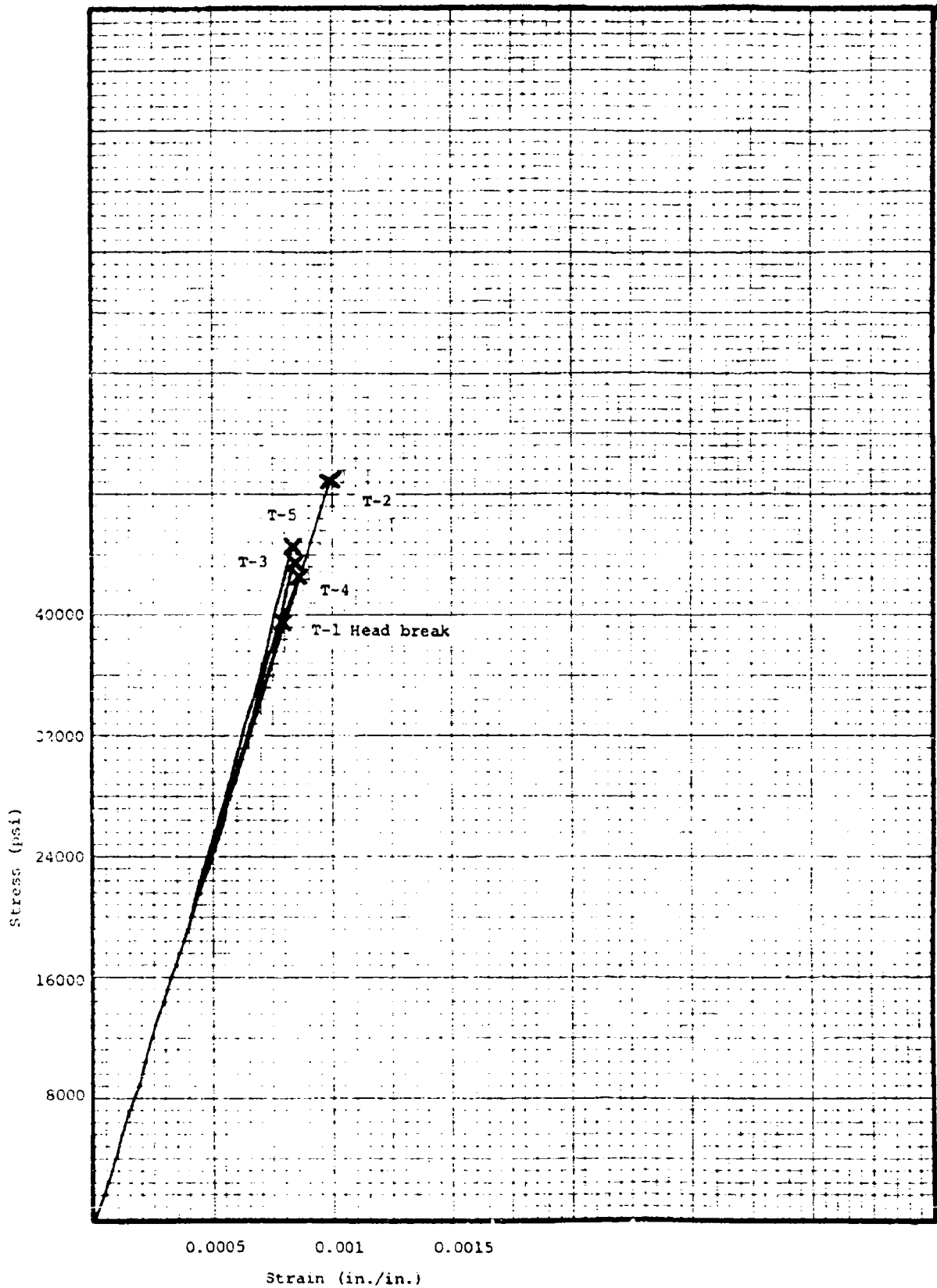
Figure 32. Tensile Stress-Strain Curves for Sapphire using Clip-on Extensometers

64
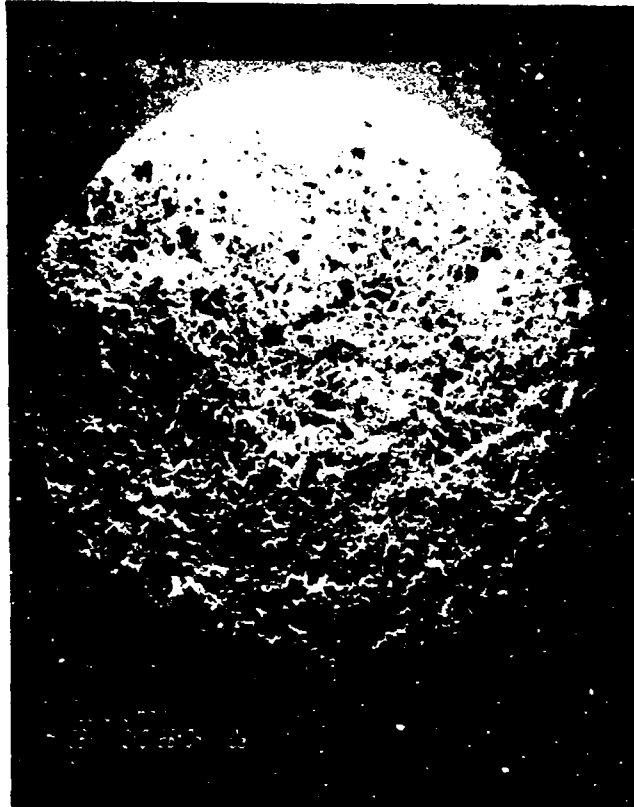
Figure 33. Failure surface of Spinel tensile specimen T-2

Figure 34. Failure surface of Spinel tensile specimen T-3
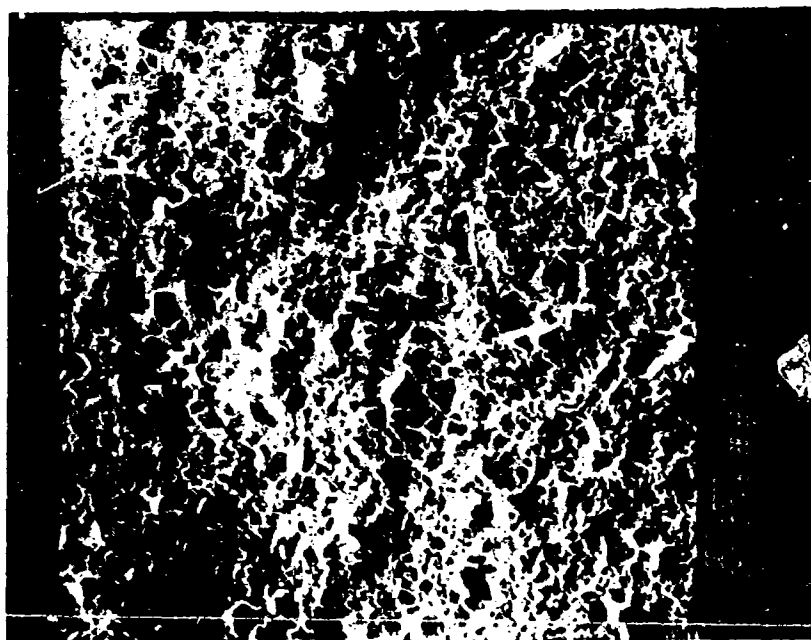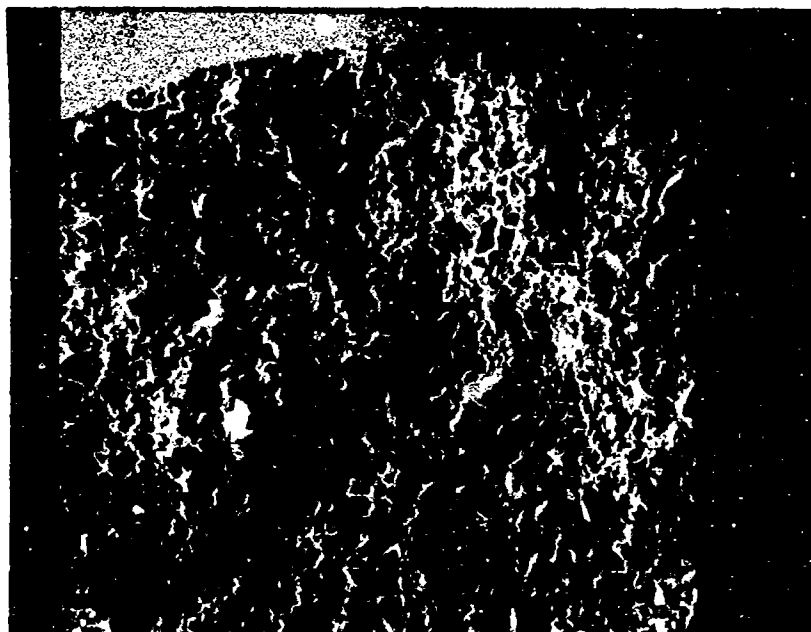
Figure 35. Higher magnification views of two zones of the Spinel tensile specimen T-3 failure surface
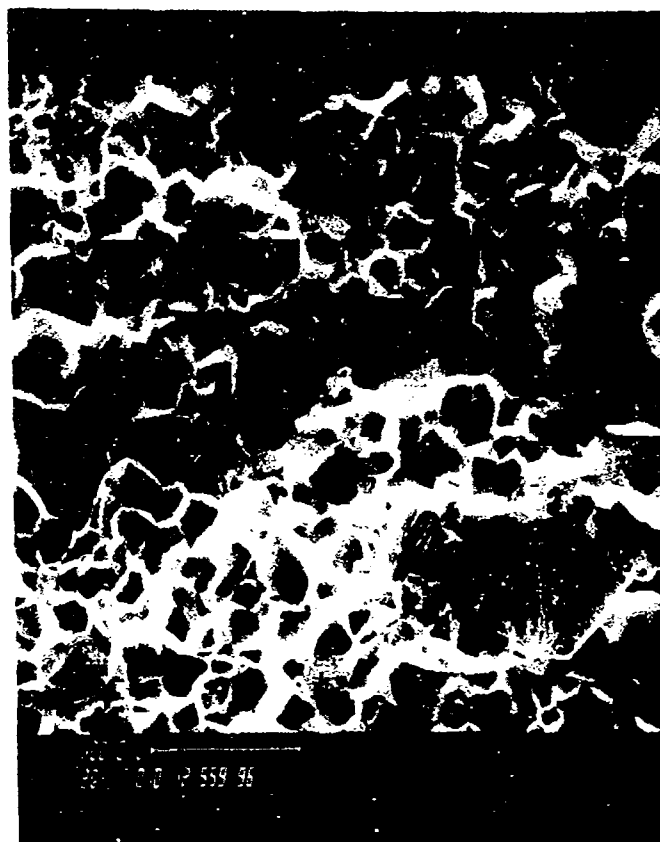
Figure 36. 200x view of fracture surface on Spinel tensile specimen T-3
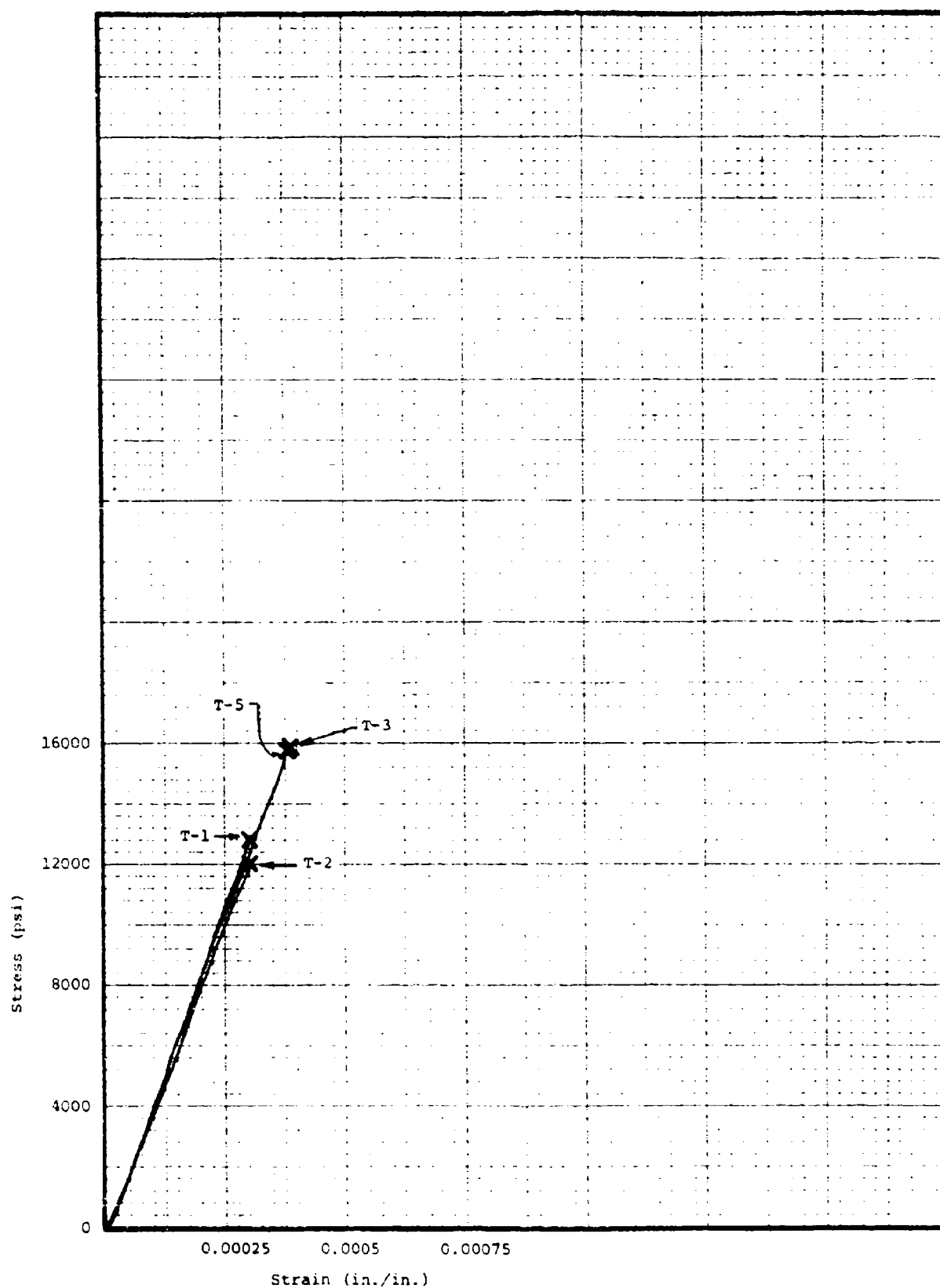
Figure 37.   Tensile Stress-Strain Curves for Spinel Specimens

69
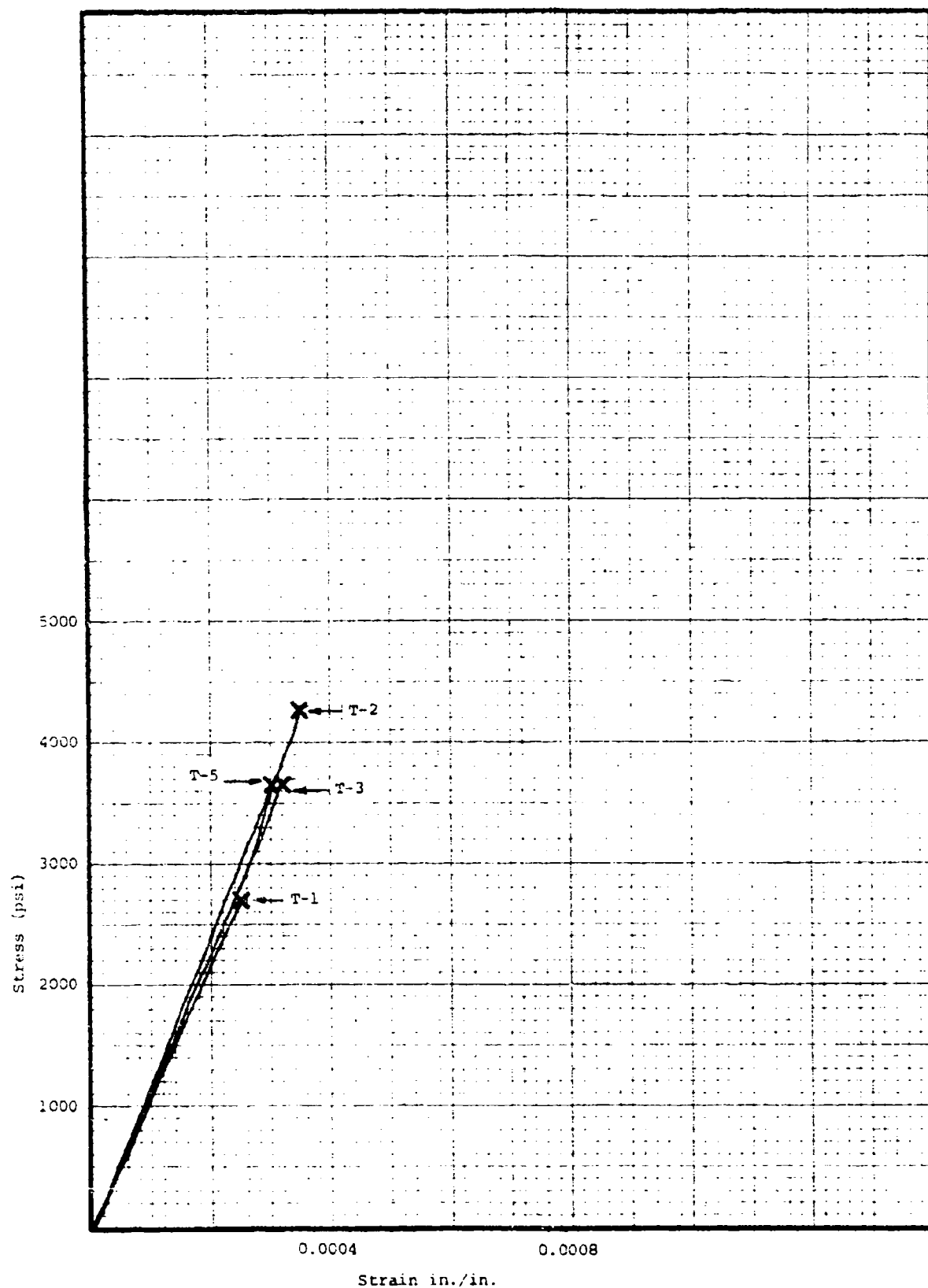
Figure 38.   Tensile Stress-Strain Response of Zinc Sulfide

70
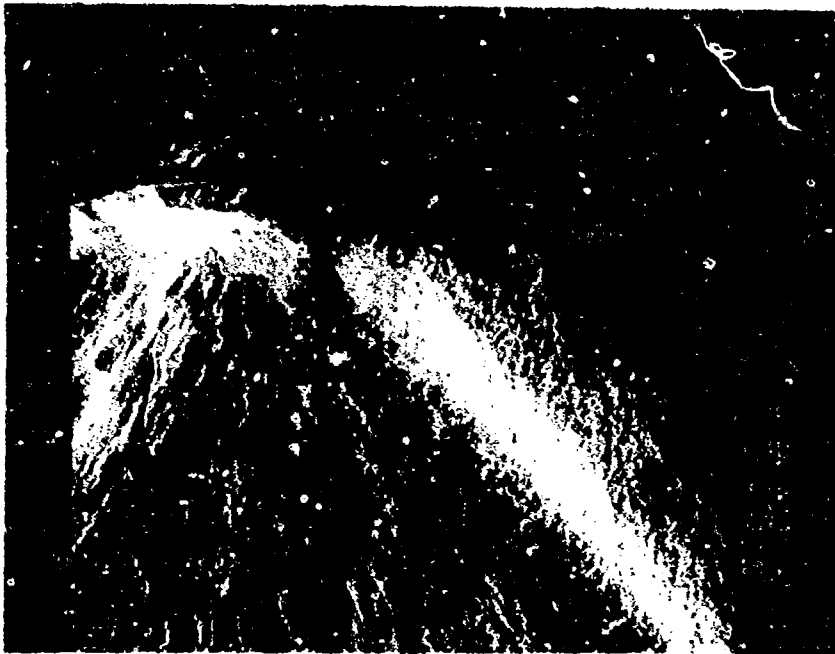
Figure 39. Fracture surface and failure initiation site for ZnS specimen T-1
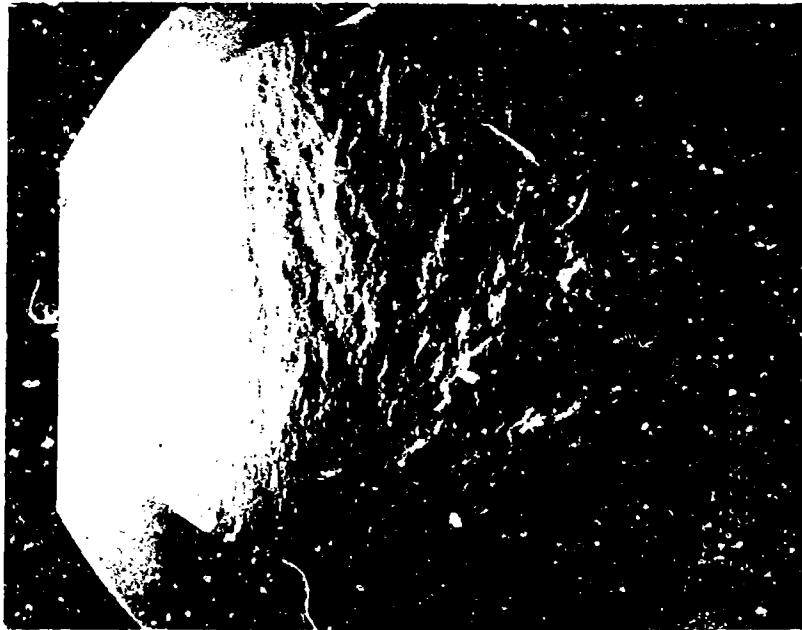
Figure 40. Fracture surface and failure initiation site for ZnS specimen T-2
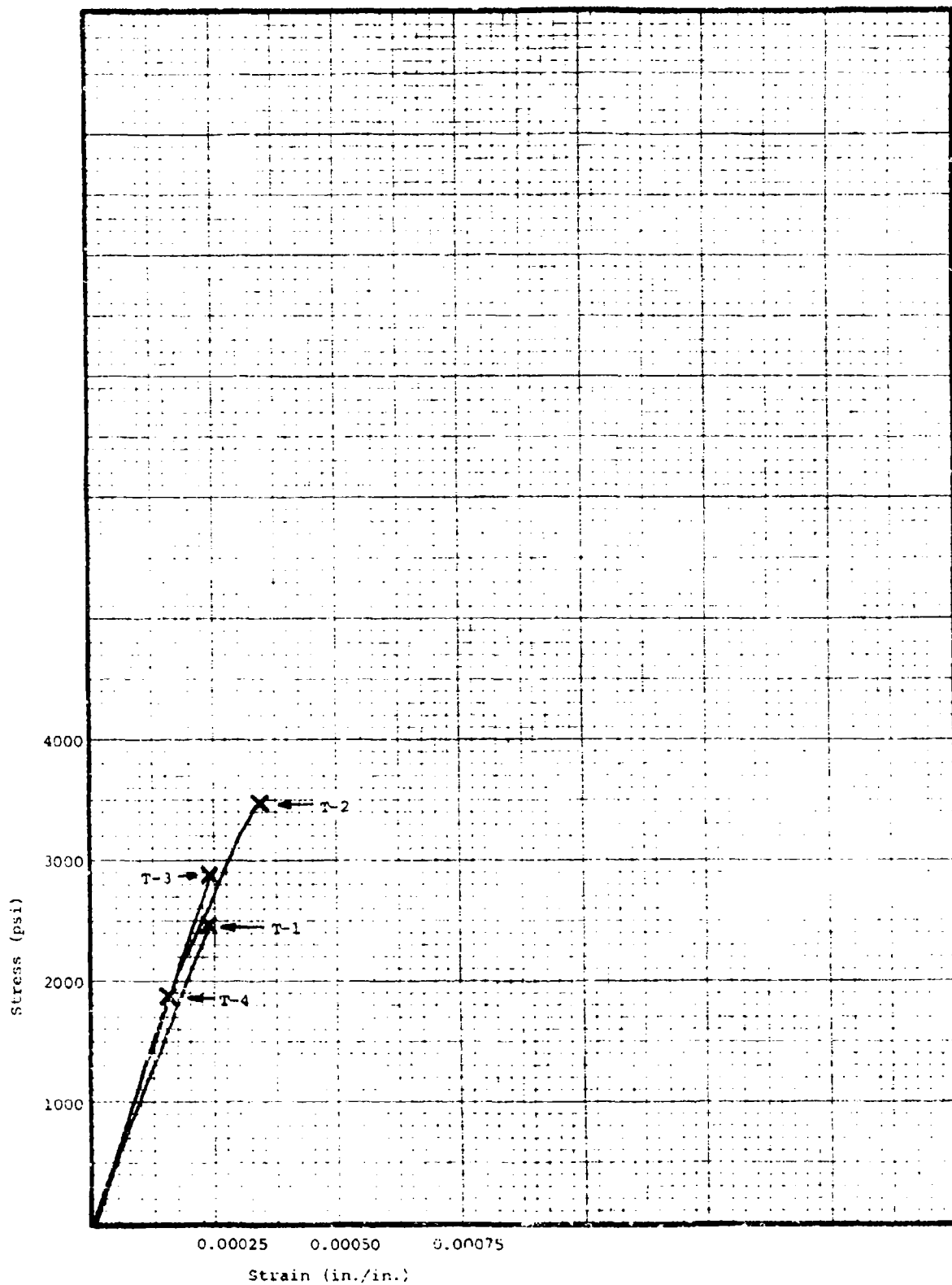
Figure 41. Tensile Stress-Strain Response for Zinc Selenide
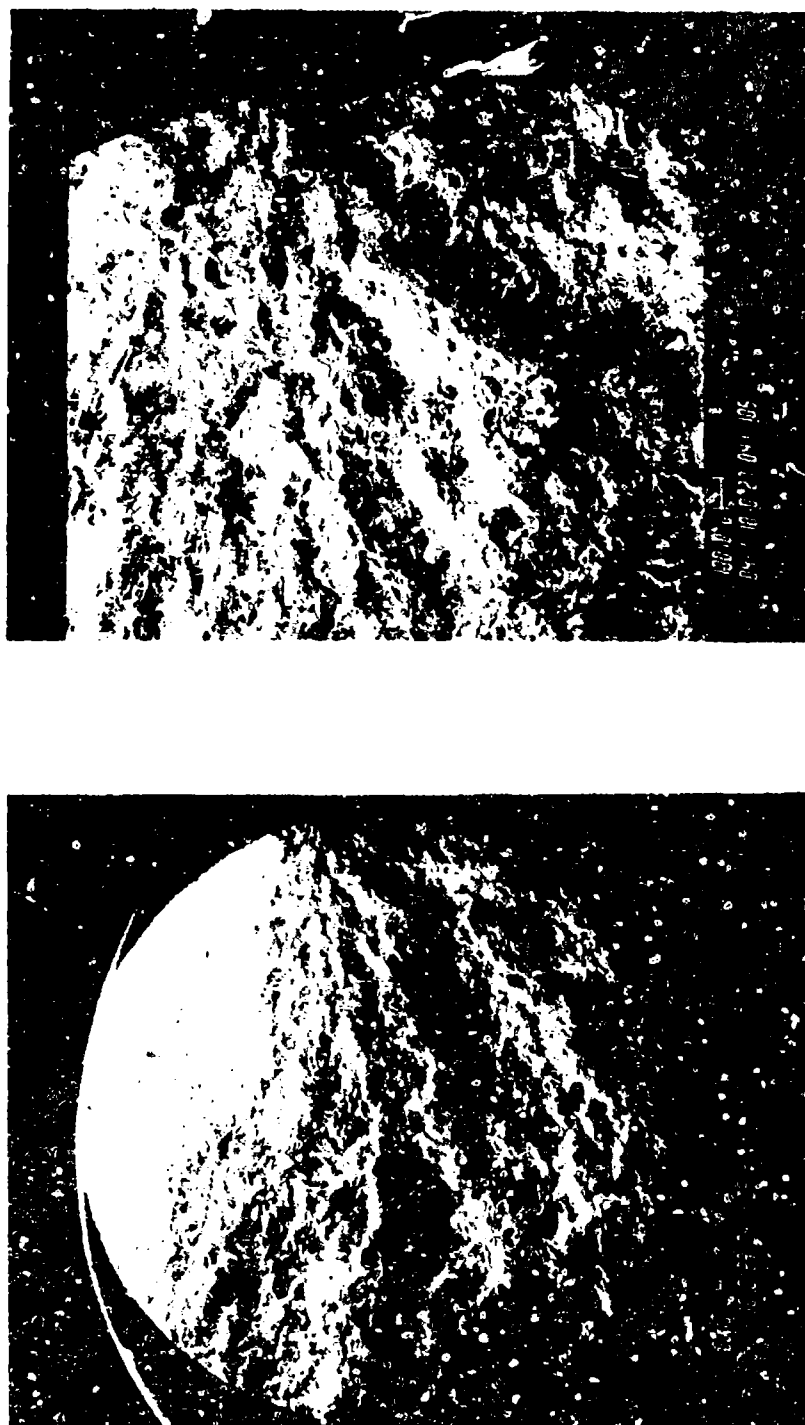
Figure 42. Fracture surface and initiation site for Zinc Selenide tensile specimen T-2

Figure 43. 10 and 50X SEM micrographs of Zinc Selenide tensile fracture surface (Specimen T-4)
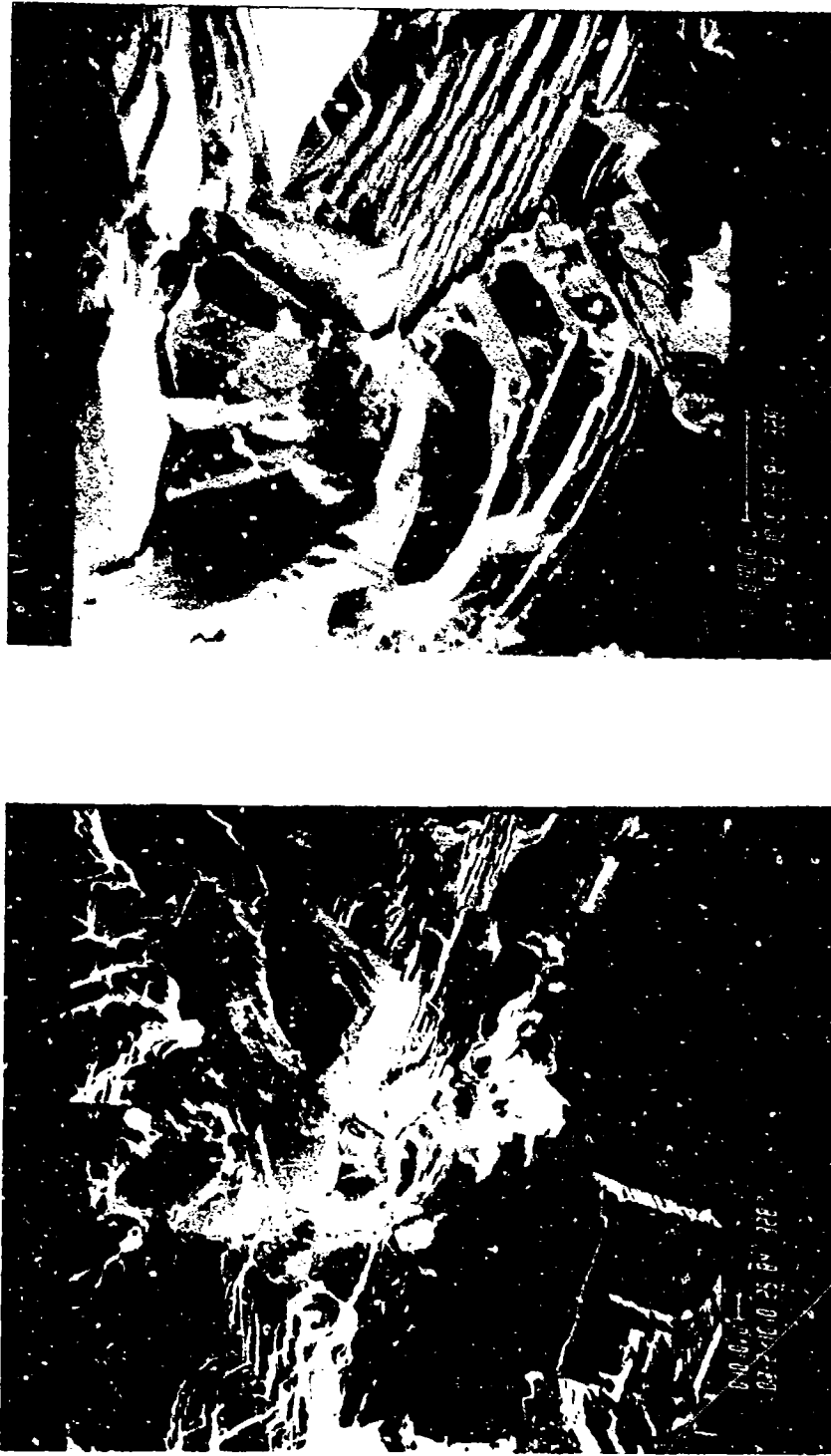
Figure 44. 300 and 1500X SEM micrographs of Zinc Selenide tensile fracture surface (Specimen T-4)
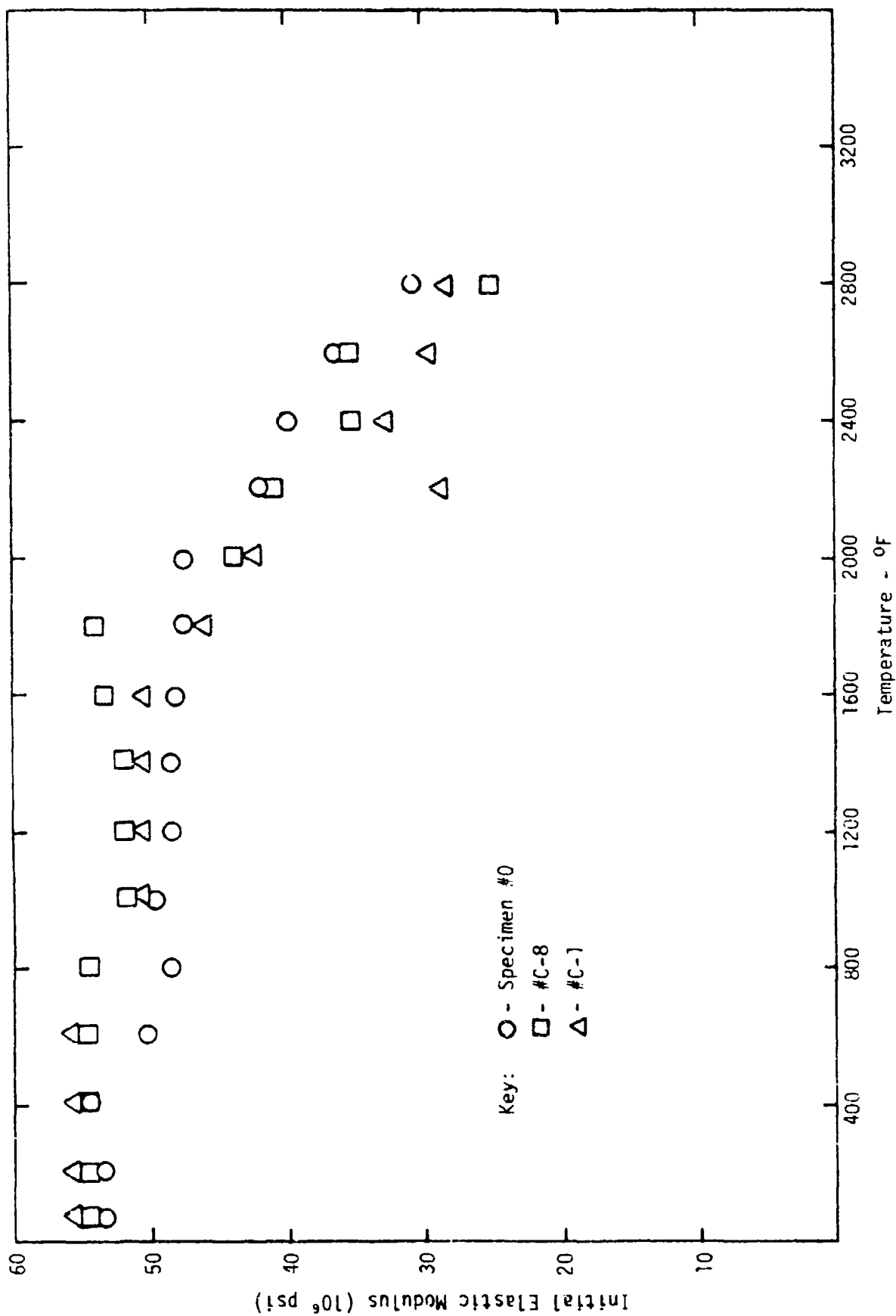
Figure 45. Compressive moduli of Sapphire
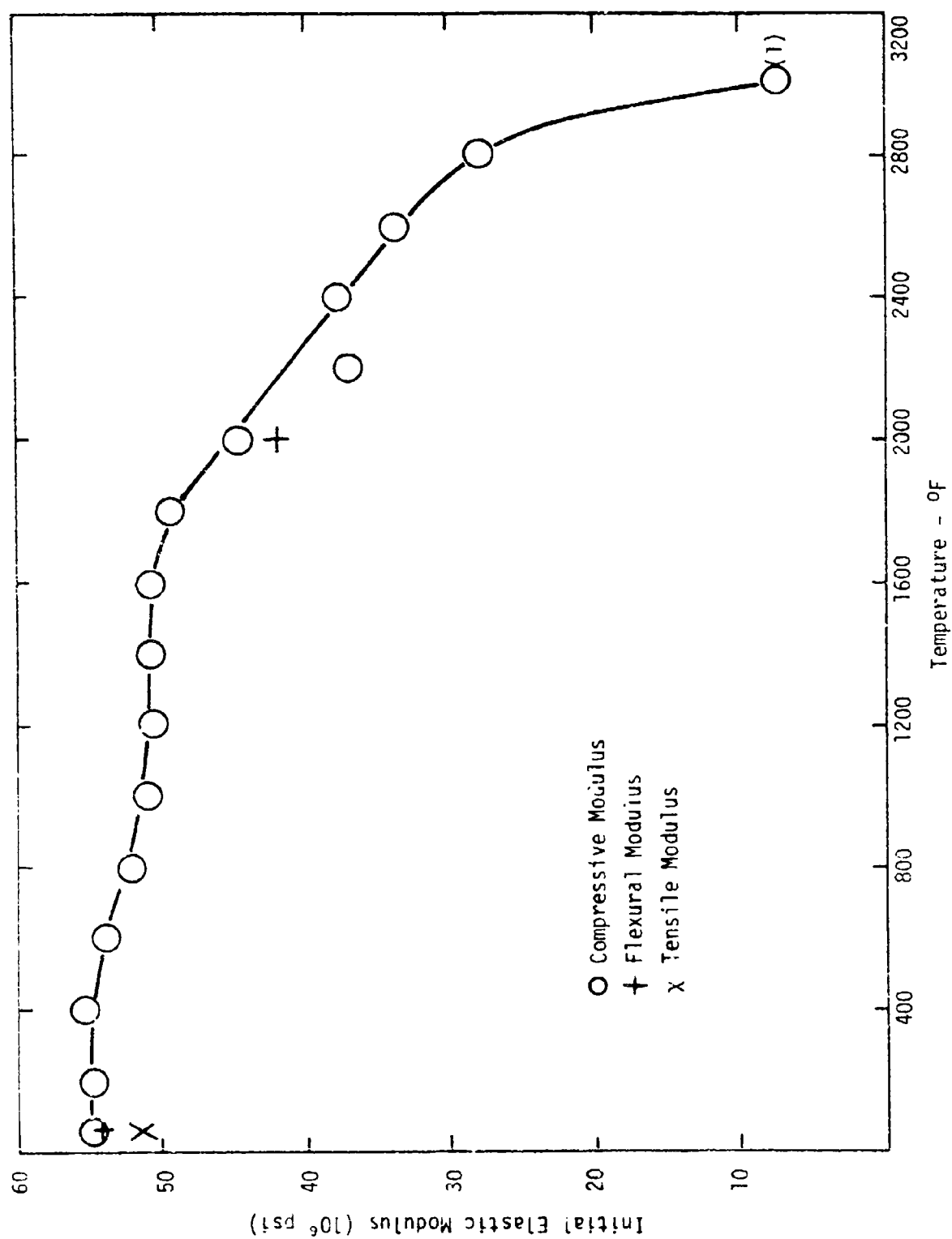
Figure 46. Average compressive modulus of Sapphire

78
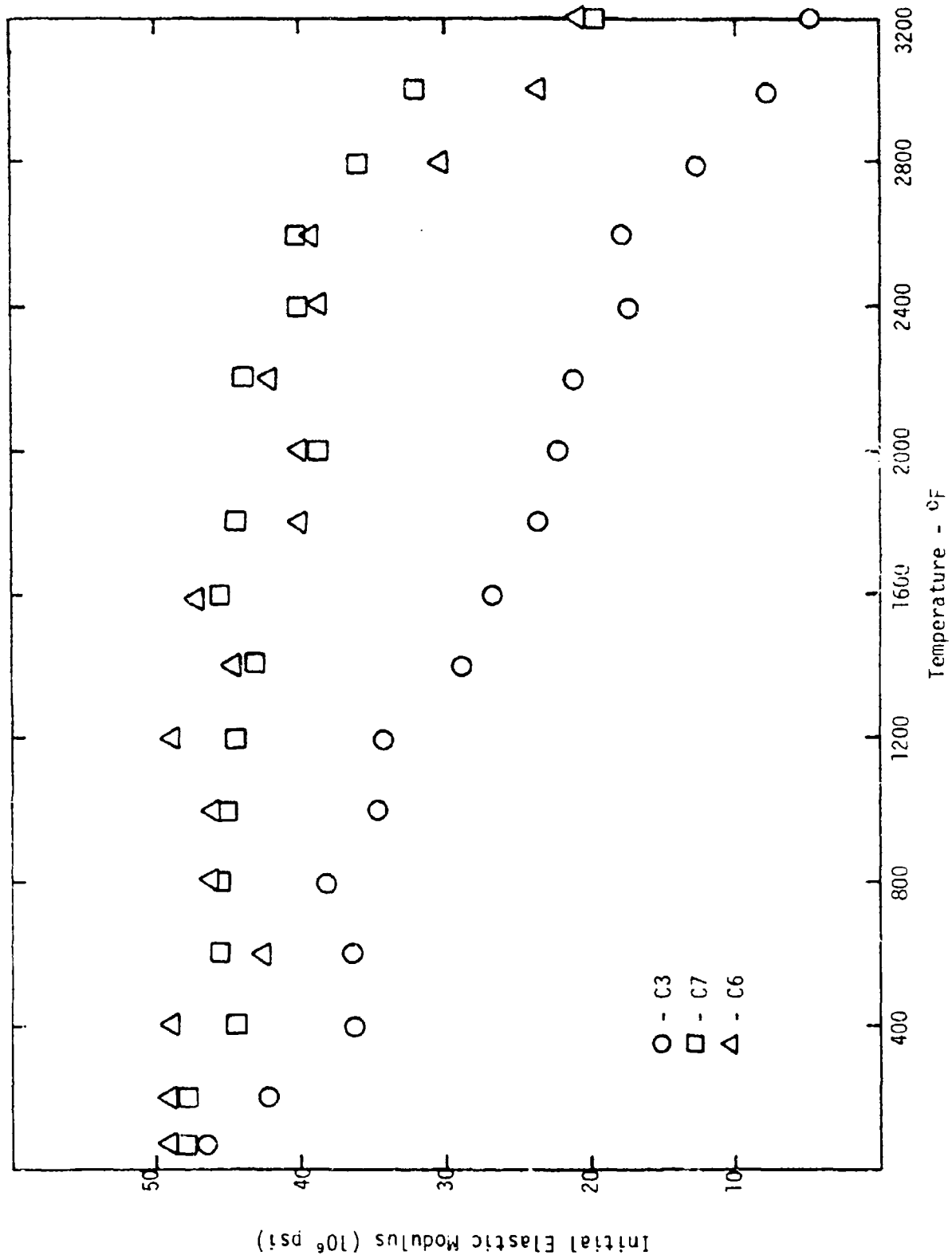
Figure 47. Compressive moduli of Spinel
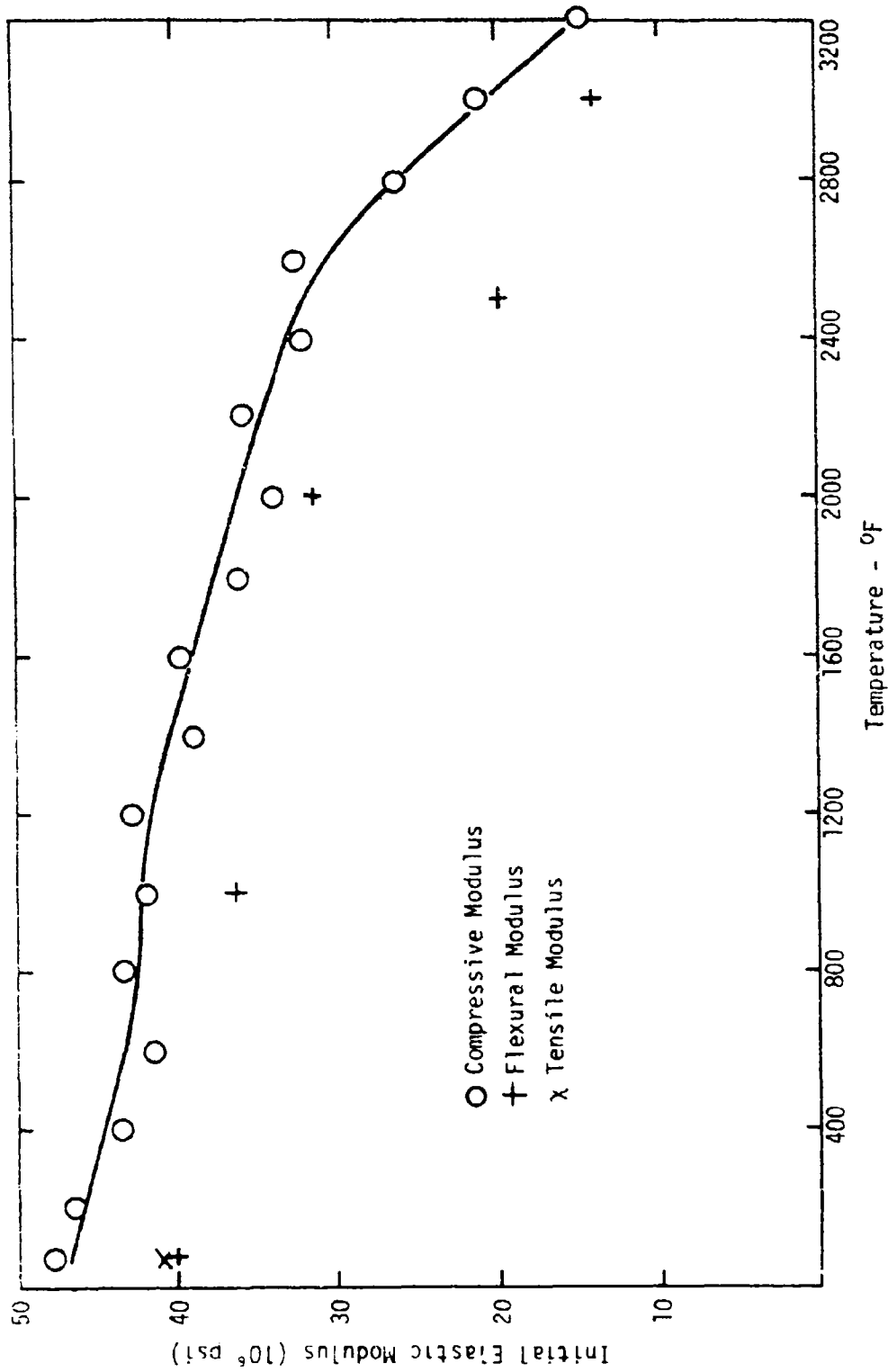
Figure 48. Average compressive moduli of Spinel
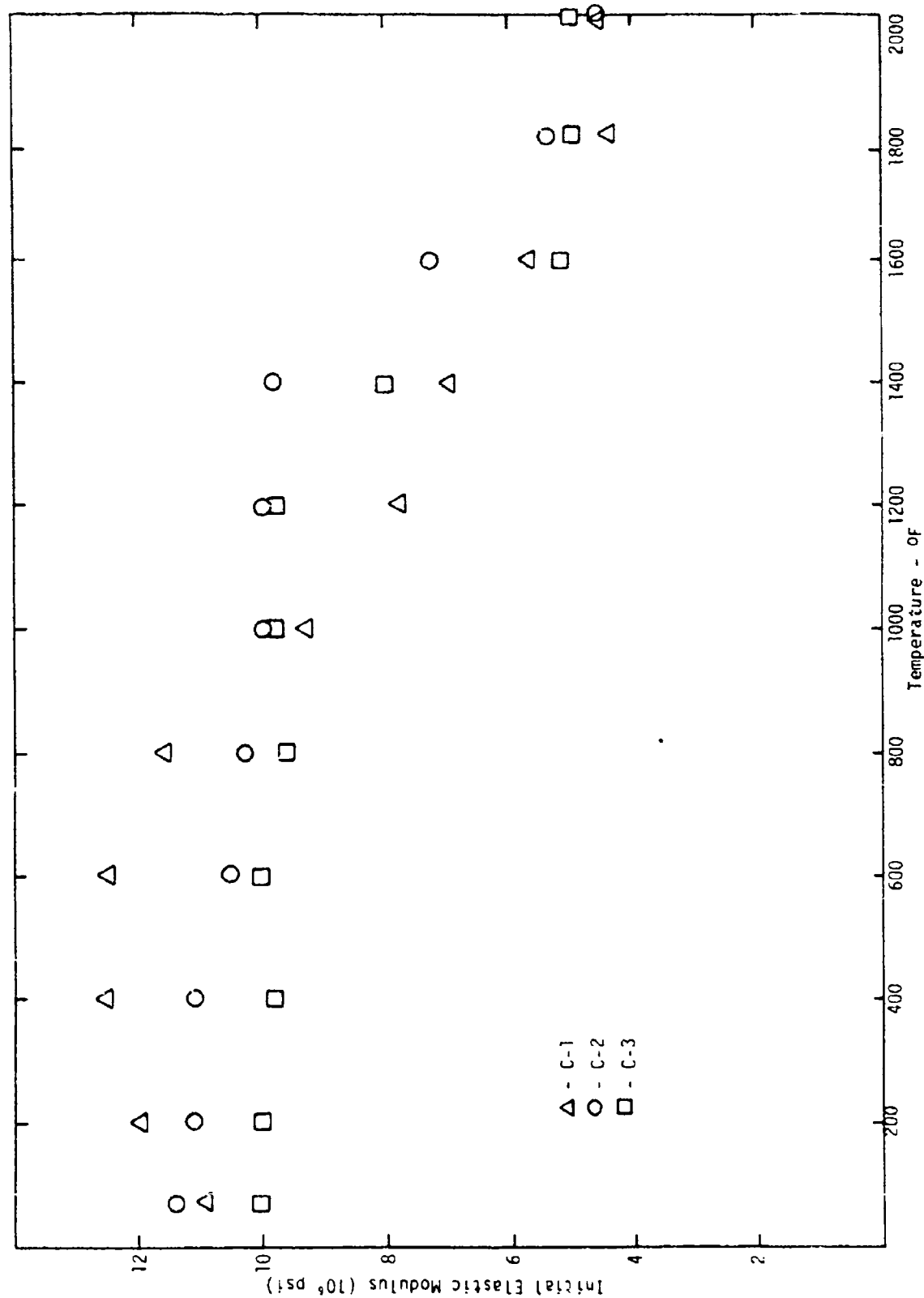
Figure 49. Initial compressive elastic modulus of ZnS.
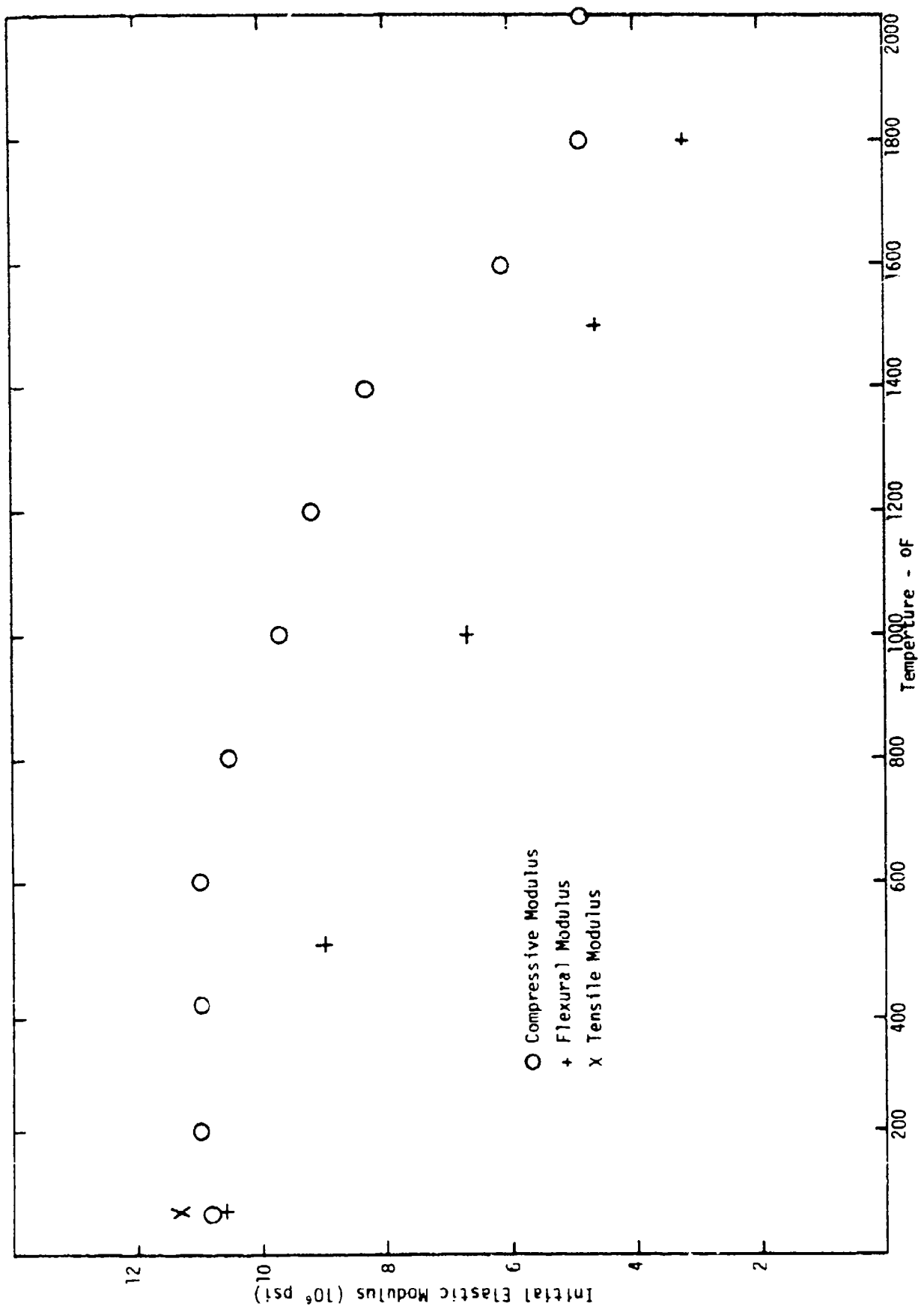
Figure 50. Average compressive moduli of ZnS
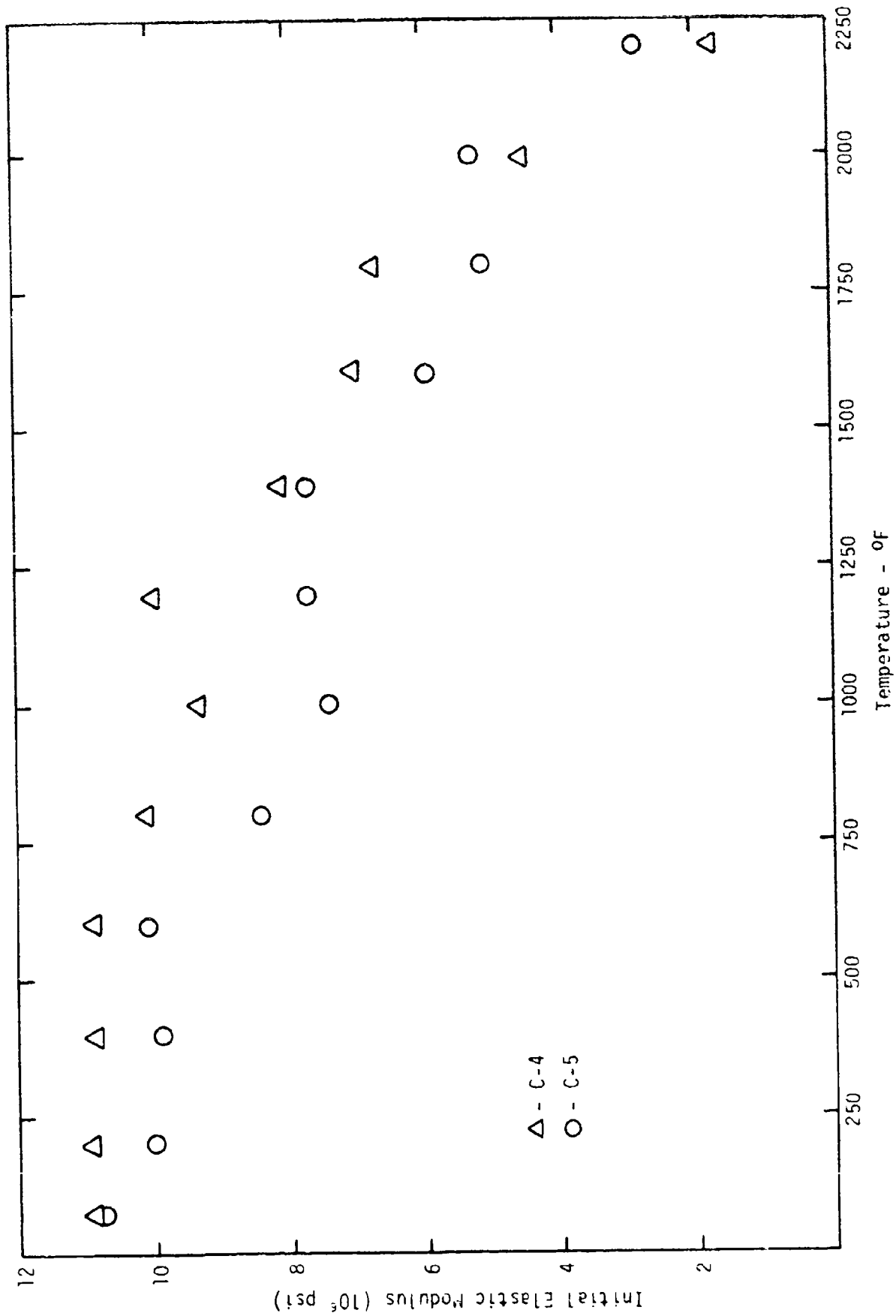
Figure 51. Compressive moduli of ZnSe
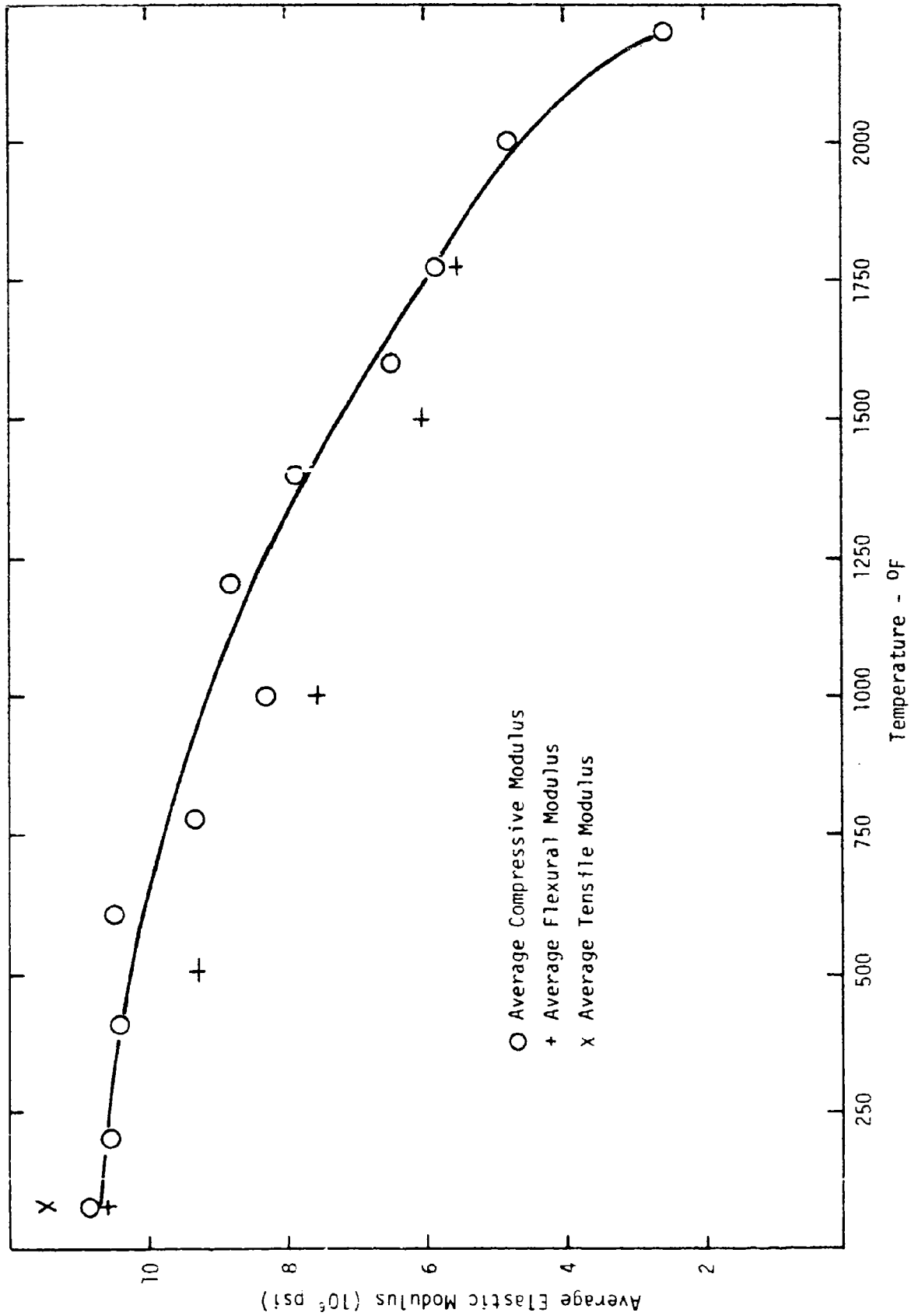
Figure 52. Average compressive modulus of ZnSe
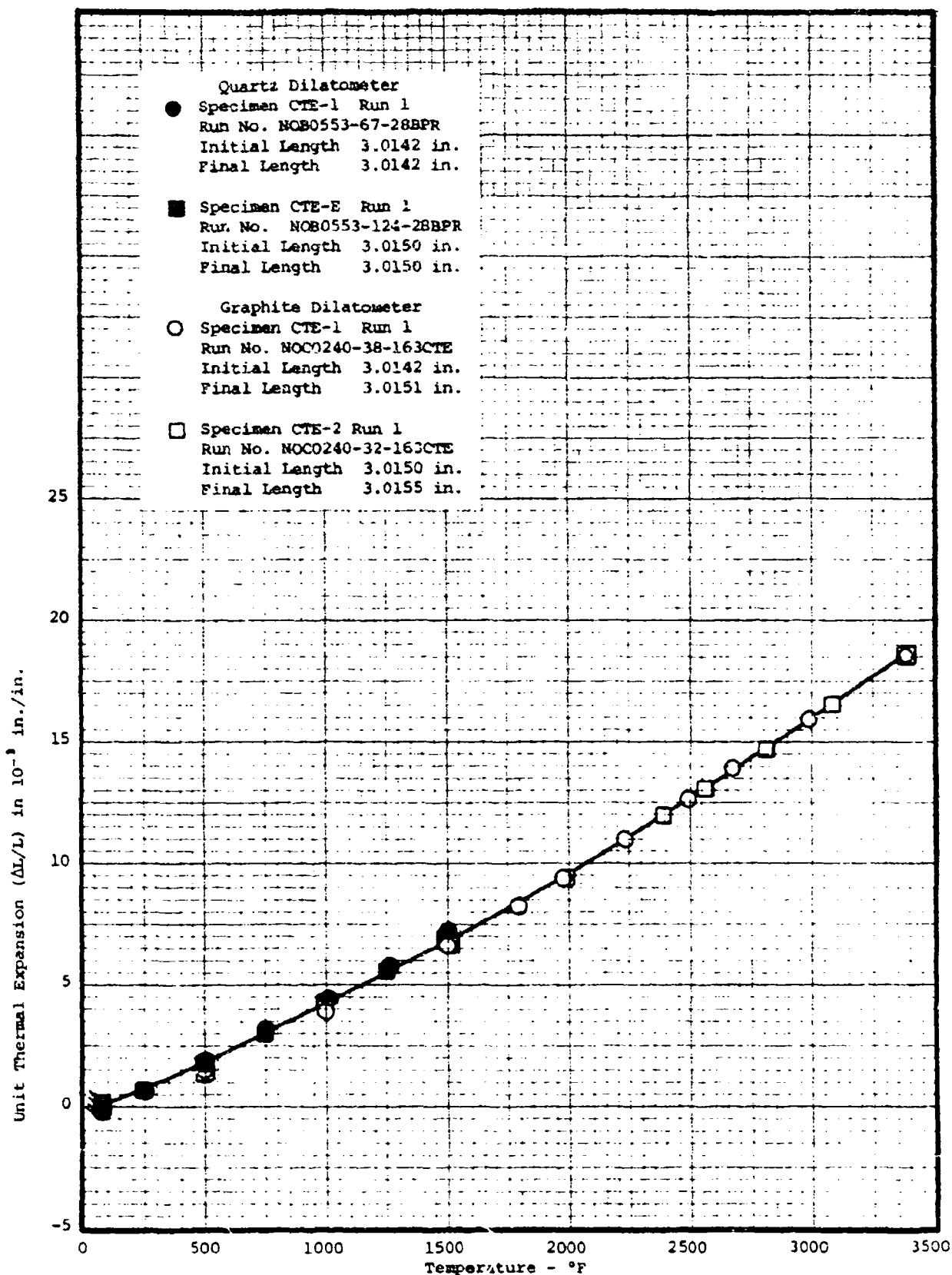
Figure 53. Thermal Expansion of Sapphire—Specimens 1 and 2

85

Quartz Dilatometer
Specimen CTE-3 Run 1
● Run No. NOB0553-74-28BPR
   Initial Length 3.0170 in.
   Final Length   3.0172 in.

■ Specimen CTE-4 Run
   Run No. NOB0553-121-28BPR
   Initial Length 3.0152 in.
   Final Length   3.0152 in.

Graphite Dilatometer
○ Specimen CTE-3 Run
   Run No. NOC0240-35-163CTE
   Initial Length 3.0164 in.
   Final Length   3.0.75 in.

□ Specimen CTE-4 Run
   Run No. NOC0240-36-171BK3
   Initial Length 3.0152 in.
   Final Length   3.0150 in.

✦ Reference Single Crystal Sapphire

Figure 54.   Thermal Expansion of Sapphire—Specimens 3 and 4

86
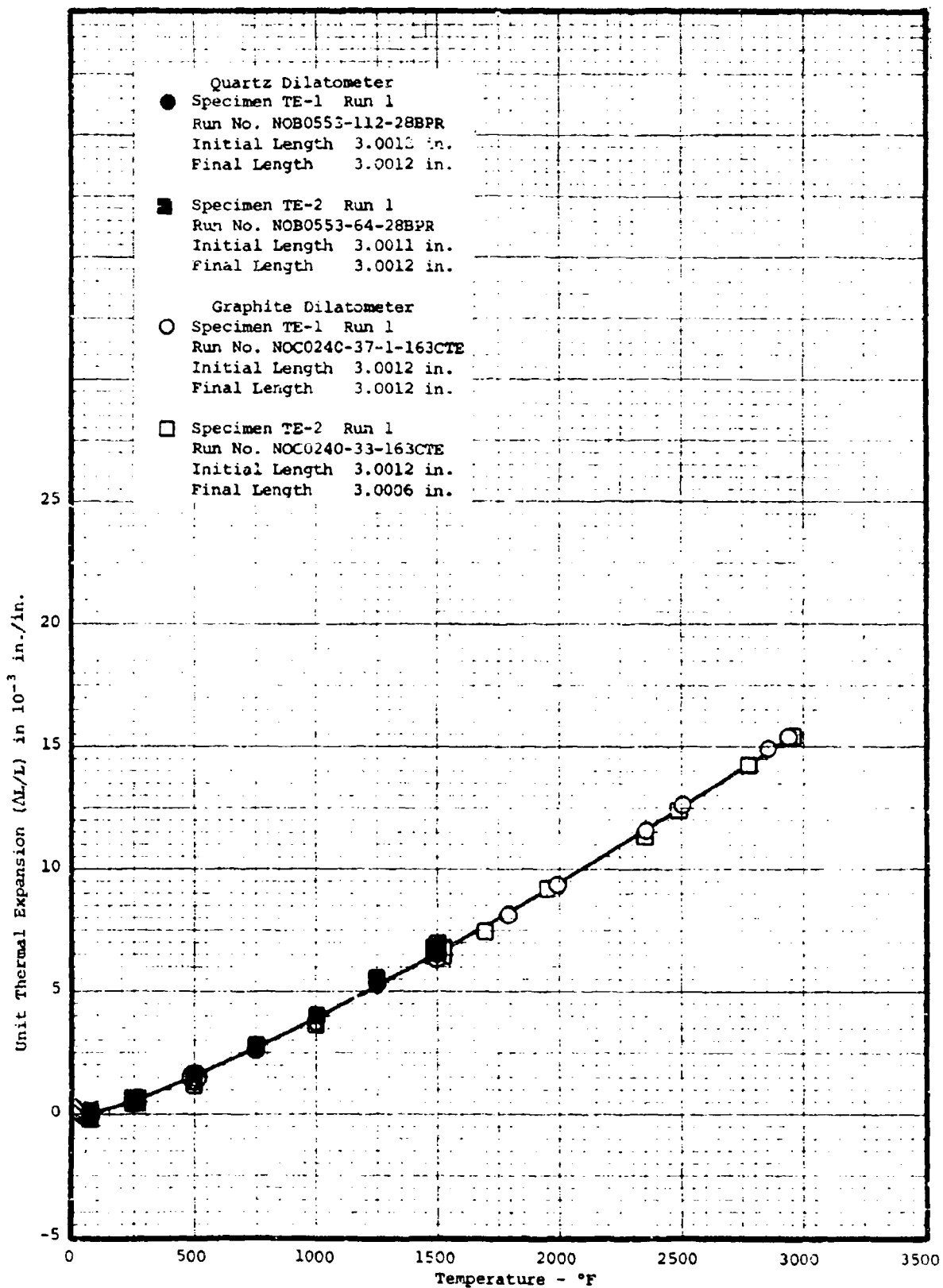
Figure 55.   Thermal Expansion of Spinel

87
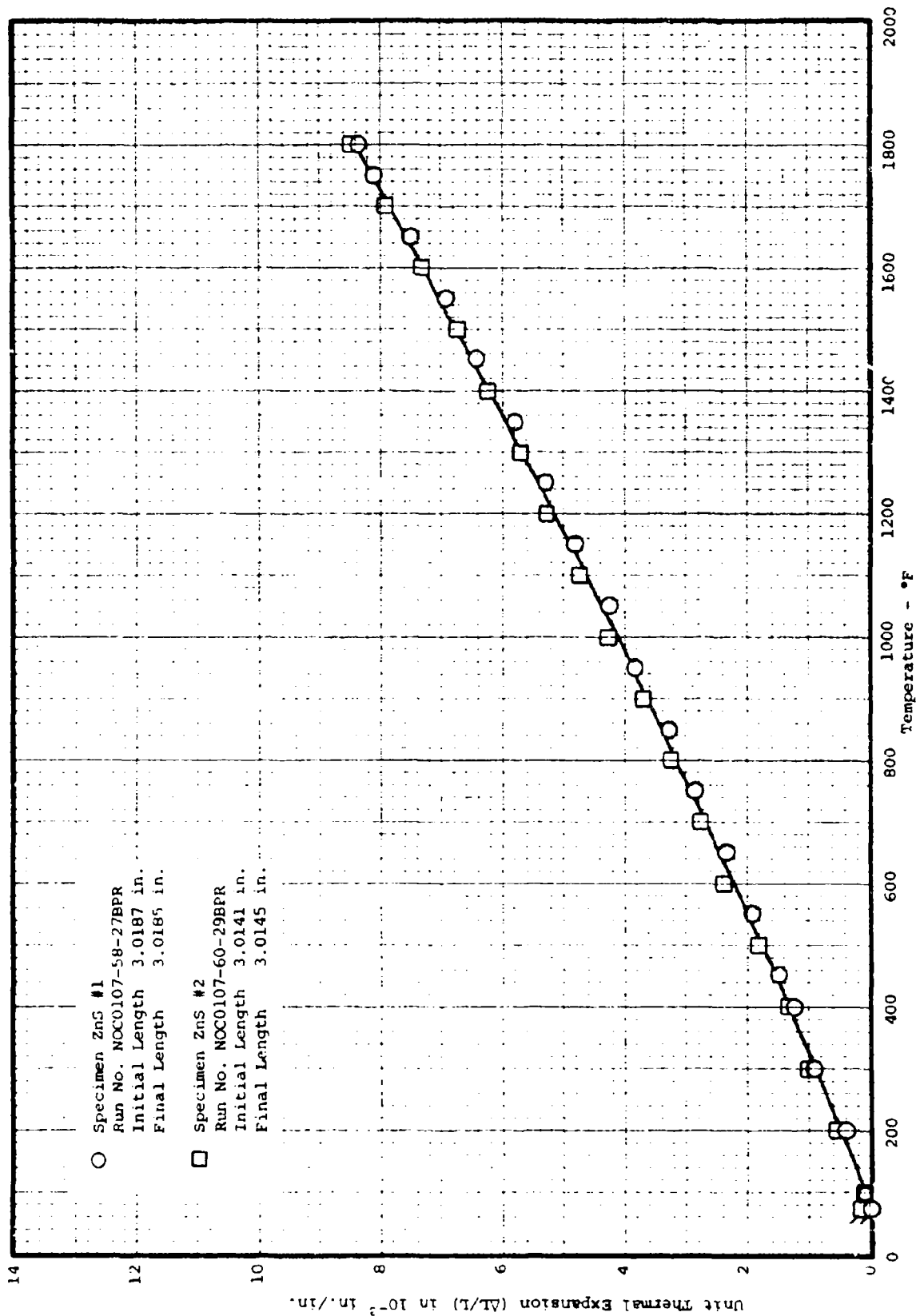
Figure 56. Thermal Expansion of ZnS

88
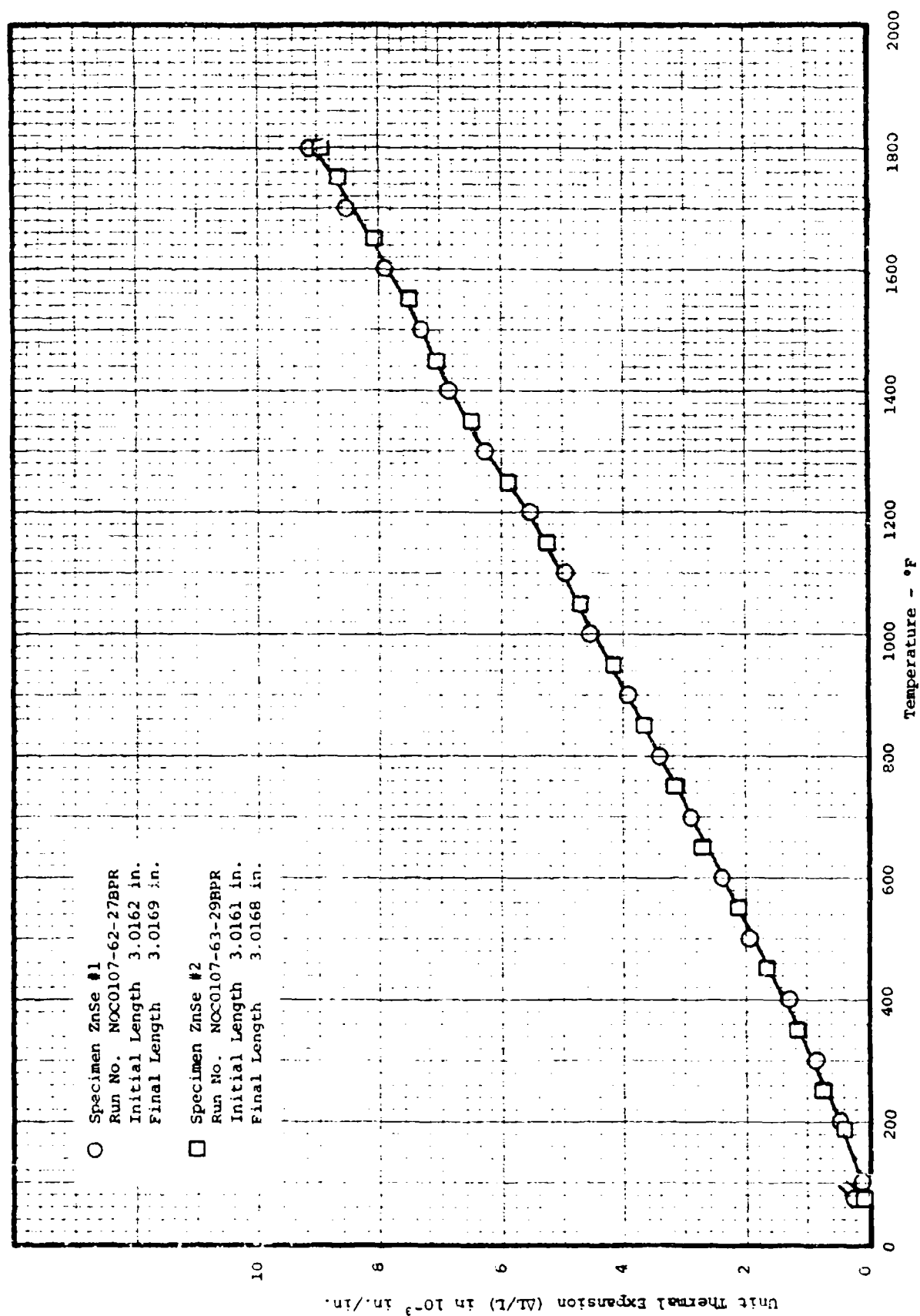
Figure 57. Thermal Expansion of ZnSe
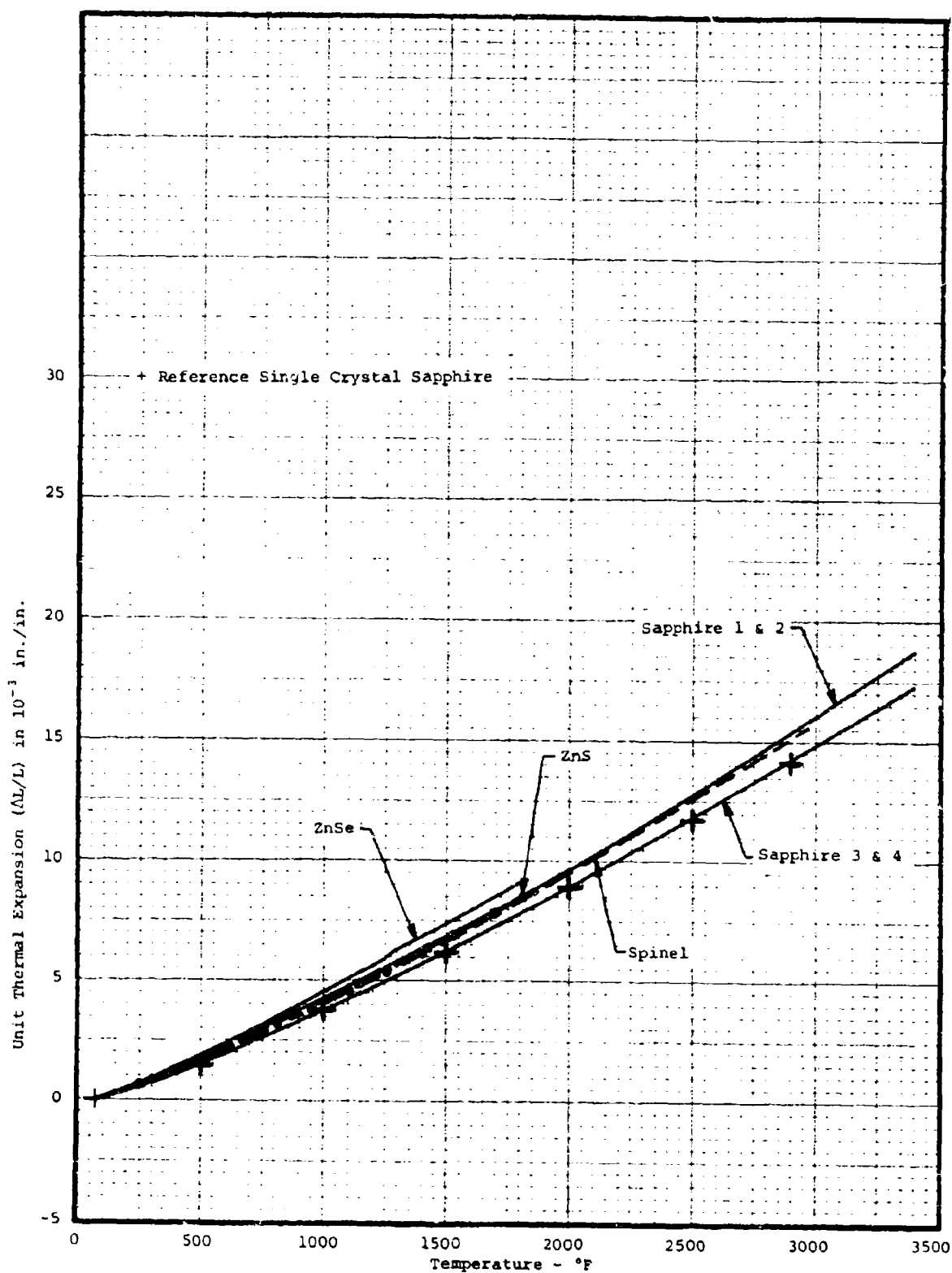
Figure 58.   Composite Plot of Thermal Expansions

90
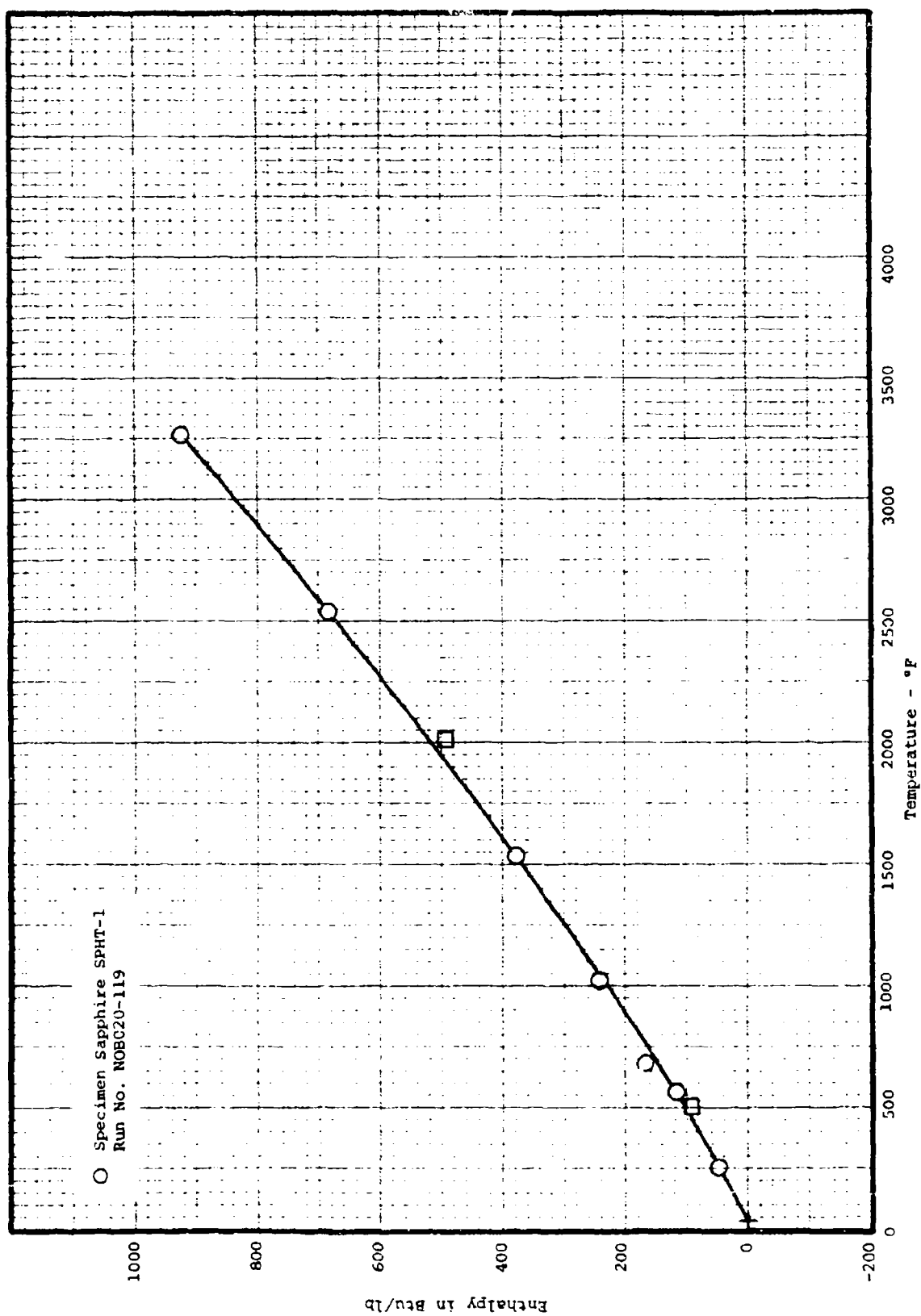
Figure 59. Enthalpy of Sapphire
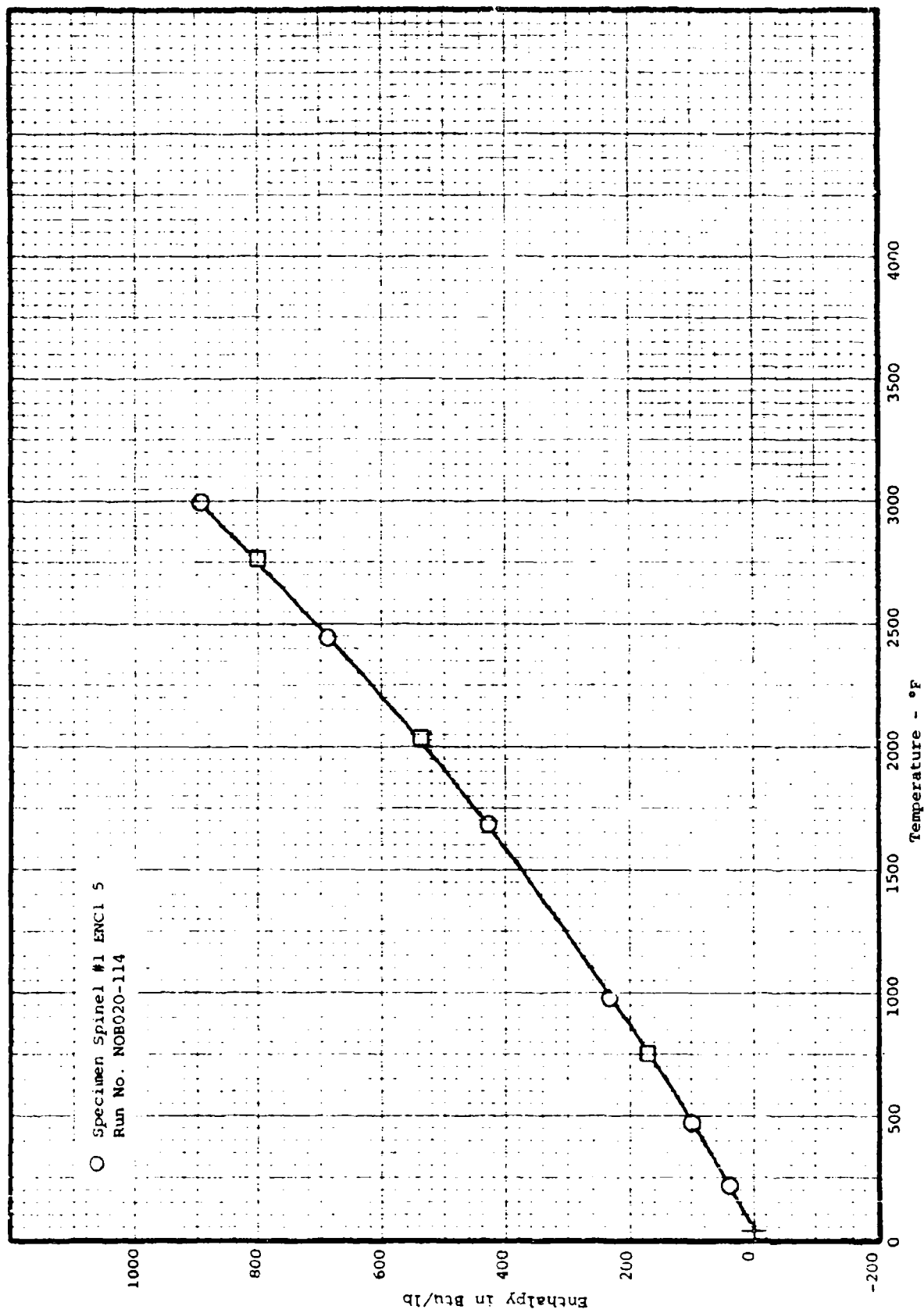
Figure 60. Enthalpy of Spinel
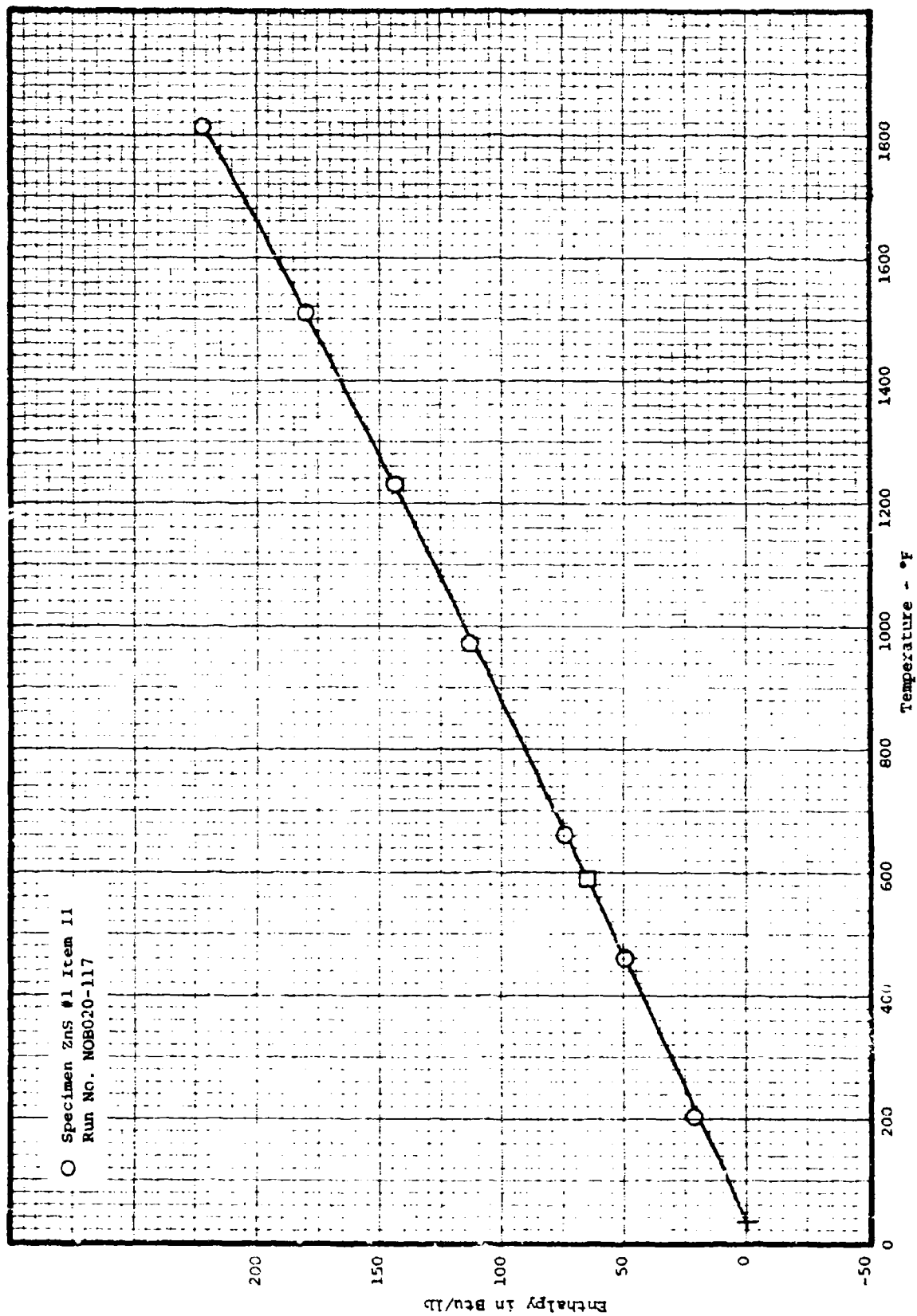
Figure 61. Enthalpy of ZnS
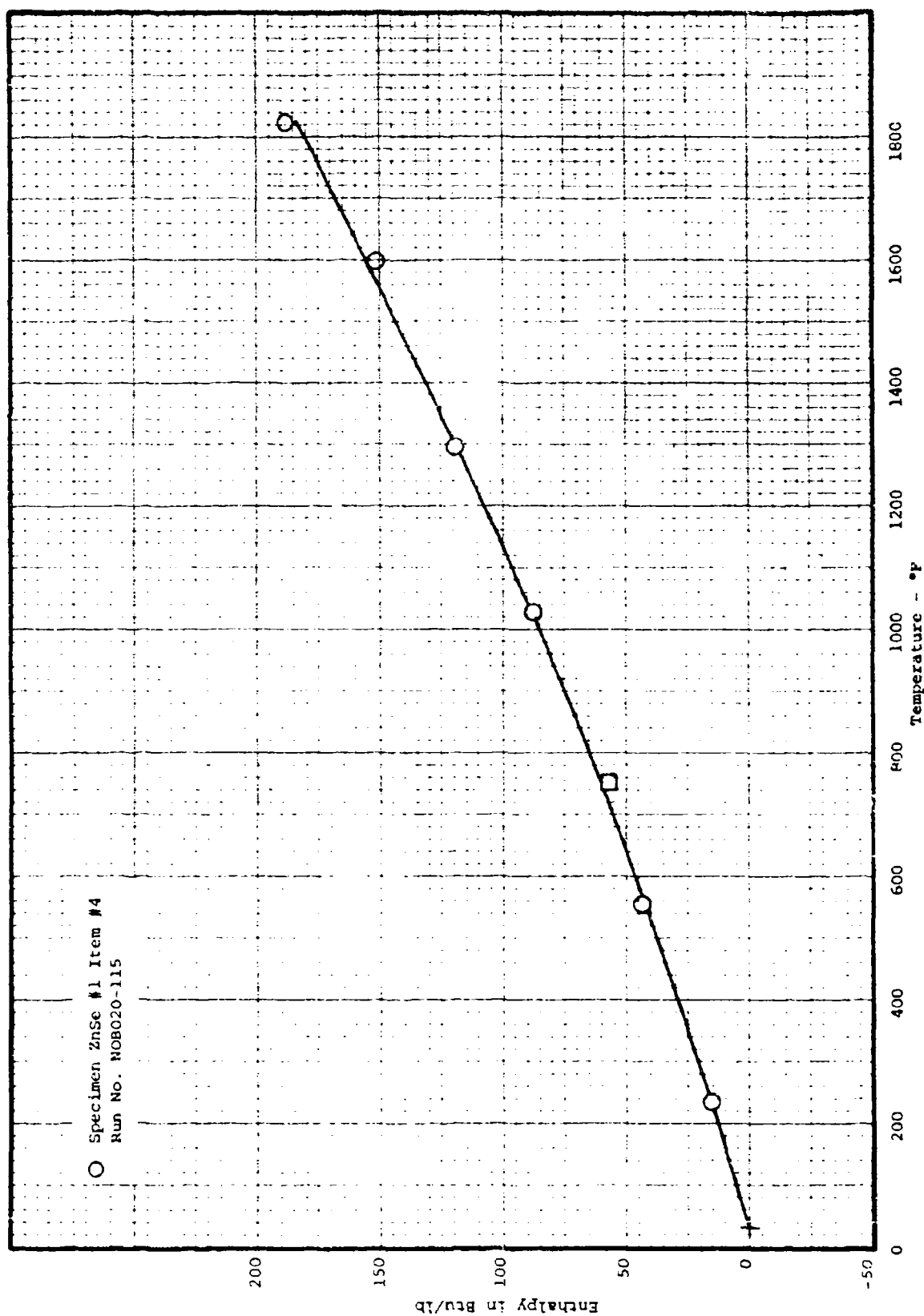
Figure 62. Enthalpy of ZnSe
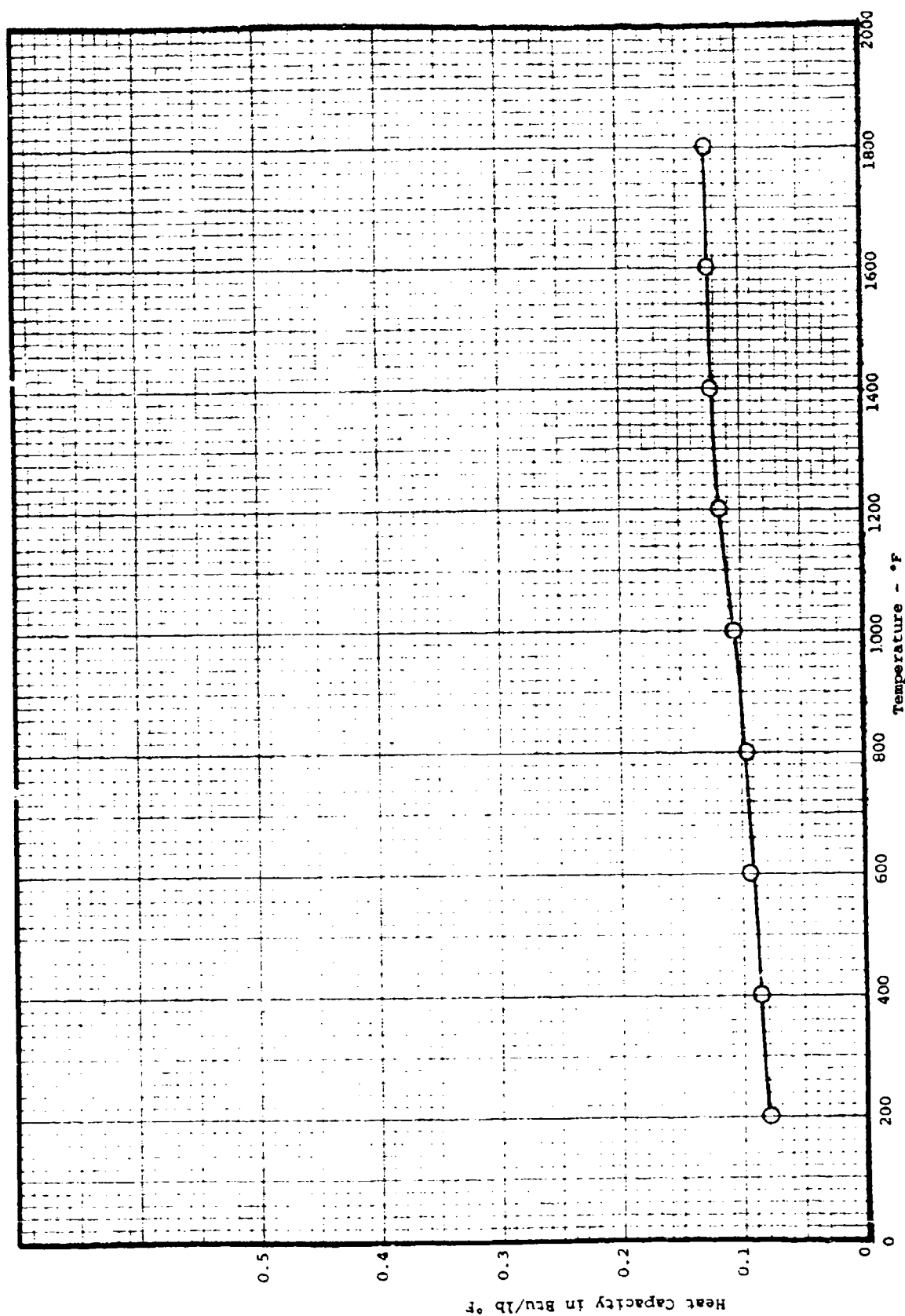
Figure 63. Heat Capacity of ZnSe
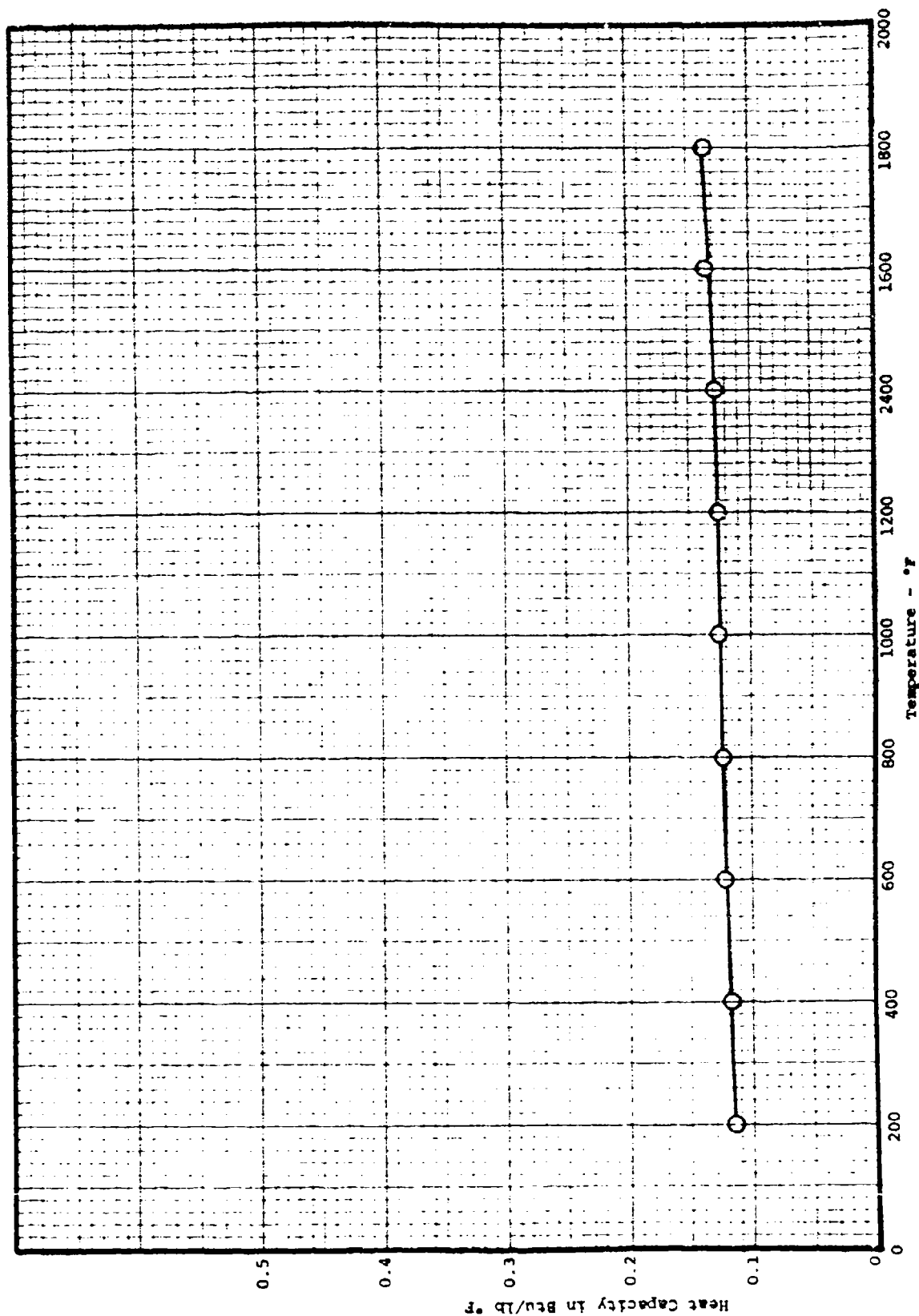
Figure 64. Heat Capacity of ZnS

96
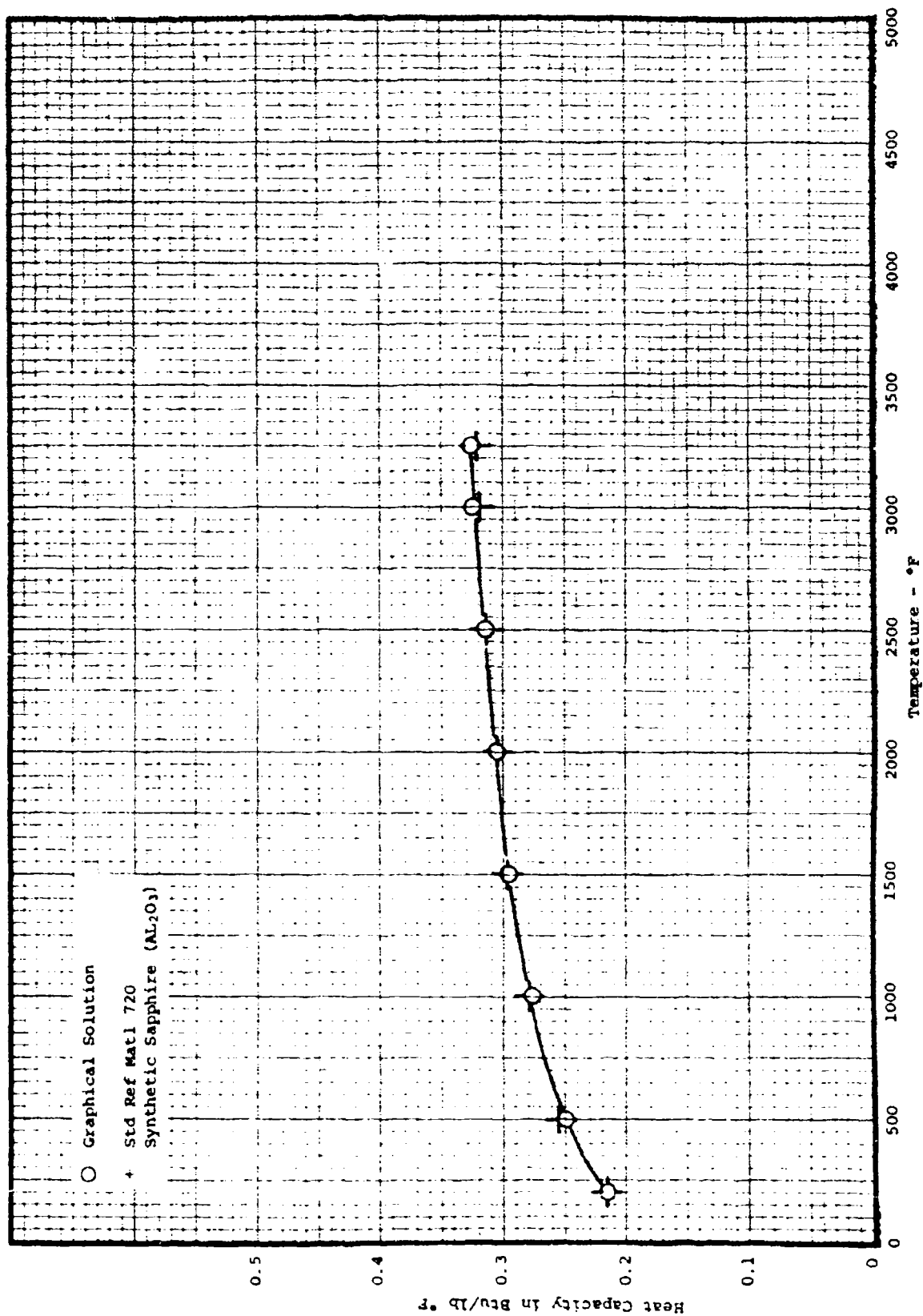
Figure 65. Heat Capacity of Sapphire

97
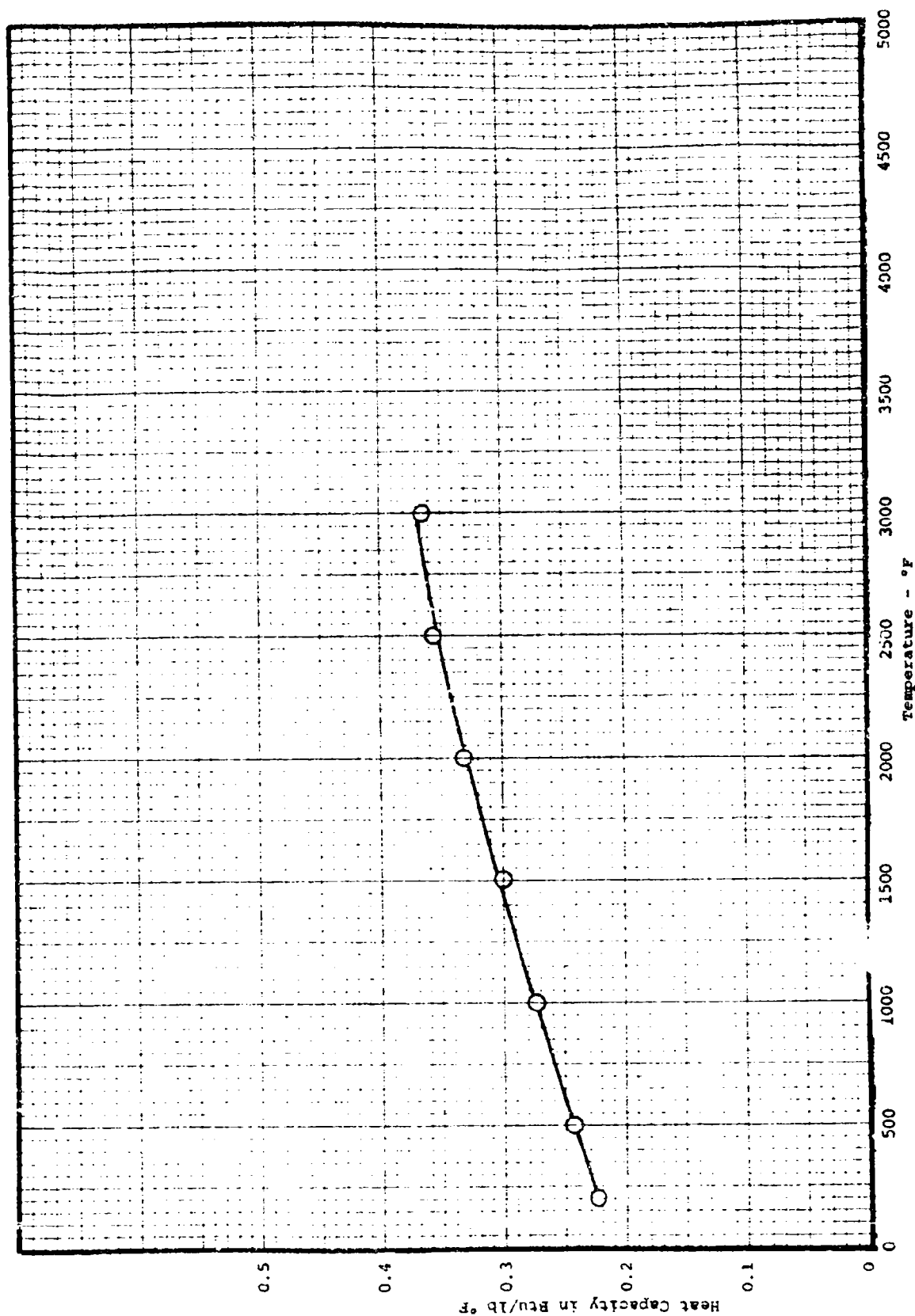
Figure 66. Heat Capacity of Spinel
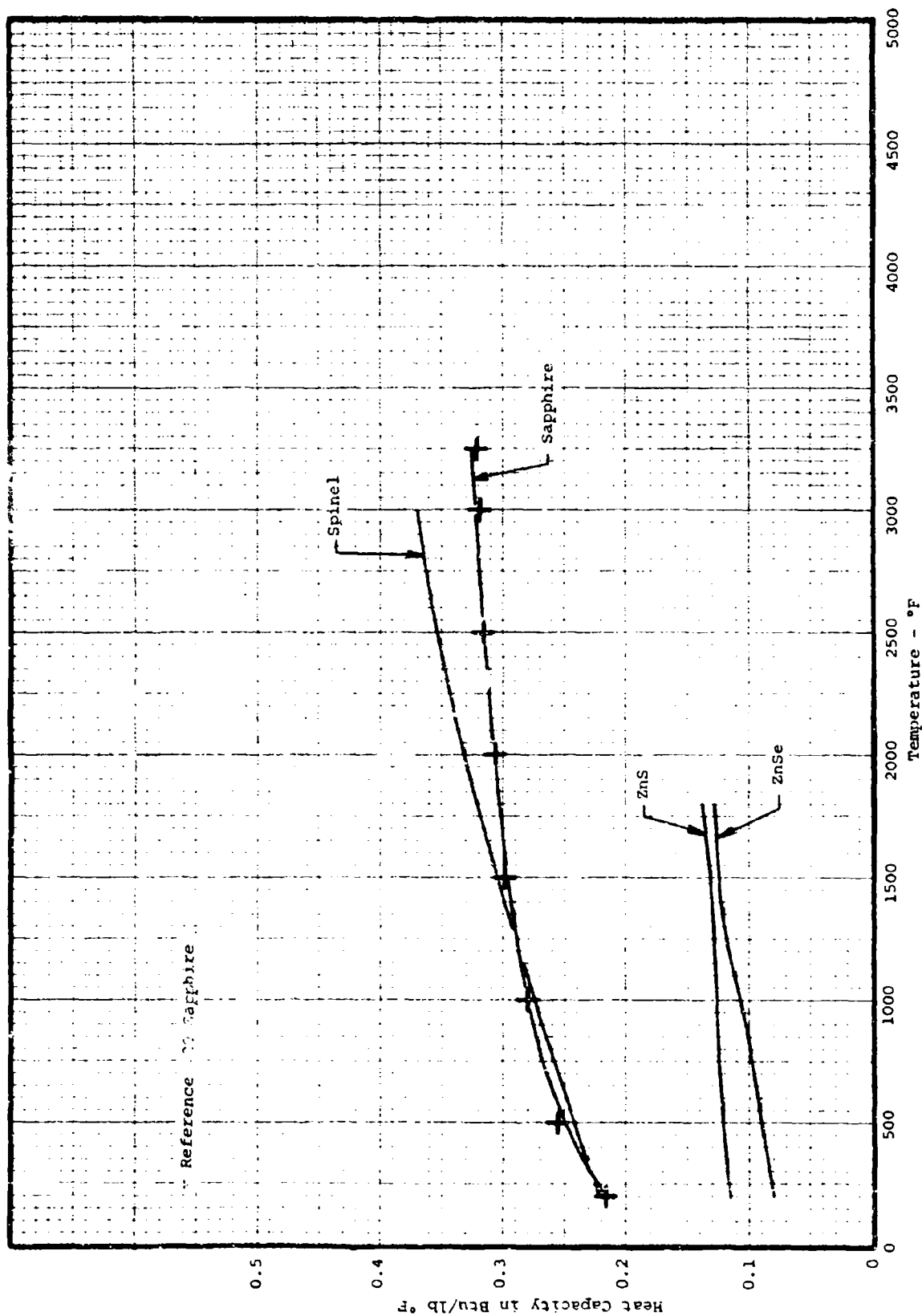
Figure 67. Composite Plot of Heat Capacities
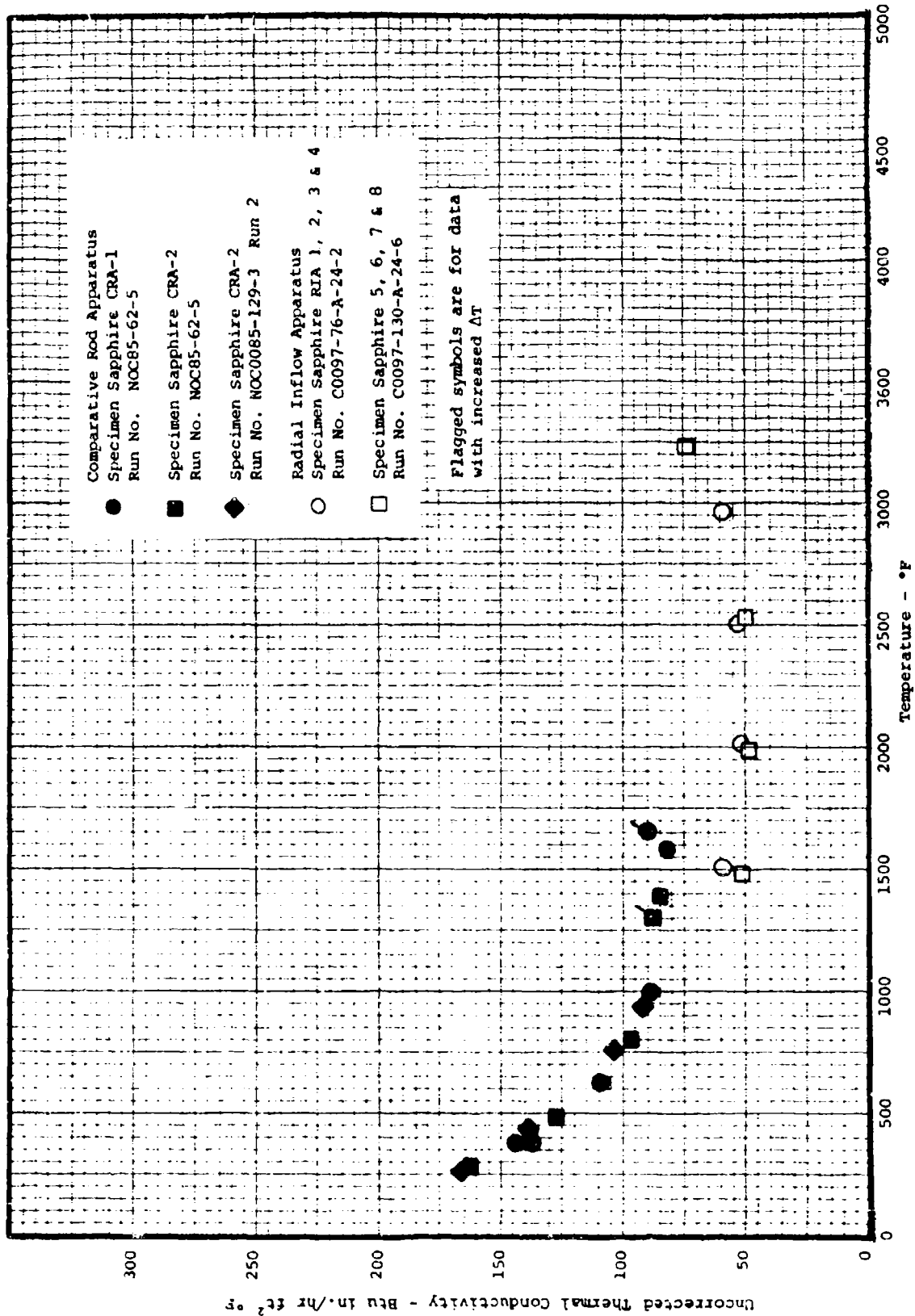
Figure 68. Uncorrected Thermal Conductivity of Sapphire
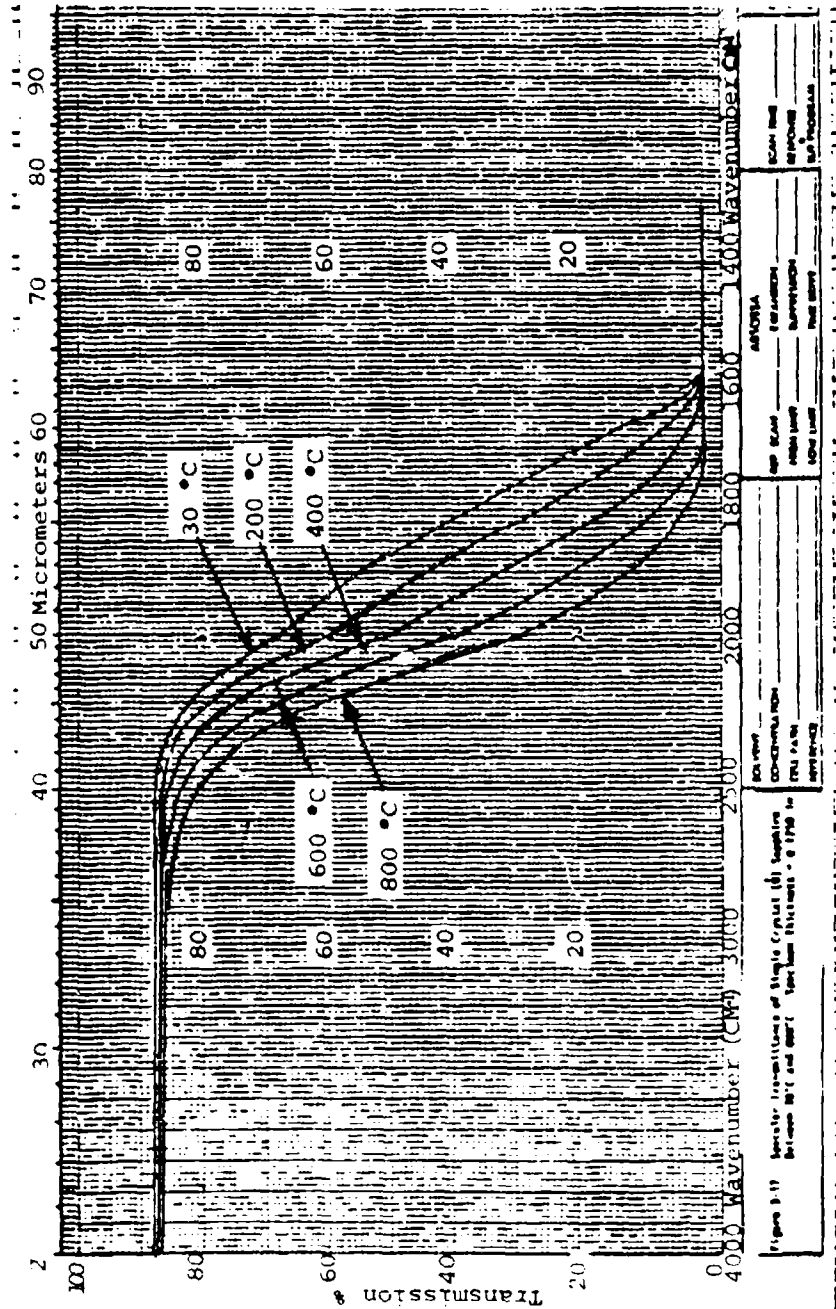
Figure 69. Transmission plot for 0.125 inch Sapphire sample (30 °C - 800 °C)
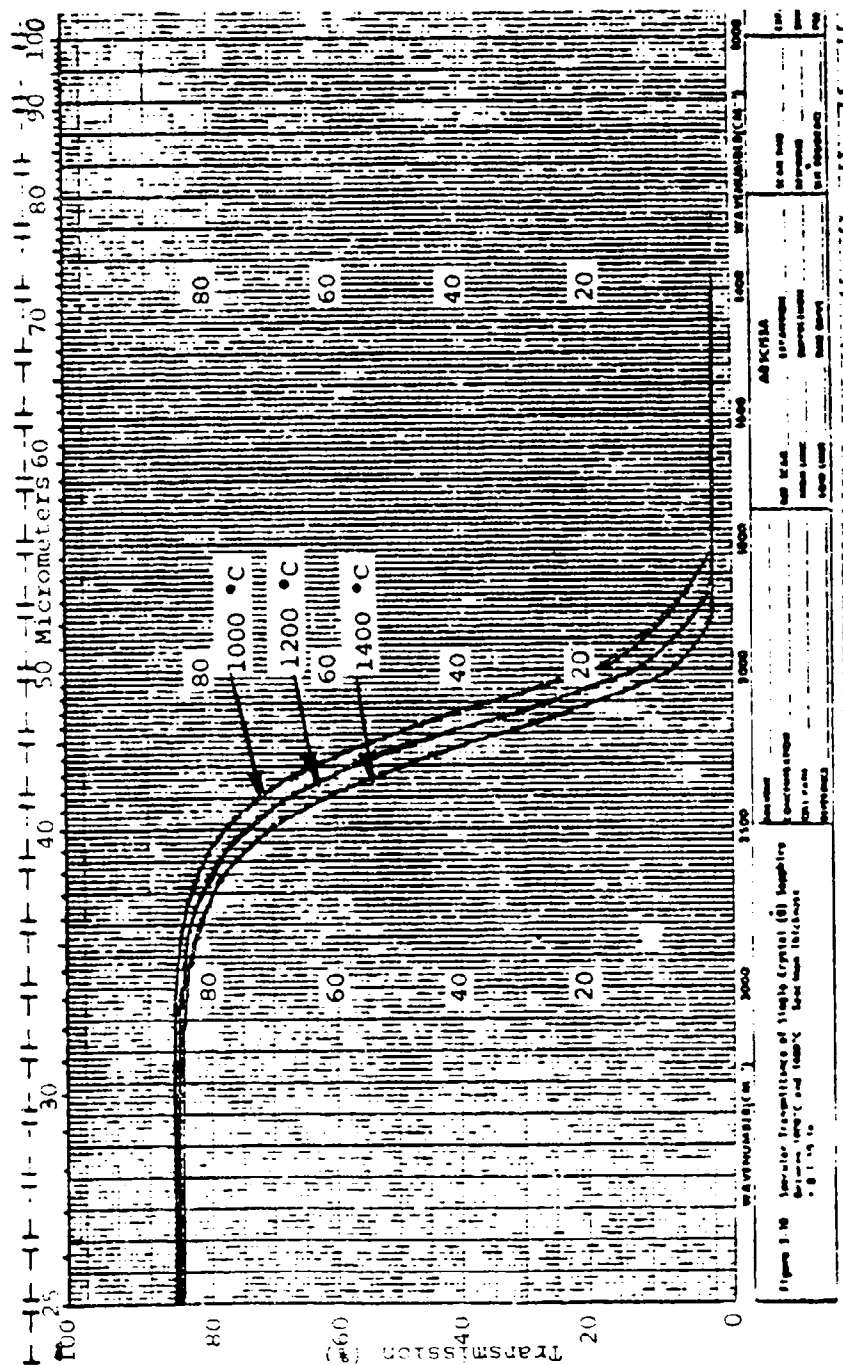
Figure 70. Transmission plot for 0.125 inch Sapphire sample (1000 °C – 1400 °C)
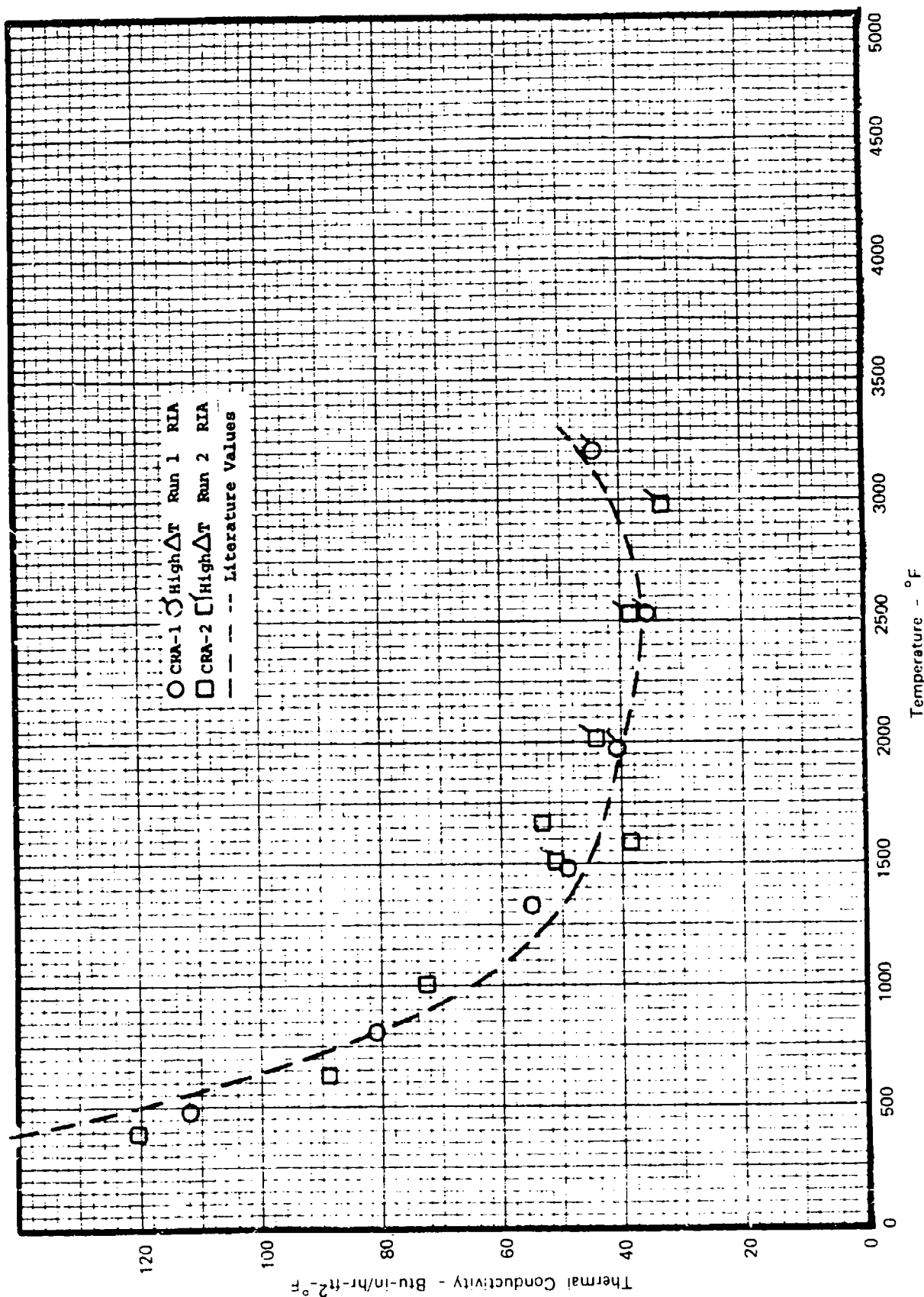
Figure 71. Calculated Thermal Conductivity for Sapphire
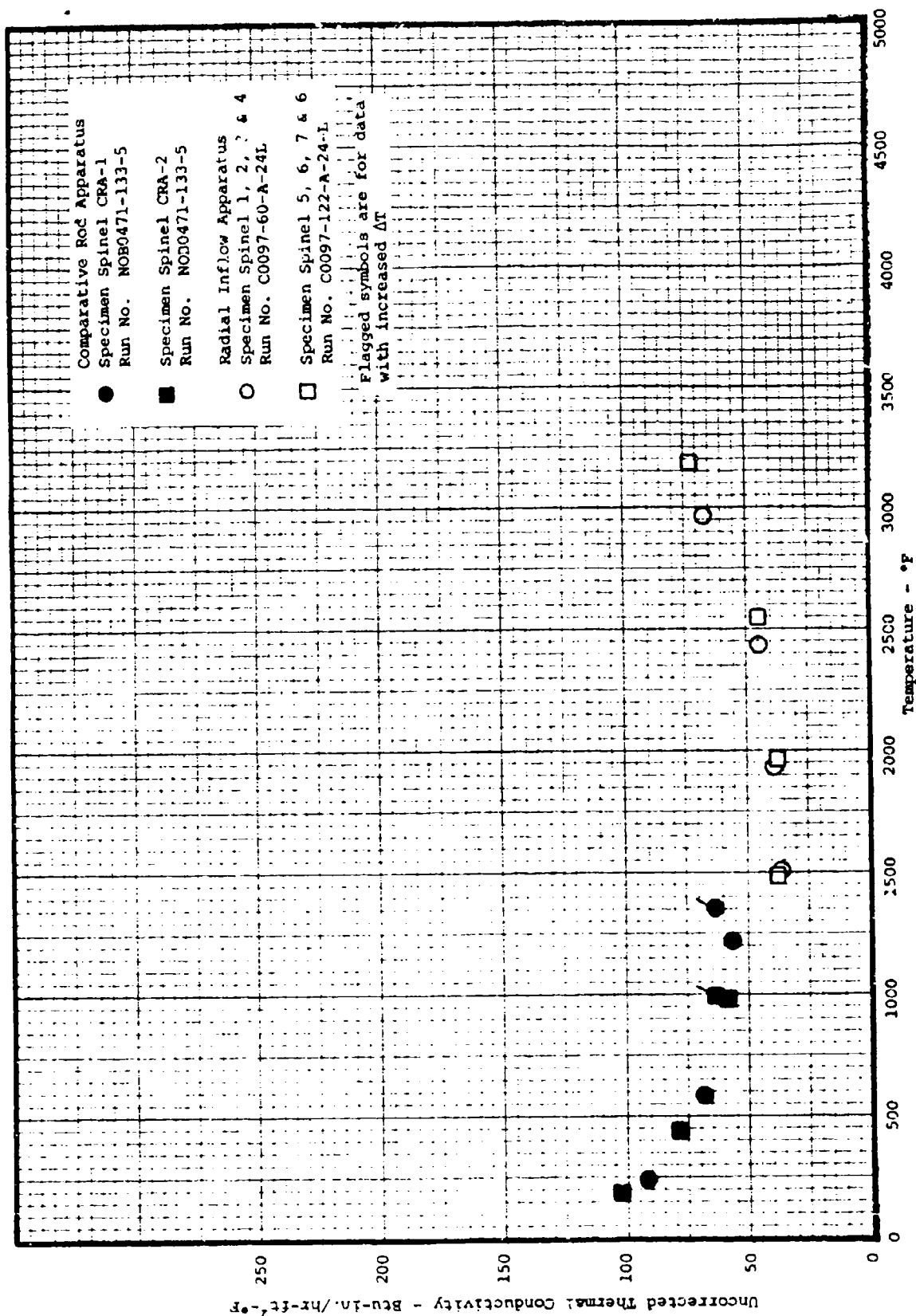
Figure 72. Uncorrected Thermal Conductivity of Spinel
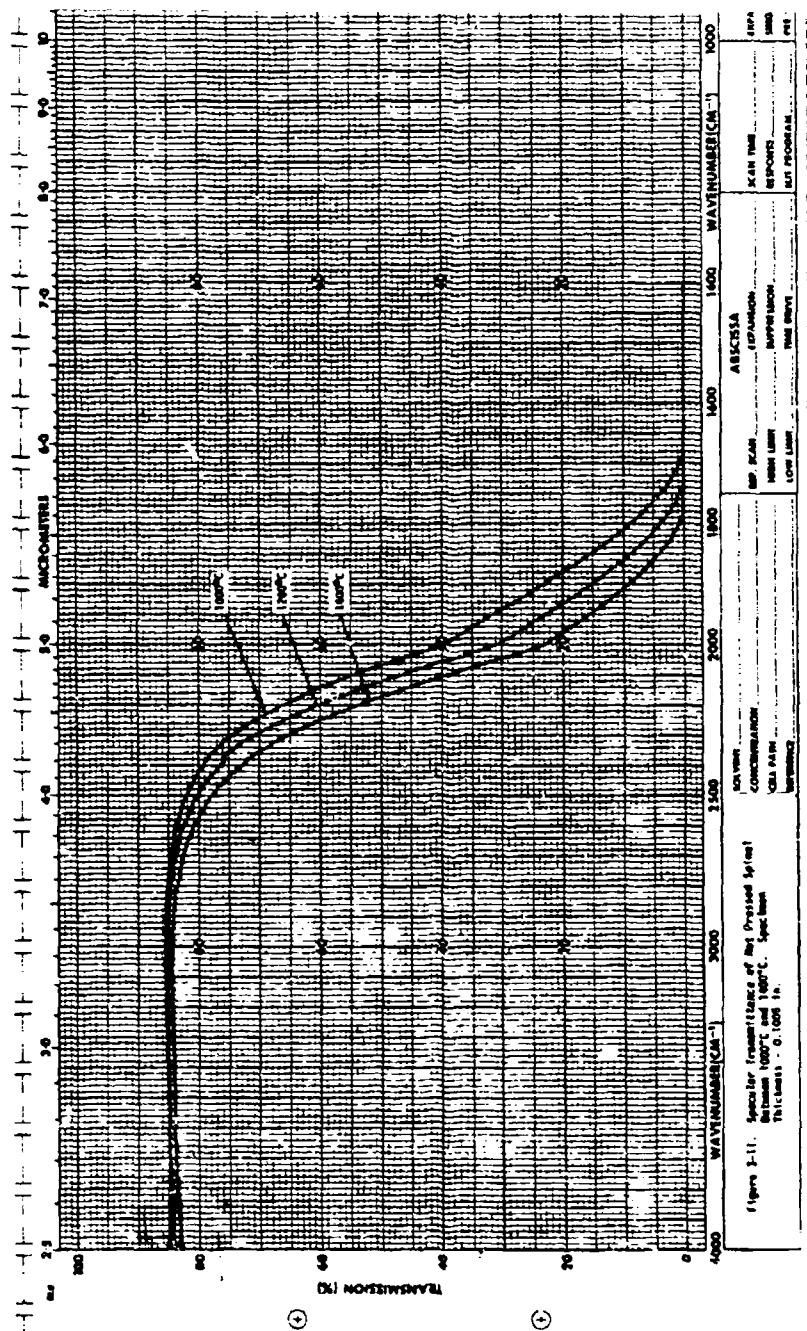
Figure 73. Transmission plot for 0.1005-inch Spinel sample (1000°C – 1400 °C)

Figure 74. Transmission plot for 0.1005-inch Spinel sample (30 °C – 800 °C)
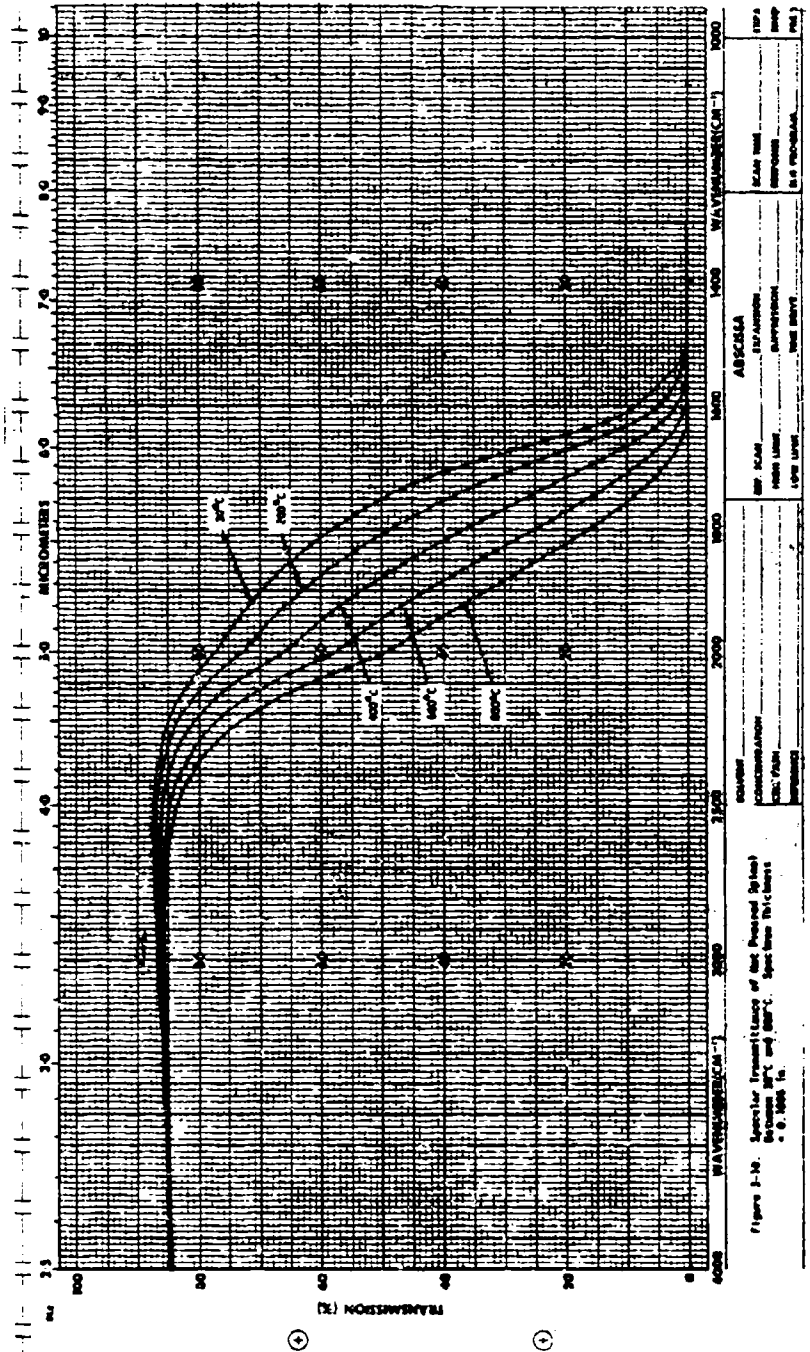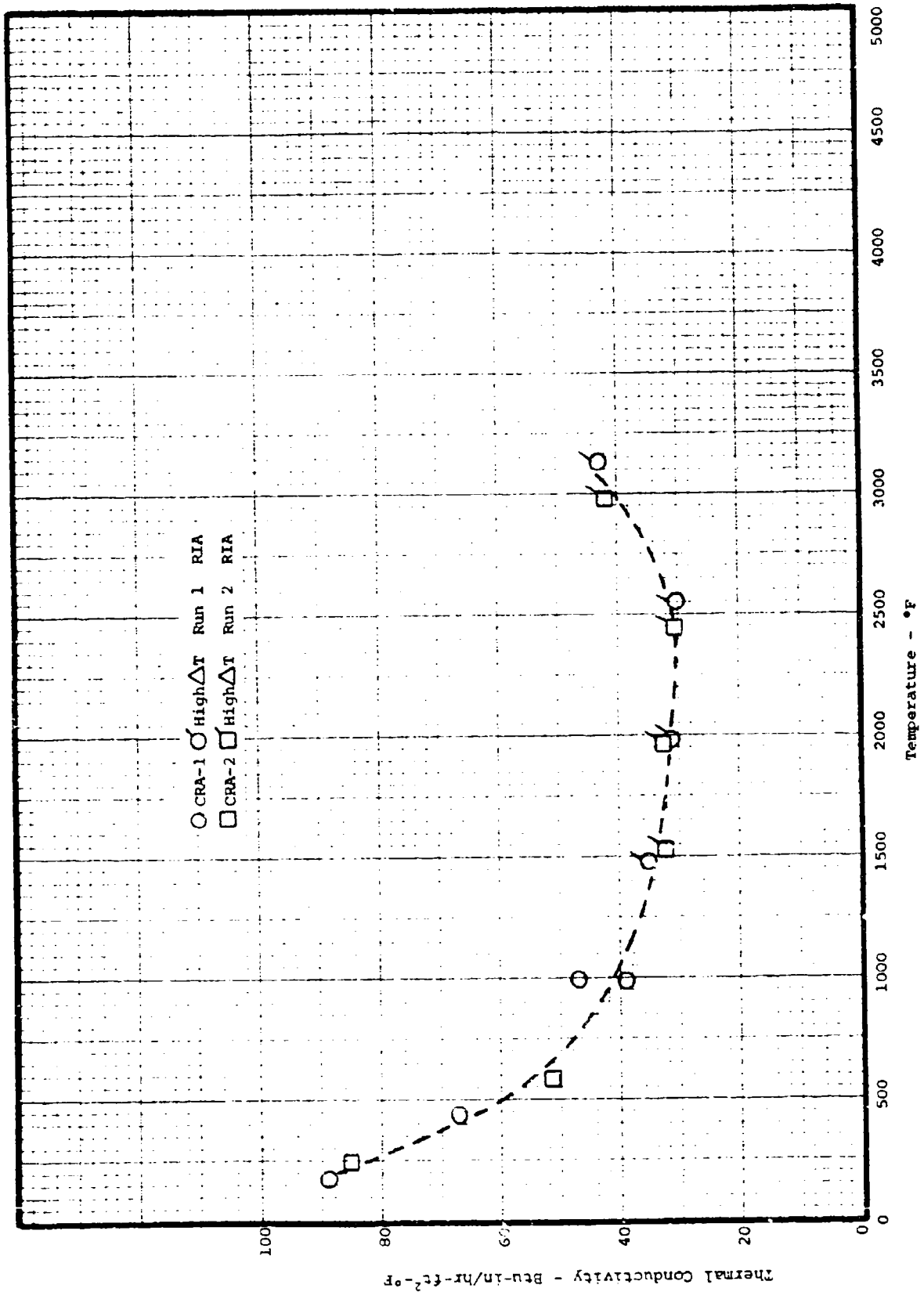
Figure 75. Calculated Thermal Conductivity of Spinel
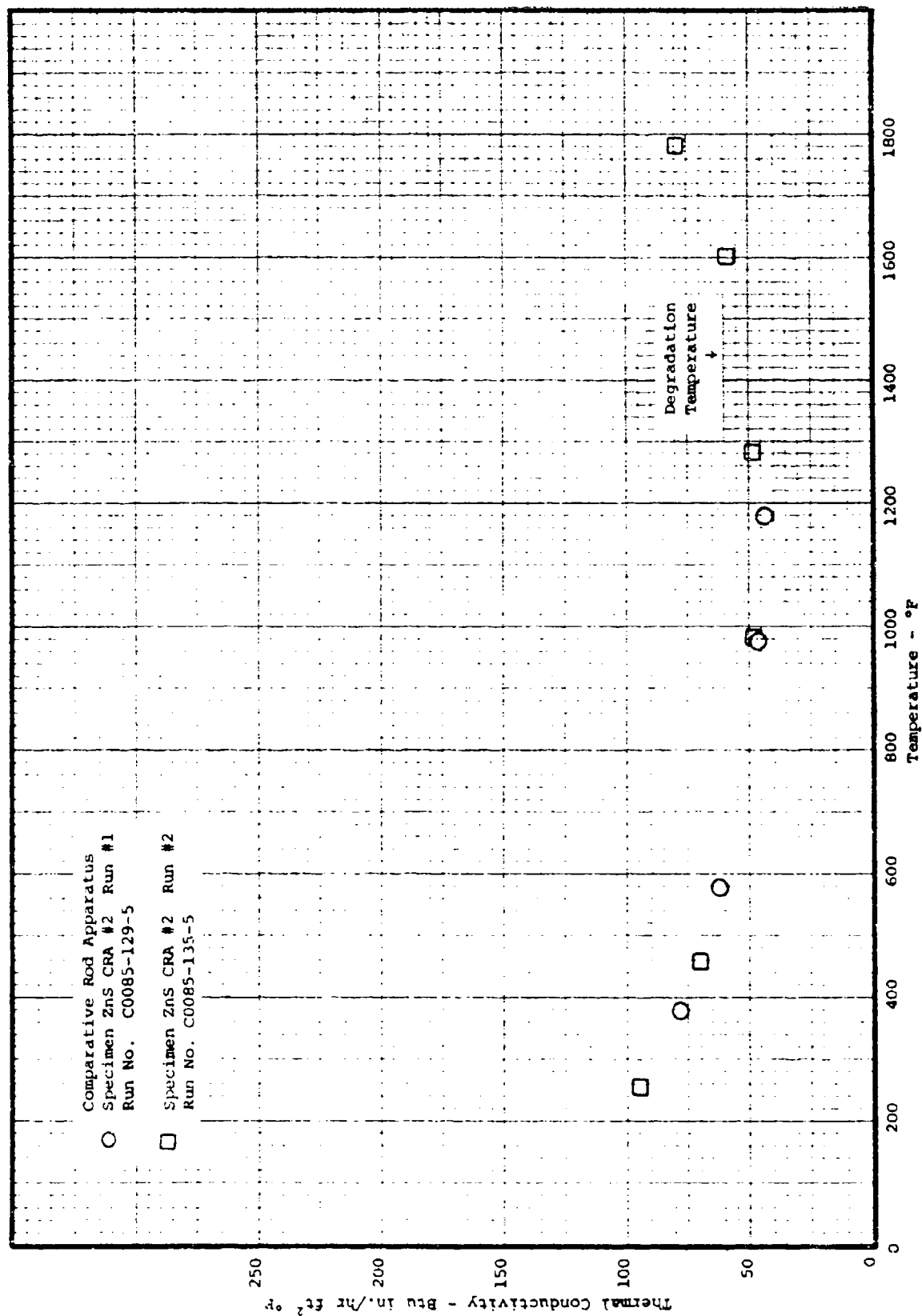
Figure 76. Thermal Conductivity of ZnS
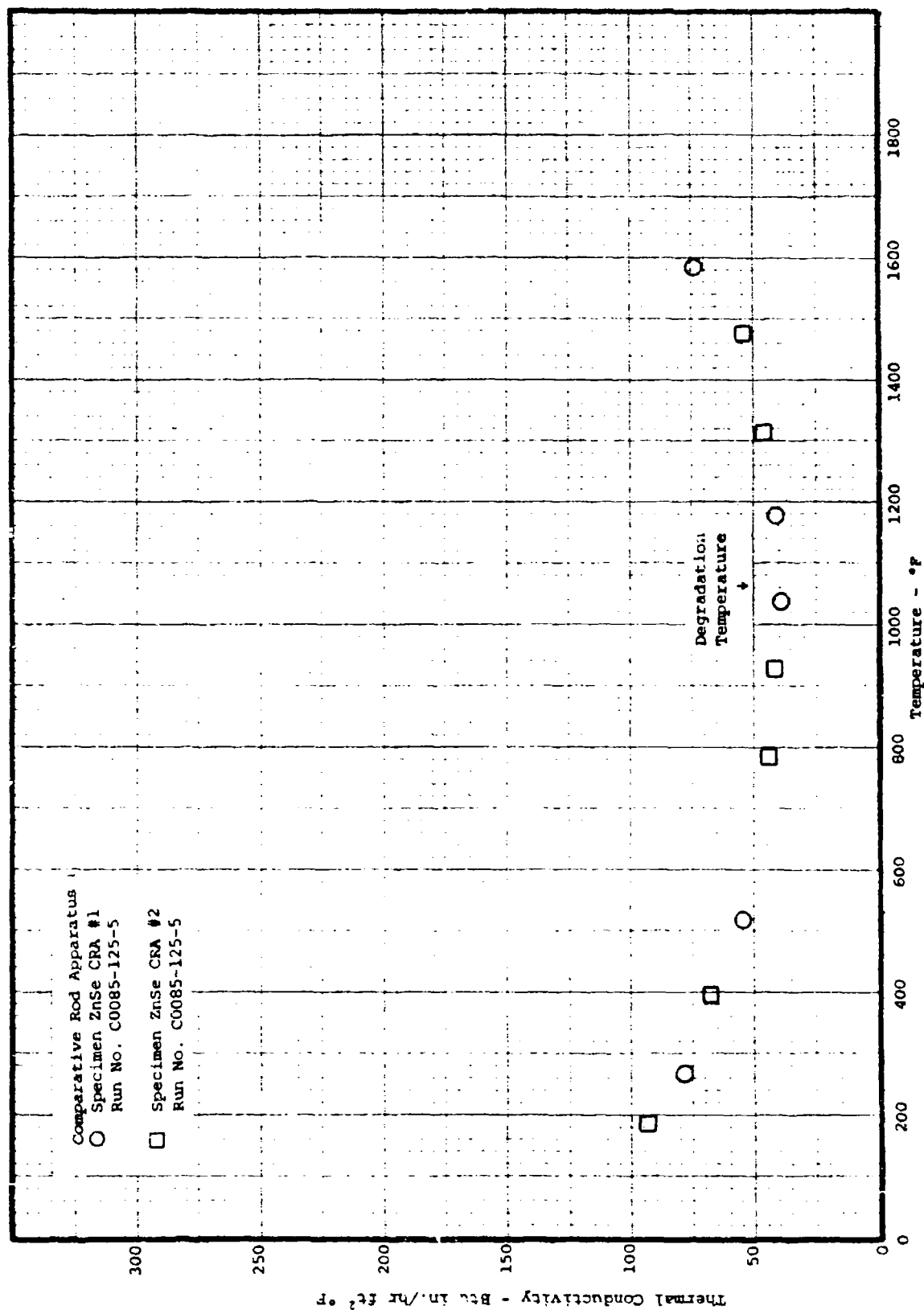
Figure 77. Thermal Conductivity of ZnSe

Table 1. Test Matrix for ZnS and ZnSe

Test[4]	Temperature - °F					
	70	500	1000	1500	1800	2000
Flexure	5 (6)[5]	5 (3)[5]	3	3	3	
Compression[1,3]	3	⟶ Every 260° ⟶				
Tension[2]	5					
Coefficient of Thermal Expansion	2					
Specific Heat	2					
Thermal Conductivity	2					

[1] Modulus measurement only

[2] Ultimate stress, strain, modulus, complete stress strain

[3] Poisson's ratio determined at 70°

[4] NDC and fractography as appropriate

[5] Number of tests for ZnS

110

Table 2. Test Matrix for Spinel

Test	Temperature - °F					
	70	1000	1500	2000	2500	3000
Flexure	6/5[1]	4	-	3	2	4
Compression	3[2],[3]	←——— Every 200° ———————————————→				
Tension	4[4]					
Coefficient of Thermal Expansion	2		2 ——————————————————→			
Specific Heat	2	2 ——————————————————————————→				
Thermal Conductivity	2		2[5] ————————————————→			

[1]Six polished and five ground equivalent to tension

[2]Modulus measurement only

[3]Poisson's ratio determined at 70°

[4]Includes complete stress-strain curve, elastic modulus, ultimate stress and ultimate strain

[5]ΔT varied

[6]NDC and fractography as appropriate

Table 3. Test Matrix for Sapphire

Test[8]	____		Temperature - °F		
	70	1500	2000	2500	3000
Flexure	5/5/5[1]		3/5[2]	3	3
Compression	3[3,4]	——————→ Every 200° —————————————→			
Tension	5				
Coefficient of Thermal Expansion	4[6]	——————→	4[6]	——————————————→	
Specific Heat	2	——————→	2	——————————————→	
Thermal Conductivity	2	——————→	2[7]	——————————————→	

[1] Five specimens fine ground (equivalent to tensile), five polished, and five at 60°

[2] Three at 0° and five at 60°

[3] Modulus measurement only

[4] Poissons ratio determined at 70°

[5] Includes complete stress-strain curve, elastic modulus, ultimate strength and ultimate strain

[6] Two at 60° and two at 0°

[7] ΔT varied

[8] NDC and fractography as appropriate

Table 4. Four Point Flexure of Sapphire

Specimen Number	Density (gms/cc)	Sonic Velocity (in./μsec)	Temperature °F	Ultimate Flexure Strength (psi)	Initial Flexural Modulus (10^6 psi)
25	3.9872	0.4386	70	107321	67.47
28	3.9819	0.4381	70	120070	61.78
26	3.9824	0.4396	70	140705	64.03
27	3.9835	0.4376	70	158903	61.51
24	3.9824	0.4401	70	123756	70.80
Average					
11	3.9834	0.4388	70	130151	65.11
10	3.9799	0.4366	70	50583	64.48
12	3.9769	0.4372	70	68621	64.71
13	3.9812	0.4376	70	88227	65.04
14	3.9824	0.4366	70	81953	65.96
	3.9839	0.4366	70	78455	66.89
	3.9808	0.4369	70	73567	64.21
Average					
29 *	3.9768	0.4085	70	88425	48.61
3 *	3.9775	0.4082	70	68451	54.20
5 *	3.9810	0.4081	70	91924	54.53
1 *	3.9750	0.4073	70	68451	52.70
7 *	3.9814	0.4086	70	50198	52.31
Average	3.9783	0.4081		73490	52.47
18	3.9790	0.4363	2000	38384	54.84
15	3.9761	0.4363	2000	109658	58.92
21	3.9756	0.4382	2000	102743	56.50
Average	3.9769	0.4369		83608	56.75
4 *	3.9816	0.4077	2000	38187	39.84
2 *	3.9756	0.4086	2000	36507	44.84
6 *	3.9776	0.4085	2000	28148	40.43
9 *	3.9788	0.4073	2000	27558	42.28
8 *	3.9784	0.4082	2000	35714	42.87
Average	3.9784	0.4081		33223	42.05
16	3.9860	0.4368	2500	97599	51.67
22	3.9824	0.4368	2500	97439	53.88
19	3.9856	0.4377	2500	73442	53.14
Average	3.9847	0.4371		89487	52.90
20	3.9768	0.4382	3000	48216	46.97
23	3.9842	0.4377	3000	53830	46.95
17	3.9767	0.4368	3000	46928	48.68
Average	3.9792	0.4276		49658	47.53

*60° specimens

113

Table 5. Four Point Flexure of Spinel

Specimen Number	Density (gms/cc)	Sonic Velocity (in./μsec)	Temperature °F	Ultimate Flexural Strength (psi)	Flexural Modulus (10^6 psi)	Comments
13	3.5689	0.3835	70	14251	40.44	
16	3.5696	0.3834	70	14642	40.12	
15	3.5710	0.3826	70	13075	37.94	
3	3.5680	0.3832	70	12986	40.15	
8	3.5684	0.3845	70	11733	39.52	
24	3.5694	0.3834	70	12970	39.60	
18	3.5637	0.3835	70	14606	43.53	
1	3.5668	0.3825	70	13581	40.15	
2	3.5677	0.3832	70	14620	39.82	
4	3.5651	0.3836	70	11916	40.19	
5	3.5667	0.3839	70	13692	40.33	Specimen was chipped Placed in compression
Average	3.6191	0.3834		13461	40.18	
14	3.5689	0.3838	1000	8775	37.67	
19	3.5674	0.3838	1000	13026	37.22	
7	3.5672	0.3839	1000	8692	33.09	
9	3.5716	0.3817	1000	9800	35.73	
Average	3.5688	0.3833		10073	35.93	
25	3.5707	0.3837	2000	9563	32.06	Specimen was chipped Placed in compression
10	3.5703	0.3824	2000	9218	34.56	
20	3.5680	0.3837	2000	9100	29.14	Specimen was chipped Placed in compression
Average	3.5697	0.3833		9294	31.92	
11	3.5751	0.3853	2500	8669	18.59	
26	3.5684	0.3837	2500	10261	20.95	
Average	3.5718	0.3845		9465	19.77	
12	3.5698	0.3870	3000	5888	12.50	
17	3.5686	0.3837	3000	8028	13.05	
27	3.5746	0.3838	3000	5656	13.63	
6	3.5660	0.3847	3000	7641	16.14	
Average	3.5698	0.3848		6803	13.83	

Table 6. Four Point Flexure of ZnS

Specimen Number	Density (gms/cc)	Sonic Velocity (in./μsec)	Temperature °F	Ultimate Flexure Strength (psi)	Initial Flexural Modulus (10^6 psi)
3	4.0712	0.2151	70	8809	10.79
16	4.0754	0.2111	70	7754	10.80
17	4.0765	0.2114	70	10870	10.35
1	4.0710	0.2146	70	10540	10.23
6	4.0741	0.2112	70	7154	10.50
11	4.0763	0.2120	70	10641	11.05
Average	4.0741	0.2126		9295	10.62
2	4.0689	0.2151	500	9693	8.98
12	4.0740	0.2115	500	11848	9.56
7	4.0726	0.2112	500	12630	8.24
Average	4.0718	0.2126		11390	9.02
19	4.0698	0.2120	1000	13700	7.10
13	4.0716	0.2116	1000	13120	5.95
8	4.0772	0.2116	1000	13970	7.04
Average	4.0736	0.2115		13600	6.70
9	4.0720	0.2114	1500	13450	4.53
14	4.0758	0.2116	1500	12970	5.80
4	4.0695	0.2149	1500	12400	4.22
Average	4.0724	0.2127		12940	4.85
15	4.0728	0.2115	1800	10035	3.18
18	4.0746	0.2115	1800	10646	3.34
10	4.0743	0.2114	1800	8840	3.05
Average	4.0737	0.2113		9840	3.19

Table 7. Four Point Flexure of ZnSe

Specimen Number	Density (gms/cc)	Sonic Velocity (in./µsec)	Temperature °F	Ultimate Flexure Strength (psi)	Initial Modulus (10^6 psi)	Comments
16	5.2406	0.1742	70	6700	10.59	10.47 Strain Gage
17	5.2371	0.1741	70	7240	11.38	
1	5.2381	0.1740	70	5240	10.18	
6	5.2429	0.1740	70	5815	10.46	
11	5.2507	0.1743	70	5900	10.53	
Average	5.24419	0.1741		6180	10.63	
7	5.2451	0.1741	500	7310	9.02	
2	5.2438	0.1740	500	10531	8.98	
19	5.2428	0.1742	500	7755	8.87	
12	5.2378	0.1741	500	8385	10.00	
20	5.2455	0.1742	500	9185	9.75	
Average	5.2778	0.1741		8633	9.32	
3	5.2438	0.1740	1000	8840	7.06	
13	5.2431	0.1742	1000	>7427	8.86	Bottomed Out
8	5.2413	0.1742	1000	6890	6.81	
Average	5.2427	0.1741		>7720	7.58	Yield ∿ 1500 psi
9	5.2421	0.1743	1500	>5170	5.87	Bottomed Out
14	5.2357	0.1742	1500	>6510	6.26	Bottomed Out
4	5.2520	0.1741	1500	>7353	6.19	Bottomed Out
Average	5.2433	0.1742		>6345	6.11	Yield ∿ 1000 psi
5	5.2407	0.1742	1800	>5700	5.23	Bottomed Out
10	5.2405	0.1742	1800	>2980	5.54	Bottomed Out
15	5.2392	0.1743	1800	>6000	6.32	Bottomed Out
Average	5.2401	0.1742		>4890	5.71	Yield ∿ 1000 psi

Table 8. Tensile Results for Sapphire

Specimen Number	Density (gms/cc)	Sonic Velocity (in./μsec)	Temperature °F	Ultimate Strength (psi)	Initial Modulus (x 10⁶ psi)	Strain to Failure (in./in.)	Comments
T-2	-	0.4029	70	49180	45.70	0.0010	
T-3	-	0.4092	70	44000	55.17	0.0008	
T-4	-	0.4076	70	43000	50.00	0.0009	
T-5	-	0.4072	70	45520	54.89	0.0008	
T-1	-	0.4072	70	39350	50.31	0.0008	Head failure
Average	-	0.4068	-	44270	51.21	0.0009	
				(45,440)			(Without T-1)

Table 9. Tensile Results for Spinel

Specimen Number	Density (gms/cc)	Sonic Velocity (in./μsec)	Temperature °F	Ultimate Strength (psi)	Initial Modulus (10⁶ psi)	Strain to Failure (in./in.)
T-1	-	0.3512	70	12960	41.37	0.00030
T-2	-	0.3525	70	12004	39.75	0.00031
T-3	-	0.3526	70	15920	40.88	0.00040
T-5	-	0.3528	70	15860	40.87	0.00039
Average		0.3523		14186	40.72	0.00035

Table 1C. Tensile Results for ZnS

Specimen Number	Density (gms/cc)	Sonic Velocity (in./μsec)	Temperature °F	Ultimate Strength (psi)	Initial Modulus (10^6 psi)	Strain to Failure (in./in.)
T-1	-	0.2166	70	2700	10.42	0.000275
T-2	-	0.2113	70	4270	11.49	0.00035
T-3	-	0.2116	70	3650	11.30	0.00032
T-5	-	0.2115	70	3640	12.20	0.00030
Average		0.2128		3565	11.35	0.00031

Table 11. Tensile Results for ZnSe

Specimen Number	Density (gms/cc)	Velocity (in./μsec)	Temperature °F	Ultimate Flexure Strength (psi)	Initial Modulus (10⁶ psi)	Strain to Failure (in./in.)
T-1	-	0.1743	70	2480	10.00	0.00024
T-2	-	0.1742	70	3460	11.73	0.00034
T-3	-	0.1726	70	2880	12.27	0.00024
T-4	-	0.1743	70	1840	12.16	0.00015
Average	-	0.1739	-	2665	11.54	0.00024

Table 12. Initial Compressive Moduli of Sapphire (10^6 psi)

Temperature °F	0	C-1	C-8	Average
70	53.1	55.9[1]	54.8[2]	54.6
200	53.1	55.9	54.8	54.6
400	54.6	55.9	54.8	55.1
600	50.0	55.9	54.8	53.6
800	48.6	-	54.8	51.7
1000	49.8	50.61	52.0	50.8
1200	48.6	50.61	52.0	50.4
1400	48.9	50.61	52.0	50.5
1600	48.0	50.61	53.33	50.6
1800	46.9	46.5	54.05	49.1
2000	46.9	42.55	43.96	44.5
2200	41.2	28.8	40.8	36.9
2400	39.8	32.8	35.4	37.8
2600	36.4	29.2	35.4	33.6
2800	30.7	28.2	25.0	27.9

[1]Strain Gage Value, 50 x 10^6 psi, $\nu = 0.29$

[2]Strain Gage Value, 52 x 10^6 psi, $\nu = 0.29$

Table 13. Initial Compressive Moduli of Spinel (10^6 psi)

Temperature °F	#3	C-6[1]	C-7	Average
70	46.5	48.8	47.6	47.6
200	42.1	48.8	47.6	46.1
400	36.3	48.8	44.4	43.2
600	36.4	42.5	45.4	41.4
800	38.1	45.9	45.4	43.1
1000	34.7	45.9	44.9	41.8
1200	34.1	48.7	44.4	42.4
1400	28.7	44.4	43.0	38.7
1600	26.7	47.0	45.4	39.7
1800	23.6	40.0	44.4	36.0
2000	22.2	40.0	38.8	33.7
2200	21.1	42.1	43.5	35.6
2400	17.2	38.5	40.0	31.9
2600	17.7	39.2	40.0	32.3
2800	12.5	30.1	35.4	26.0
3000	7.7	23.5	32.0	21.0
3200	4.6	20.6	19.7	14.9

[1]Strain Gage Modulus = 47 x 10^6 psi, ν = 0.315

Table 14. Initial Compressive Moduli of ZnS (10^6 psi)

Temperature °F	C-2	C-3	C-1	Average
70	11.4	10.0[1]	10.9	10.8
200	11.1	10.0	12.0	11.0
400	11.1	9.8	12.5	11.0
600	10.5	10.0	12.5	11.0
800	10.3	9.6	11.6	10.5
1000	10.0	9.8	9.3	9.7
1200	10.0	9.8	7.8	9.2
1400	9.8	8.0	7.0	8.3
1600	7.3	5.2	5.7	6.1
1800	5.0	5.0	4.4	4.8
2000	4.7	5.0	4.6	4.8
2200	4.3	3.6	3.8	3.9
2400			3.5 (1.3)	

[1]Strain Gage Modulus = 10.9 (ν = 0.38?)

Table 15. Initial Compressive Moduli of ZnSe (10^6 psi)

Temperature °F	C-4	C-5	Average
70	10.9[1]	10.8	10.8
200	10.9	10.0	10.5
400	10.9	9.9	10.4
600	10.9	10.1	10.5
800	10.1	8.4	9.3
1000	9.3	7.4	8.3
1200	10.0?	7.7	8.8
1400	8.1	7.7	7.9
1600	7.0	5.9	6.5
1800	6.7	5.1	5.9
2000	4.5	5.2	4.8
2200	1.7	2.8	2.3

[1]Strain Gage Modulus = 10.2×10^6 psi, ν = 0.21

Table 16. Thermal Expansion of 60° Sapphire Measured in Quartz Dilatometer

Specimen and Run Number	Temperature °F	Observed Total Elongation (10^{-3} in.)	Observed Unit Elongation (10^{-3} in./in.)	Unit Correction for Dilatometer Motion (10^{-3} in./in.)	Corrected Specimen Unit Elongation (10^{-3} in./in.)
Specimen: Sapphire CTE-1	70	0.0	0.0	0.0	0.0
Run No: NOB0553-67-28 BPR	250	1.73	0.57	0.06	0.63
Initial Length: 3.0142 in.	500	5.03	1.67	0.14	1.81
Final Length: 3.0142 in.	750	8.83	2.93	0.21	3.14
Initial Weight: 52.2365 gm	1010	12.63	4.19	0.26	4.45
Final Weight: 52.2360 gm	1268	16.44	5.45	0.31	5.76
	1515	20.81	6.90	0.38	7.28
	69	- 0.23	-0.08	0.0	-0.08

Table 17. Thermal Expansion of 60° Sapphire Measured in Quartz Dilatometer

Specimen and Run Number	Temperature °F	Observed Total Elongation (10⁻³ in.)	Observed Unit Elongation (10⁻³ in./in.)	Unit Correction for Dilatometer Motion (10⁻³ in./in.)	Corrected Specimen Unit Elongation (10⁻³ in./in.)
Specimen: Sapphire CTE-2	72	0.0	0.0	0.0	0.0
Run No: NOB0553-124-28 BPR	250	1.51	0.50	0.06	0.56
Initial Length: 3.0150 in.	500	4.76	1.58	0.14	1.72
Final Length: 3.0150 in.	750	8.44	2.80	0.20	3.00
Initial Weight: 52.2847 gm	1000	11.98	3.97	0.25	4.22
Final Weight: 52.2849 gm	1250	15.68	5.20	0.31	5.51
	1500	19.78	6.56	0.37	6.93
	71	-0.02	-0.01	0	-0.01

126

Table 18. Thermal Expansion of 60° Sapphire Measured in Graphite Dilatometer

Specimen and Run No.	Temp °F	Time	Observed Total Elongation (10^{-3} in.)	Observed Unit Elongation (10^{-3} in./in.)	Unit Correction for Dilatometer Motion (10^{-3} in./in.)	Corrected Specimen Unit Elongation (10^{-3} in./in.)
Specimen: Sapphire CTE-1	70	8:12	0.0	0.0	0.0	0.0
Run No: N0C0240-38-163 CTE	500	8:30	3.69	1.22	0.32	1.54
Initial Length: 3.0142 in.	1000	8:50	8.99	2.98	0.95	3.93
Final Length: 3.0151 in.	1500	9:10	14.42	4.78	1.78	6.56
Initial Weight: 52.2360 gm	1797	9:23	17.84	5.92	2.32	8.24
Final Weight: 51.8083 gm	1979	9:30	20.20	6.70	2.68	9.38
	2235	9:37	23.30	7.73	3.22	10.95
	2493	9:45	26.70	8.86	3.82	12.68
	2674	9:54	29.19	9.68	4.26	13.94
	2982	10:08	33.18	11.01	4.98	15.99
	3382	10:24	37.89	12.57	6.00	18.57
	70	7:53	0.36	0.12	0.0	0.12

Table 19. Thermal Expansion of 60° Sapphire Measured in Graphite Dilatometer

Specimen and Run No.	Temp °F	Time	Observed Total Elongation (10⁻³ in.)	Observed Unit Elongation (10⁻³ in./in.)	Unit Correction for Dilatometer Motion (10⁻³ in./in.)	Corrected Specimen Unit Elongation (10⁻³ in./in.)
Specimen: Sapphire CTE-2	70	8:14	0.0	0.0	0.0	0.0
Run: NOC0240-32-163 CTE	500	8:36	3.63	1.20	0.32	1.52
Initial Length: 1000	1000	9:00	9.13	3.03	0.95	3.98
3.0150 in.						
Final Length:	1511	9:20	14.56	4.83	1.81	6.64
3.0155 in.						
Initial Weight:	1989	9:35	20.13	6.68	2.72	9.40
52.2849 gm	2392	9:52	25.23	8.37	3.60	11.97
Final Weight:	2563	9:57	27.46	9.11	4.00	13.11
51.9249 gm	2816	10:07	30.73	10.19	4.58	14.77
	3078	10:23	34.13	11.32	6.12	16.53
	3382	10:33	37.93	12.58	6.00	18.58
	70	7:45	0.43	0.14	0.0	0.14

Table 20. Thermal Expansion of 0° Sapphire Measured in Quartz Dilatometer

Specimen and Run Number	Temperature °F	Observed Total Elongation (10⁻³ in.)	Observed Unit Elongation (10⁻³ in./in.)	Unit Correction for Dilatometer Motion (10⁻³ in./in.)	Corrected Specimen Unit Elongation (10⁻³ in./in.)
Specimen: Sapphire CTE-3 Run No: N0B0553-74-28 BPR	72	0.0	0.0	0.0	0.0
	250	1.48	0.49	0.06	0.55
Initial Length: 3.0170 in.	500	4.18	1.39	0.14	1.53
Final Length: 3.0172 in.	750	7.59	2.52	0.21	2.73
Initial Weight: 52.1587 gm	1000	10.85	3.60	0.25	3.85
Final Weight: 52.1584 gm	1250	14.20	4.71	0.31	5.02
	1500	17.80	5.90	0.37	6.27

Table 21. Thermal Expansion of 0° Sapphire Measured in Quartz Dilatometer

Specimen and Run Number	Temperature °F	Observed Total Elongation (10^{-3} in.)	Observed Unit Elongation (10^{-3} in./in.)	Unit Correction for Dilatometer Motion (10^{-3} in./in.)	Corrected Specimen Unit Elongation (10^{-3} in./in.)
Specimen: Sapphire CIE-4 Run: NOB0553-121-28 BPR Initial Length: 3.0152 in. Final Length: 3.0152 in. Initial Weight: 52.1414 gm Final Weight: 52.1412 gm	72	0.0	0.0	0.0	0.0
	250	1.29	0.43	0.06	0.49
	500	4.13	1.37	0.14	1.51
	750	7.23	2.40	0.20	2.60
	1000	10.68	3.54	0.25	3.79
	1250	14.21	4.71	0.31	5.02
	1500	17.87	5.93	0.38	6.31
	72	0.10	0.03	0.0	0.03

Table 22. Thermal Expansion of 0° Sapphire Measured in Graphite Dilatometer

Specimen and Run No.	Temp °F	Time	Observed Total Elongation (10⁻³ in.)	Observed Unit Elongation (10⁻³ in./in.)	Unit Correction for Dilatometer Motion (10⁻³ in./in.)	Corrected Specimen Unit Elongation (10⁻³ in./in.)
Specimen: Sapphire CTE-3	70	8:25	0.0	0.0	0.0	0.0
Run No: NOC0240-35-163 CTE	500	8:40	2.69	0.89	0.32	1.21
Initial Length: 3.0165 in.	1000	8:58	8.19	2.72	0.95	3.67
Final Length: 3.0175 in.	1500	9:18	12.69	4.21	1.78	5.99
Initial Weight: 52.1584 gm	1787	9:36	16.19	5.37	2.32	7.69
Final Weight: 51.8023 gm	1964	9:44	18.02	5.97	2.68	8.65
	2391	9:58	23.09	7.65	3.60	11.25
	2563	10:05	24.94	8.27	4.00	12.27
	2765	10:15	27.29	9.05	4.47	13.52
	2997	10:25	30.19	10.01	5.02	15.03
	3382	10:38	34.24	11.35	6.00	17.35
	70	7:50	0.88	0.29	0.0	0.29

Table 23. Thermal Expansion of 0° Sapphire Measured in Graphite Dilatometer

Specimen and Run No.	Temp °F	Time	Observed Total Elongation (10^{-3} in.)	Observed Unit Elongation (10^{-3} in./in.)	Unit Correction for Dilatometer Motion (10^{-3} in./in.)	Corrected Specimen Unit Elongation (10^{-3} in./in.)
Specimen: Sapphire CTE-4	70	8:15	0.0	0.0	0.0	0.0
Run: NOC0240-36-171 BK3	772	8:33	6.38	2.12	0.35	2.47
Initial Length: 3.0152 in.	1469	8:55	13.96	4.63	1.17	5.80
Final Length: 3.0150 in.	1908	9:08	19.18	6.36	1.93	8.29
Initial Weight: 52.1412 gm	2064	9:16	21.35	7.08	2.19	9.27
Final Weight: 51.9550 gm	2250	9:26	23.28	7.72	2.53	10.25
	2473	9:36	26.18	8.68	2.89	11.57
	2785	9:51	30.19	10.01	3.47	13.48
	3038	10:04	33.70	11.18	3.93	15.11
	3402	10:17	38.08	12.63	4.66	17.29
	70	7:54	-0.02	-0.01	0.0	-0.01

132

Table 24. Thermal Expansion of Spinel Measured in Quartz Dilatometer

Specimen and Run Number	Temperature °F	Observed Total Elongation (10^{-3} in.)	Observed Unit Elongation (10^{-3} in./in.)	Unit Correction for Dilatometer Motion (10^{-3} in./in.)	Corrected Specimen Unit Elongation (10^{-3} in./in.)
Specimen: Spinel TE-1 Run No: N080553-112-28 BPR	73	0.0	0.0	0.0	0.0
Initial Length: 3.0012 in.	250	1.36	0.45	0.06	0.51
Final Length: 3.0012 in.	500	4.48	1.49	0.14	1.63
Initial Weight: 45.5467 gm	750	7.58	2.53	0.20	2.73
Final Weight: 45.5460 gm	1000	11.12	3.71	0.25	3.96
	1250	15.21	5.07	0.3i	5.38
	1500	18.71	6.23	0.38	6.61
	75	0.03	0.01	0.0	0.01

133

Table 25. Thermal Expansion of Spinel Measured in Quartz Dilatometer

Specimen and Run Number	Temperature °F	Observed Total Elongation (10^{-3} in.)	Observed Unit Elongation (10^{-3} in./in.)	Unit Correction for Dilatometer Motion (10^{-3} in./in.)	Corrected Specimen Unit Elongation (10^{-3} in./in.)
Specimen: Spinel TE-2 Run No: NOBO553-64-28 BPR	72	0.0	0.0	0.0	0.0
Initial Length: 3.0011 in.	250	1.28	0.43	0.06	0.49
Final Length: 3.0012 in.	500	4.52	1.51	0.15	1.66
Initial Weight: 44.7132 gm	750	8.06	2.68	0.21	2.89
Final Weight: 44.7132 gm	1000	11.82	3.94	0.25	4.19
	1250	16.09	5.36	0.31	5.67
	1500	20.22	6.74	0.37	7.11
	70	0.26	0.09	0.0	0.09

Table 26. Thermal Expansion of Spinel Measured in Graphite Dilatometer

Specimen and Run No.	Temp °F	Time	Observed Total Elongation (10^{-3} in.)	Observed Unit Elongation (10^{-3} in./in.)	Unit Correction for Dilatometer Motion (10^{-3} in./in.)	Corrected Specimen Unit Elongation (10^{-3} in./in.)
Specimen: Spinel #1 Run No: NOC0240-37-163 CTE Initial Length: 3.0012 in. Final Length: 3.0010 in. Initial Weight: 45.5450 gm Final Weight: 45.5166 gm	70	8:15	0.0	0.0	0.0	0.0
	500	8:31	3.27	1.09	0.32	1.41
	1000	8:53	8.23	2.74	0.95	3.69
	1500	9:20	13.73	4.57	1.78	6.35
	1782	9:26	17.60	5.86	2.31	8.17
	1989	9:37	19.98	6.66	2.72	9.38
	2351	9:51	24.11	8.03	3.50	11.53
	2513	9:59	26.30	8.76	3.87	12.63
	2865	10:17	30.58	10.19	4.71	14.90
	2946	10:28	31.68	10.56	4.87	15.43
	70	7:53	- 0.24	- 0.08	0.0	- 0.08

Table 27. Thermal Expansion of Spinel Measured in Graphite Dilatometer

Specimen and Run No.	Temp °F	Time	Observed Total Elongation (10^{-3} in.)	Observed Unit Elongation (10^{-3} in./in.)	Unit Correction for Dilatometer Motion (10^{-3} in./in.)	Corrected Specimen Unit Elongation (10^{-3} in./in.)
Specimen: Spinel #2 Run No: NOCO240-33-163 CTE Initial Length: 3.0012 in. Final Length: 3.0006 in. Initial Weight: 44.7132 gm Final Weight: 44.6968 gm	70	8:44	0.0	0.0	0.0	0.0
	500	9:00	3.05	1.02	0.32	1.34
	1000	9:30	8.22	2.74	0.95	3.69
	1500	9:45	14.22	4.74	1.78	6.52
	1697	9:56	15.97	5.32	2.12	7.44
	1968	10:08	19.64	6.54	2.69	9.23
	2351	10:17	23.64	7.88	3.50	11.38
	2493	10:30	25.92	8.61	3.82	12.43
	2775	10:40	29.28	9.76	4.50	14.26
	2957	10:50	31.67	10.55	4.92	15.47
	70	7:44	- 0.45	- 0.15	0.0	- 0.15

136

Table 28. Thermal Expansion of Zinc Sulfide Measured in Quartz Dilatometer

Specimen	Time	Specimen Temperatures - °F			Observed Total Elongation 10^{-3} in.	Observed Unit Elongation 10^{-3} in./in.	Unit Elongation Correction for Dilatometer Motion 10^{-3} in./in.	Corrected Specimen Unit Elongation 10^{-3} in./in.
		Top	Bottom	Average				
Specimen: ZnS-1		Initial Length: 3.0187 in.			Initial Weight: 54.2000 gm			
Run: NOCO107-58-27 BPR		Final Length: 3.0185 in.			Final Weight: 54.1873 gm			
	1:45	70	70	70	0.0	0.0	0.0	0.0
	1:56	100	100	100	0.13	0.04	0.01	0.05
	2:04	200	200	200	1.05	0.35	0.05	0.40
	2:15	300	300	300	2.49	0.82	0.09	0.91
	2:20	400	400	400	3.34	1.11	0.12	1.23
	2:26	450	450	450	4.12	1.36	0.14	1.50
	2:36	550	550	550	5.32	1.76	0.17	1.93
	2:47	650	650	650	6.50	2.15	0.21	2.36
	2:55	750	750	750	7.92	2.62	0.23	2.85
	3:00	850	850	850	9.12	3.02	0.26	3.28
	3:10	950	950	950	10.72	3.55	0.29	3.84
	3:16	1050	1050	1050	11.92	3.95	0.31	4.26
	3:25	1150	1150	1150	13.51	4.48	0.33	4.81
	3:30	1250	1250	1250	14.92	4.94	0.37	5.31
	3:35	1350	1350	1350	16.32	5.41	0.39	5.80
	3:40	1450	1450	1450	18.12	6.00	0.42	6.42
	3:45	1550	1550	1550	19.52	6.47	0.45	6.92
	3:50	1650	1650	1650	21.23	7.03	0.48	7.51
	4:00	1750	1750	1750	22.94	7.60	0.51	8.10
	4:03	1800	1800	1800	23.62	7.82	0.52	8.34
	1:05	70	70	70	-0.06	-0.02	0.0	-0.02

Table 29. Thermal Expansion of Zinc Sulfide Measured in Quartz Dilatometer

Specimen: ZnS-2
Run: NOC0107-60-29 BPR

Initial Length: 3.0141 in. Final Length: 3.0145 in.
Initial Weight: 54.1187 gm Final Weight: 54.0729 gm

Specimen Time	Specimen Temperatures - °F			Observed Total Elongation 10⁻³ in.	Observed Unit Elongation 10⁻³ in./in.	Unit Elongation Correction for Dilatometer Motion 10⁻³ in./in.	Corrected Specimen Unit Elongation 10⁻³ in./in.
	Top	Bottom	Average				
1:45	70	70	70	0.0	0.0	0.0	0.0
1:52	100	100	100	0.19	0.06	0.01	0.07
2:00	200	200	200	1.33	0.46	0.05	0.51
2:14	300	300	300	2.64	0.88	0.08	0.96
2:20	400	400	400	3.60	1.19	0.11	1.30
2:27	500	500	500	5.03	1.67	0.14	1.81
2:37	600	600	600	6.68	2.22	0.17	2.39
2:45	700	700	700	7.78	2.58	0.20	2.78
2:54	800	800	800	9.07	3.01	0.23	3.24
3:03	900	900	900	10.40	3.45	0.26	3.71
3:11	1000	1000	1000	12.03	3.99	0.28	4.27
3:17	1100	1100	1100	13.38	4.44	0.31	4.75
3:24	1200	1200	1200	14.93	4.95	0.33	5.28
3:30	1300	1300	1300	16.18	5.37	0.36	5.73
3:35	1400	1400	1400	17.68	5.87	0.39	6.25
3:40	1500	1500	1500	19.18	6.36	0.41	6.77
3:46	1600	1600	1600	20.76	6.89	0.45	7.34
3:51	1700	1700	1700	22.39	7.43	0.48	7.91
4:00	1800	1800	1800	23.98	7.96	0.51	8.47
1:06	70	70	70	0.39	0.13	0.0	0.13

Table 30. Thermal Expansion of ZnSe Measured in Quartz Dilatometer

Specimen	Time	Specimen Temperatures - °F			Observed Total Elongation 10⁻³ in.	Observed Unit Elongation 10⁻³ in./in.	Unit Elongation Correction for Dilatometer Motion 10⁻³ in./in.	Corrected Specimen Unit Elongation 10⁻³ in./in.
		Top	Bottom	Average				
	2:00	70	70	70	0.0	0.0	0.0	0.0
	2:09	189	189	189	1.02	0.34	0.04	0.38
	2:18	250	250	250	2.02	0.67	0.06	0.73
	2:23	350	350	350	3.30	1.09	0.09	1.18
	2:35	450	450	450	4.65	1.54	0.12	1.66
	2:44	550	550	550	5.90	1.96	0.16	2.12
	2:51	650	650	650	7.70	2.55	0.18	2.73
	2:55	750	750	750	8.90	2.95	0.22	3.17
	3:00	850	850	850	10.32	3.42	0.24	3.66
	3:06	950	950	950	11.75	3.90	0.27	4.17
	3:13	1050	1050	1050	13.30	4.41	0.30	4.71
	3:18	1150	1150	1150	14.90	4.94	0.32	5.26
	3:22	1250	1250	1250	16.70	5.54	0.35	5.89
	3:27	1350	1350	1350	18.54	5.15	0.37	6.52
	3:32	1450	1450	1450	20.05	6.65	0.40	7.05
	3:38	1550	1550	1550	21.32	7.07	0.43	7.50
	3:46	1650	1650	1650	22.88	7.59	0.46	3.05
	3:53	1750	1750	1750	24.68	8.18	0.49	8.67
	3:57	1900	1750	1800	25.42	8.43	0.51	8.94
	1:38	70	70	70	0.19	0.06	0.0	0.06

Specimen: ZnSe-2
Run: NOCO107-63-29 BPR

Initial Length: 3.0161 in.
Final Length: 3.0168 in.

Initial Weight: 69.6984 gm
Final Weight: 69.6562 gm

139

Table 31. Thermal Expansion of ZnSe Measured in Quartz Dilatometer

Specimen	Time	Specimen Temperatures - °F			Observed Total Elongation 10^{-3} in.	Observed Unit Elongation 10^{-3} in./in.	Unit Elongation Correction for Dilatometer Motion 10^{-3} in./in.	Corrected Specimen Unit Elongation 10^{-3} in./in.
		Top	Bottom	Average				
Specimen: ZnSe-1 Run: NOCu107-62-27 BPR	2:00	70	70	70	0.0	0.0	0.0	0.0
	2:09	100	100	100	0.14	0.05	0.01	0.06
	2:19	200	200	200	1.24	0.41	0.05	0.46
	2:27	300	300	300	2.31	0.77	0.09	0.86
	2:34	400	400	400	3.53	1.17	0.12	1.29
	2:42	500	500	500	5.37	1.78	0.16	1.94
	2:49	600	600	600	6.67	2.21	0.19	2.40
	2:56	700	700	700	8.02	2.66	0.22	2.88
	3:02	800	800	800	9.52	3.16	0.25	3.41
	3:08	900	900	900	11.04	3.66	0.28	3.94
	3:14	1000	1000	1000	12.82	4.25	0.30	4.55
	3:17	1100	1100	1100	13.97	4.63	0.33	4.96
	3:22	1200	1200	1200	15.72	5.21	0.35	5.56
	3:27	1300	1300	1300	17.79	5.90	0.38	6.28
	3:32	1400	1400	1400	19.47	6.46	0.41	6.87
	3:37	1500	1500	1500	20.77	6.89	0.43	7.32
	3:43	1600	1600	1600	22.42	7.43	0.46	7.89
	3:51	1700	1700	1700	24.32	8.06	0.49	8.55
	3:59	1800	1800	1800	26.02	8.63	0.52	9.15
	1:38	70	70	70	0.63	0.21	0.0	0.21

Initial Length: 3.0162 in.
Final Length: 3.0169 in.
Initial Weight: 69.6893 gm
Final Weight: 69.6592 gm

140

TABLE 32. Enthalpy of Sapphire Measured in the Adiabatic Calorimeter

Specimen	Run	Initial Cup Temp. °F	Final Cup Temp. °F	Change in Cup Temp. °F	Initial Sample Temp. °F	Initial Weight of Sample gm	Final Weight of Sample gm	Enthalpy $h = \frac{k}{Ws}(t_2-t_1)$ Btu/lb	Enthalpy Btu/lb Above 85 °F Ref.	Above 32 °F Ref.
NOB02O										
HC-1	119	71.55	73.59	2.04	254.5	6.3107	6.3105	38.92	36.46	47.87
HC-1	119	73.00	81.13	8.13	678.0	6.3105	6.3104	155.10	154.09	167.82
HC-1	120	78.04	90.04	12.0	1022	6.3104	6.3104	228.93	230.17	243.12
HC-2	152	104.182	108.957	4.775	501	7.4668	7.4668	76.99	81.77	92.17
NOC0215										
HC-1	35	86.174	91.696	5.522	567	6.3104	6.3104	105.35	106.84	118.58

141

Table 33. Enthalpy of Sapphire in Ice Calorimeter

Specimen Number	SRI Run Number	Drop Temperature °F	Initial Weight Grams	Final Weight Grams	Enthalpy from Drop Temperature to 32 °F Btu/lb
HC-1	36	2541	6.3104	6.3104	681.6
HC-1	37	3270	6.3104	6.3104	922.13
HC-2	40	2014	7.4668	7.4686	493.31
HC-1	31	1529	6.3104	6.3104	378.36

TABLE 34. Enthalpy of Spinel Measured in the Adiabatic Calorimeter

Specimen	Run	Initial Cup Temp. °F	Final Cup Temp. °F	Change in Cup Temp. °F	Initial Sample Temp. °F	Initial Weight of Sample gm	Final Weight of Sample gm	Enthalpy $h = \frac{k}{W_s}(t_2-t_1)$ Btu/lb	Enthalpy Btu/lb Above 85 °F Ref.	Enthalpy Btu/lb Above 32 °F Ref.
NOB020										
HC-1	114	77.64	82.74	5.10	223	21.3527	21.3526	28.75	28.29	39.16
HC-1	116	81.44	96.48	15.04	473	21.3526	21.3520	84.80	86.83	99.31
HC-1	118	74.71	111.86	37.15	984	21.3520	21.3514	209.76	215.95	228.73
NOC0215										
HC-2	32	78.261	105.565	27.304	751	21.6590	21.6574	151.77	156.61	169.07

143

Table 35. Enthalpy of Spinel in Ice Calorimeter

Specimen Number	SRI Run Number	Drop Temperature °F	Initial Weight Grams	Final Weight Grams	Enthalpy from Drop Temperature to 32 °F Btu/lb
	NOCO215				
HC-1	36	1679	21.3514	21.3617	421.93
HC-1	37	2448	21.3617	21.3564	688.0
HC-1	38	2992	21.3564	21.3276	894.9
HC-2	41	2032	21.6574	21.6658	534.24
HC-2	51	2765	21.6658	21.6558	798.81

TABLE 36. Enthalpy of Zinc Sulfide Measured in the Adiabatic Calorimeter

Specimen	Run	Initial Cup Temp. °F	Final Cup Temp. °F	Change in Cup Temp. °F	Initial Sample Temp. °F	Initial Weight of Sample gm	Final Weight of Sample gm	Enthalpy $h = \frac{k}{Ws}(t_2-t_1)$ Btu/lb	Enthalpy Btu/lb Above 85 °F Ref.	Enthalpy Btu/lb Above 32 °F Ref.
NOB020										
HC-1	114	75.50	77.64	2.14	204	16.9873	16.9864	15.17	14.29	20.65
HC-1	115	75.18	81.44	6.26	460	16.9864	16.9849	44.37	43.24	49.35
HC-1	117	73.94	83.65	9.71	662	16.9849	16.9835	68.83	68.67	74.98
HC-1	117	73.61	88.65	15.04	976	16.9835	16.9828	106.61	107.04	113.41
NOC0215										
HC-1	33	85.478	104.455	18.977	1229	16.9828	16.9758	134.58	136.91	143.25
HC-2	34	78.261	86.435	8.174	590	16.3852	16.9843	57.94	58.10	64.20

Table 37. Enthalpy of Zinc Sulfide in Ice Calorimeter

Specimen Number	SRI Run Number	Drop Temperature °F	Initial Weight Grams	Final Weight Grams	Enthalpy from Drop Temperature to 32 °F Btu/lb
	NOC0215				
HC-1	38	1513	16.9758	16.9748	180
HC-1	39	1813	16.9748	16.9207	222.0

146

TABLE 38. Enthalpy of Zinc Selenide Measured in the Adiabatic Calorimeter

Specimen	Run	Initial Cup Temp. °F	Final Cup Temp. °F	Change in Cup Temp. °F	Initial Sample Temp. °F	Initial Weight of Sample gm	Final Weight of Sample gm	Enthalpy $h = \frac{k}{Ws}(t_2 - t_1)$ Btu/lb	Enthalpy Btu/lb Above 85 °F Ref.	Enthalpy Btu/lb Above 32 °F Ref.
NOB020										
HC-1	115	82.74	84.77	2.03	237	21.7212	21.7186	11.25	11.23	15.26
HC-1	116	83.97	90.94	6.97	556	21.7186	21.7158	38.64	39.14	43.55
HC-1	118	75.01	89.61	14.60	1028	21.7158	21.4124	82.09	82.50	87.10
NOC0215										
HC-2	33	105.217	114.130	9.044	752	21.6856	21.6806	50.22	51.75	56.69
HC-1	34	104.318	121.409	17.091	1293	21.4124	18.4949	111.24	114.89	119.73

Table 39.   Enthalpy of Zinc Selenide in Ice Calorimeter

Specimen Number	SRI Run Number	Drop Temperature °F	Initial Weight Grams	Final Weight Grams	Enthalpy from Drop Temperature to 32 °F Btu/lb
	NOC0215				
HC-1	39	1598	18.4949	18.4510	151.0
HC-1	40	1823	18.4510	18.1609	188.07

Table 40. Sapphire Summary of Properties[1,2]

Temperature - °F

	Units	70	1500	2000	2500	3000
Flexural Modulus	10^6 psi	64.8 [52.4]	--	56.8 [42.0]	52.9	47.5
Flexural Strength	10^3 psi	130 (73.6) [73.5]	--	83.6 [33.2]	89.5	49.5
Compressive Modulus	10^6 psi	[54.6]	[50.5]	[44.5]	[35.7]	---
Poisson's Ratio	---	0.29				
Tensile Modulus	10^6 psi	[51.2]				
Tensile Strength	10^3 psi	[44.3]				
Tensile Ultimate Strain	10^{-3} in./in.	[0.88]				
Thermal Conductivity	Btu-in./hr-ft^2-°F	120[3]	46	40	37	42
Thermal Expansion	10^{-3} in./in.	0	6.25 [0.675]	8.8 [9.3]	11.7 [13.7]	14.7 [17]
Specific Heat	Btu/lb-°F	0.215	0.295	0.305		0.321

[1]Values in parenthesis are 60/40 polish
[2]Values in brackets are 60° orientation
[3]At 500 °F

149

Table 41. Spinel Summary of Properties

	Units	Temperature - °F					
		70	1000	1500	2000	2500	3000
Flexural Modulus	10^6 psi	40.2	35.9	-	31.9	19.8	13.8
Flexural Strength	10^3 psi	13.5	10.1	-	9.3	9.5	6.8
Compressive Modulus	10^6 psi	47.6	41.8	39.2	33.7	32.1	21.0
Poisson's Ratio	-	0.31					
Tensile Modulus	10^6 psi	40.7					
Tensile Strength	10^3 psi	14.2					
Tensile Ultimate Strain	10^{-3} in./in.	0.35					
Thermal Conductivity	Btu-in./hr-ft^2-°F	60 (500)	41	34	31	31	41
Thermal Expansion	10^{-3} in./in.	0	4.0	6.51	9.5	12.5	15.8
Specific Heat	Btu/lb-°F	0.22	0.274	0.303	0.331	0.352	0.37

Table 42. Zinc Sulfide Summary of Properties

| | Units | Temperature - °F | | | | | |
		70	500	1000	1500	1800
Flexural Modulus	10^6 psi	10.6	9.0	6.7	4.9	3.2
Flexural Strength	10^3 psi	9.3	11.4	13.6	12.9	9.8
Compressive Modulus	10^6 psi	10.8	11.0	9.7	7.2	4.8
Poisson's Ratio	-	0.38				
Tensile Modulus	10^6 psi	11.3				
Tensile Strength	10^3 psi	3.6				
Tensile Ultimate Strain	10^{-3} in./in.	0.31				
Thermal Conductivity	Btu-in./hr-ft²-°F	-	67	45	52	80
Thermal Expansion	10^{-3} in./in.	0	1.75	4.15	6.72	8.4
Specific Heat	Btu/lb-°F	0.115	0.120	0.125	0.130	0.135

Table 43. Zinc Selenide Summary of Properties

	Units	Temperature - °F				
		70	500	1000	1500	1800 °F
Flexural Modulus	10^6 psi	10.6	9.3	7.6	6.1	5.7
Flexural Strength	10^3 psi	6.2	8.6	7.7	>6.3	>4.9
Compressive Modulus	10^6 psi	10.8	10.5	8.3	7.2	5.9
Poisson's Ratio	--	0.21				
Tensile Modulus	10^6 psi	11.5				
Tensile Strength	10^3 psi	2.7				
Tensile Ultimate Strain	10^{-3} in./in.	0.24				
Thermal Conductivity	Btu-in./hr-ft^2-°F	--	55	40	55	--
Thermal Expansion	10^{-3} in./in.	--	1.85	4.45	7.3	9.05
Specific Heat	Btu/lb-°F	0.080	0.090	0.106	0.123	0.128

Table 44. Comparison of Predicted Tensile Loads at Failure to
Measured Tensile and Flexural Strengths at 70°

Material	Average 70° Flexural Strength (psi)	Average 70° Tensile Strength (psi)	Average Predicted Value (see Part 1) at Failure (psi)
Zinc Selenide	6,180	2,665	2,598
Zinc Sulfide	9,295	3,565	6,105
Sapphire (60°)	73,490	44,270	28,600
Spinel	13,461	14,186	15,433

Table 45. Comparison of Properties of Four Optical Materials

Property	Units	Spinel	Sapphire	ZnS	ZnSe
70° Flexural Strength	10³ psi	13.5	130.2/73.5*	9.3	6.2
70° Flexural Modulus	10⁶ psi	40.2	64.3/52.4*	10.6	10.6
70° Compressive Modulus	10⁶ psi	47.6	54.6*	10.8	10.8
70° Poisson's Ratio	-	0.31	0.29*	0.38?	0.21
70° Tensile Modulus	10⁶ psi	40.7	51.2*	11.3	11.5
70° Tensile Strength	10³ psi	14.2	44.3*	3.6	2.7
70° Tensile Ultimate Strain	10⁻³ in./in.	0.35	0.88*	0.31	0.24
500° Thermal Conductivity	Btu-in./hr-ft²-°F	60	120	67	55
1500° Thermal Conductivity	Btu-in./hr-ft²-°F	34	46	52	55
1500° Thermal Expansion	10⁻³ in./in.	6.51	6.25/6.75	6.72	7.30
500° Specific Heat	Btu/lb-°F	0.242	0.250	0.120	0.090

*60° Orientation

Appendix

SENSITIVITY STUDIES

The sensitivity studies in Reference 8 were conducted on Pyroceram® using nominal properties available prior to the data set developed under that effort. The analysis was conducted on a radome structure at aerodynamic heating condition somewhat exceeding those anticipated for the IR windows for which the materials under this effort were evaluated. The analysis was conducted using state of the art aerodynamic heating codes. the Asthma code for indepth heating analysis and SAAS-III body-of-revelation finite-element structural analysis. The material properties were modeled as elastic with equal tensile and compressive moduli which varied as a function of temperature.

Prior to initiating the testing effort, the peak stressed volumes and areas were calculated. These were comparable to the tensile specimens used in that effort. Note that the volume and surface areas are about the same as would be involved in the ID surface of an IR Dome despite the much larger size of the full radome as shown in Figure A-1.

The sensitivity studies were conducted by varying the properties listed in Table A-1 one at a time. As can be seen the most sensitive parameters in terms of stress generation were the stiffnesses and thermal expansion.

Appendix

SENSITIVITY STUDIES

The sensitivity studies in Reference 8 were conducted on Pyroceram® using nominal properties available prior to the data set developed under that effort. The analysis was conducted on a radome structure at aerodynamic heating condition somewhat exceeding those anticipated for the IR windows for which the materials under this effort were evaluated. The analysis was conducted using state of the art aerodynamic heating codes, the Asthma code for indepth heating analysis and SAAS-III body-of-revelation finite-element structural analysis. The material properties were modeled as elastic with equal tensile and compressive moduli which varied as a function of temperature.

Prior to initiating the testing effort, the peak stressed volumes and areas were calculated. These were comparable to the tensile specimens used in that effort. Note that the volume and surface areas are about the same as would be involved in the ID surface of an IR Dome despite the much larger size of the full radome as shown in Figure A-1.

The sensitivity studies were conducted by varying the properties listed in Table A-1 one at a time. As can be seen the most sensitive parameters in terms of stress generation were the stiffnesses and thermal expansion.
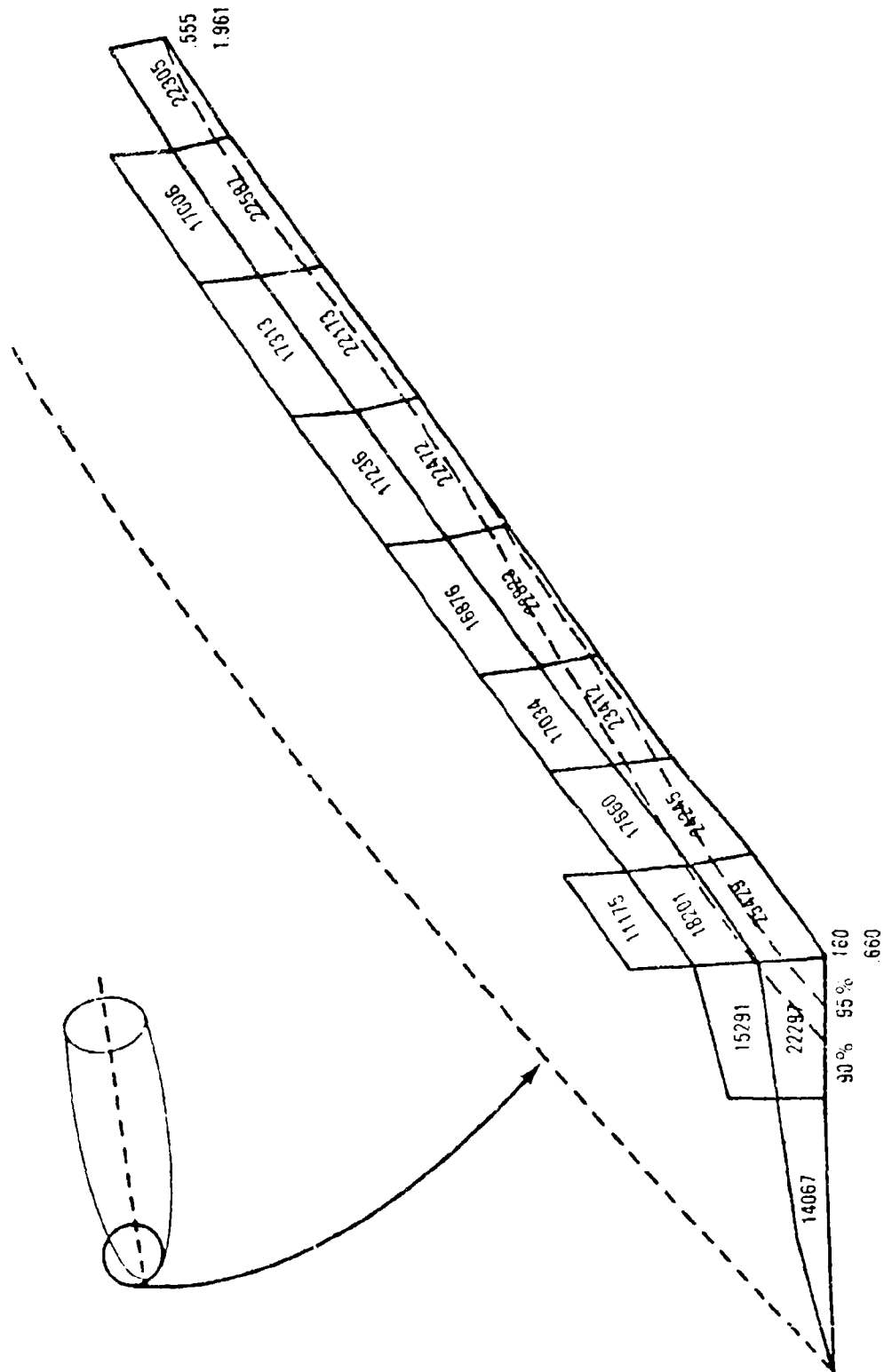
Figure A-1. Peak Stressed Volume and Surface Area for Radome Discussed in Part 1

TABLE A-1. Sensitivity Study Summary.

Error introduced	Parameter	Error in backface temp. rise, %	Error in max. theta stress, %
5%	Velocity	10	9
5%	Thermal conductivity	1.2	1.2
5%	Thickness	1.5	1.5
100%	Emissivity	0.1	0.1
1/8 in.	Strain gauge location	---	6
1/8 in.	Thermocouple location	8.5	---
-15% baseline	Modulus		-15
+11% baseline	Modulus		+11
+11% constant f(T)	Modulus		+4
Linear/2nd slope	Expansion		-3
-30% linear/2nd slope	Expansion		-34
-40% linear/2nd slope	Expansion		-47
-50% linear/2nd slope	Expansion		-52

REFERENCES

1. Tanzilli and Bleiler. Specular Spectral Transmittance Behaviour and Absorption Coefficient and Emittance Estimates for Five Infrared Window Materials at Elevated Temperatures. Hughes Aircraft Report No. 9T21-2E6-1, Dec. 1982.

2. Siegel, Howell. Thermal Radiation Heat Transfer. New York, McGraw-Hill, 1981.

3. Condon. "Radiative Transport in Hot Glass," J. Quan. Spectrosc. & Radiat. Transfer, Vol. 8, pp. 369-385, 1968.

4. Buzoukiwa, Men. "Use of Fused Quartz as a Reference Standard in Comparative Methods of Thermal Conductivity Measurements," Inzhenerno-Fizicheskii Zhurnal, Vol. 23, No. 44 (October, 1972), pp. 669-672.

5. Krieth and Black. Basic Heat Transfer. New York, Harper-Row, 1972.

6. Rosenhow and Hartnett. Handbook of Heat Transfer. New York, McGraw-Hill, 1973.

7. Sparrow and Cejs. Radiation Heat Transfer. New York, McGraw-Hill, 1978.

8. Koenig, J. R. Presentation to AMRAAM JSPO, 1980.

9. Powell, Ho, and Liley. Thermal Conductivity of Selected Materials. Washington, D.C., U.S. Dept. of Commerce, 1966. (USDC Pub. No. NSRDS-NBS-8.)

10. Goldsmith, Waterman, and Hirschhorn. Handbook of Thermophysical Properties of Solid Materials, Vol. 3. New York, MacMillan, 1961.

INITIAL DISTRIBUTION

2 Naval Air Systems Command (AIR-7226)
9 Naval Sea Systems Command
    SEA-09B312 (2)
    SEA-62R11, D. Bean (5)
    SEA-62Z3 (2)
1 Commander in Chief, U.S. Pacific Fleet (Code 325)
1 Commander, Third Fleet, Pearl Harbor
1 Commander, Seventh Fleet, San Francisco
2 Naval Academy, Annapolis (Director of Research)
3 Naval Ship Weapon Systems Engineering Station, Port Hueneme
    Code 5711, Repository (2)
    Code 5712 (1)
2 Naval Surface Weapons Center, Dahlgren
    G-23, D. McClure (1)
    K-21, F. Moore (1)
2 Naval Surface Weapons Center, White Oak Laboratory, Silver Spring
    G20, J. East (1)
    SURFMAT, W. T. Messick (1)
1 Naval War College, Newport
2 Army Ballistic Missile Defense Systems Command, Huntsville
    BMDSC-HNV, G. Flowers (1)
    BMDSC-LEH, R. Smith (1)
1 Army Missile Command, Redstone Arsenal (DRSMI-ROA, T. Morgan)
1 Air Force Armament Division, Eglin Air Force Base (AD/XRG)
1 Air Force Intelligence Service, Bolling Air Force Base (AFIS/INTAX, Maj. R. Lecklider)
5 Air Force Wright Aeronautical Laboratories, Wright-Patterson Air Force Base
    AFWAL/AADM, A. Blume (1)
    AFWAL/MLP, M. Minges (1)
    AFWAL/MLPJ (1)
    AFWAL/MLPO
      D. Evans (1)
      E. Kuhl (1)
1 Lewis Research Center (NASA), Cleveland, OH (H. Schock)
2 Defense Technical Information Center
1 Acurex Corporation, Huntsville, AL (F. Strobel)
1 Aerojet Electro Systems Company, Azusa, CA (MS 170/8433, J. Buch)
1 CVD, Inc., Woburn, MA (R. Taylor)
1 Coors Porcelain Company, Golden, CO (D. Roy)
1 Crystal Systems, Salem, MA (F. Schmidt)
1 Ford Aerospace and Communication Corporation, Newport Beach, CA (Library)
1 General Dynamics Corporation, Pomona Division, Pomona, CA (R. Hallse), Via NAVPRO
1 General Electric Company, Optoelectronics Systems Operation, Syracuse, NY (Library)
1 Hughes Aircraft Company, Canoga Park, CA (D. Quan)
1 ITT Research Institute, Chicago, IL (GACIAC, C. Smoots)
1 Martin-Marietta Aerospace, Orlando, FL (S. H. Hawkins)
1 McDonnell Douglas Corporation, St. Louis, MO (J. Reilly, Dept. E451, Bldg. 1071,
  Level 4, Rm. 413)
2 Raytheon Company, Lexington, MA
    Research Division
      R. Gentilman (1)
      J. Pappas (1)
1 Raytheon Manufacturing Company, Missile Systems Division, Bedford, MA (P. Miles)
1 Southern Research Institute, Birmingham, AL (J. Koenig)
1 Teledyne Brown Engineering, Huntsville, AL (M/S 44, D. McMahon)
1 Texas Instruments, Dallas, TX (Technical Library)
1 The Boeing Company, Seattle, WA (Technical Library)
1 The Johns Hopkins University, Applied Physics Laboratory, Laurel, MD (W. J. Tropf)